EFFECTS OF LEAFLET STIFFNESS ON THE DYNAMIC MOTION OF THE AORTIC HEART VALVE

by

Hiroatsu Sugimoto

BS, Carnegie Mellon University, 1999

Submitted to the Graduate Faculty of

School of Engineering in partial fulfillment

of the requirements for the degree of

Master of Science

University of Pittsburgh

2003

UNIVERSITY OF PITTSBURGH

SCHOOL OF ENGINEERING

This thesis was presented

by

Hiroatsu Sugimoto

It was defended on

April 14, 2003

and approved by

James F. Antaki, Ph. D., Associate Professor
Department of Bioengineering

George D. Stetton, Ph. D., Assistant Professor
Department of Bioengineering

Thesis Advisor: Michael S. Sacks, Ph. D., Associate Professor
Department of Bioengineering

ABSTRACT

EFFECTS OF LEAFLET STIFFNESS ON THE DYNAMIC MOTION OF THE AORTIC HEART VALVE

Hiroatsu Sugimoto, BS

University of Pittsburgh, 2003

The effects of valve leaflet mechanical properties on the dynamic geometry and function of the aortic heart valve are, to date, not well understood. This is largely due to the complex anatomy and solid-fluid interactions inherent in valve function. In the present study, the effects of leaflet stiffness on the dynamic aortic valve leaflet 3D geometry were quantified using a novel, non-contacting imaging system over the complete cardiac cycle. The imaging system utilized a structured laser-light imaging method, incorporated into a physiological flow loop, to project a high density matrix of laser dots onto the leaflet surface. The resulting dot pattern defined the leaflet surface, and was imaged by a pair of borescopes equipped CCD cameras providing stereographic views. From the image pairs, 3D dot coordinates were recovered using the direct linear transformation method. Five native porcine aortic heart valves were imaged, and then mechanically stiffened using a 0.625% aqueous glutaraldehyde fixation for 24 hours while under 4 mmHg transvalvular pressure. The valve was then re-imaged under near-identical flow conditions. Area, dimensional, surface curvature, and measurements were performed. We observed that: 1) the native valve elongates in the radial direction by ~30% when fully opened, and exhibited small, high frequency

shifts in shape; 2) the stiffened leaflet demonstrated a more stabile shape, as well as focal regions of prolonged, high curvature; 3) the stiffened leaflet opens and closes faster by ~10 ms compared to native leaflet; 4) for both native and stiffened states, the aortic valve opened from basal region leading to free edge 5) when closing, both the native and stiffened state valve close with both free edge and circumferential together. Clearly, valve leaflet undergo complex geometric changes during the cardiac cycle, and leaflet mechanical properties (mainly stiffness) have a profound affect on leaflet dynamic geometry.

Overall, the primary findings of this study were the extensive radial distension in the native state, and that an increase in leaflet mechanical stiffness induces high bending areas. The physiological function and advantage of the radial distension is currently unknown, but may affect the local hemodynamic patterns during valve operations, especially in the sinus regions. Our findings for the stiffened tissue have implications to valve design. For example, the high bending observed in the stiffened state correlated with known locations of tissue deterioration previously reported in our laboratory. Thus, in order to minimize leaflet tissue damage, methods of chemical modification utilized in bioprosthetic heart valves that maintain leaflet flexibility are necessary to minimize the onset and progression of tissue damage.

ACKNOWLEDGEMENTS

I would like to thank my advisor, Dr. Michael Sacks for his willingness to share with me his wealth of wisdom, patience, and encouragement as he guided me in this work. This would not have been possible without his help and effort.

I express my appreciation to, Dr. James Antaki and Dr. George Stetton for their assistance, advice, and for serving as members of the thesis committee. I also like to thank Dr. Arun Iyengar, Mr. Matt Ogle, and Dr. Michael Scott for their assistance in this research.

I would like to thank the Department of BioEngineering faculty members, staff, and graduate students for making the program a strong one with friendly atmosphere. Thanks to Dr. Claire Gloeckner, for looking over my thesis when it was far from complete.

Finally, I would like to express my deepest gratitude to my mother for her belief in me, whole-hearted love, and support.

TABLE OF CONTENTS

LIST OF TABLES

LIST OF FIGURES

1.0 INTRODUCTION

The function of a heart valve is very basic: to allow blood to flow in only one direction. Native valves can withstand 80-120 mmHg of trans-valvular pressure and will operate in excess of 3 billion cycles during an individual's lifetime. Although it is clear that the normal heart valve performs its function flawlessly, the details of how it performs its function are fully understood. Further, when a valve is diseased because of congenital defects or tissue calcification, a prosthetic replacement is needed to restore valvular function. Valve repairs are limited due to the complex valvular anatomy, so that medical treatment almost exclusively replacement as opposed to repair. (1)

Worldwide, there are ~300,000 people each year who undergo heart valve replacement surgery because of rheumatic fever, birth defects, aneurysms, or other ailments. The first attempt at heart valve replacement using allografts (i.e. from a human valve from a cadaver), which are limited in supply and include disease transmission. Dr. Alain Carpentier, in the 1960s, attempted to alleviate this problem with the development of the first xenograft porcine aortic valve. Although the first implantations were failures because of biocompatibility problems, the Carpentier valve marked the beginning of heart valve replacement.

Currently, approximately one-half of heart valve patients receive bioprosthetic heart valves replacements. The other half receives mechanical heart valves, which are composed of rigid, synthetic materials. Mechanical valves will generally last the

patient's life, but require continual anti-coagulant therapy. While bioprosthetic heart valves generally do not require anti-coagulant therapy the average lifespan of bioprosthetic valve is 8 ~ 12 years, and even shorter for younger patients. (2) For an elderly patient, a bioprosthetic valve is a preferred option as they would likely not live long enough to require repeated surgeries to replace the failed valves. For a younger patient with birth defects, the prospect of facing risky open heart surgery every 10 years is a grim one. Most patients younger than 65 years old therefore receive a mechanical valve and live with anti-coagulation therapy for the rest of their life. However, the anti-coagulation therapy requires constant monitoring and imparts the patient with a life-long increased risk of serious bleeding and hemorrhage. (3, 4) Therefore, neither current mechanical nor bioprosthetic replacement heart valves represent an ideal solution.

Most current heart valve research is focused improving bioprosthetic heart valve durability, since mechanical prosthesis are considered a mature technology. However, investigators focus on improved biocompatibility through novel chemical treatment methods. As the ultimate design paradigm, improving our understanding of how the natural valve, designed over millions of years, can guide the development of improved bioprosthetic valves. Yet, our knowledge of native valve function remains rather limited. This is particularly the case in valve dynamic behavior, where studies have been very limited due to the technical difficulties involved.

The purpose of the present study was to improve our understanding of the dynamic function of the native aortic valve. A novel optical-based valve imaging system was developed to quantify leaflet motion and shape for the study of heart valve

dynamics. The system features a structured laser-light projection technique, which eliminates the need for physical markers, to obtain images of the complete valve leaflet surface dynamically with high temporal resolution. The system employs multiple cameras along with boroscopes to obtain unobstructed views of the entire surface and has higher spatial resolution, at least three times the resolution obtained with current physical marker techniques (5) (6). Furthermore, detailed studies of effects of increased leaflet stiffness on the aortic valve dynamic geometry during the cardiac cycle were performed. The resulting changes in leaflet motion were quantified and implications to valve function discussed.

1.1 Anatomy and Physiology of the Heart and Heart Valves

The Heart. The function of the heart is to perfuse the body with blood (Figure 1). It consists of four chambers including an atrium and a ventricle on each of the left and right sides of the heart. The two chambers on the right are responsible for the perfusion of the pulmonary system. The two chambers on the left perfuse the rest of the body and brain. Oxygenated blood from the left side of the heart flows to the rest of the body, including the brain, bringing nutrients and oxygen and carrying away waste and carbon dioxide, and then blood is returned to the right side of the heart. The right side of the heart circulates blood through the pulmonary system, where the red blood cells exchange CO_2 for O_2 from the lungs. Blood returns to the left side of the heart and the cycle continues. (7)

To expel blood, the muscle fibers rapidly contract and shorten, which decreases the actual volume within the heart. Since blood is composed primarily of water and is therefore incompressible, the pressure increases due to the shortening. When the pressure inside the chamber exceeds the pressure on the other side of the outlet valve, the valve opens and fluid is ejected out. The contraction of the muscle cells that make up the chamber walls is synchronized. The timing of the contraction of the four chambers is synchronized by the nervous system of the heart (Purkinje fibers). The proper coordination of the muscle fibers within each chamber and between the chambers is essential to proper functioning. (8)

The heart is composed of cardiac muscle fibers supported by collagen fiber. This muscle type is different from the skeletal and smooth muscle found in the rest of the body. These specialized cells must work constantly, contracting every second without a pause, for several billion contractions over a human lifespan.

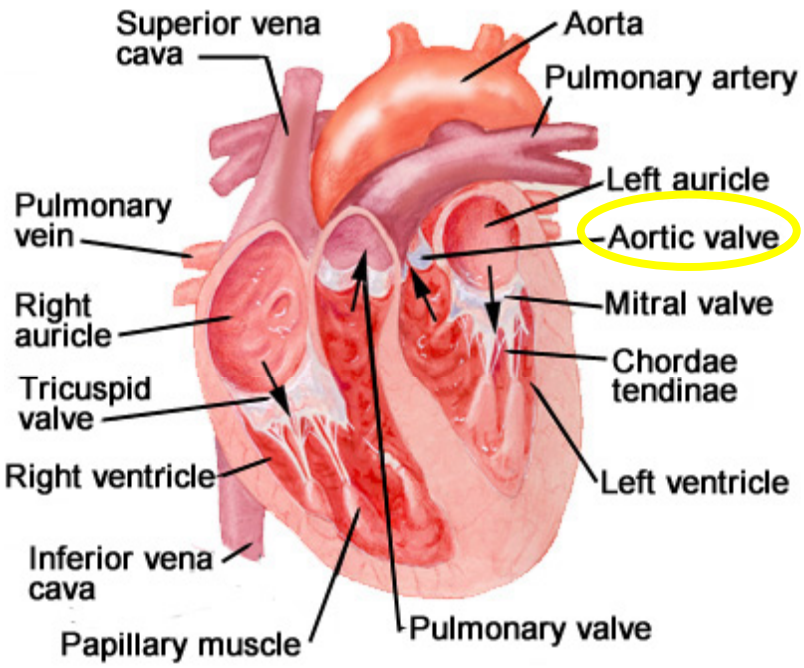

Figure 1 Anatomical structure of the heart with anatomical features marked. (Image courtesy of http://www.surgery.com/**)**

The heart valve. On each side of the heart a one-way valve separates the atrium and ventricle. The atrium collects blood and pumps it into the ventricle. The ventricle pumps blood out of the heart through another valve to keep blood from returning. Of the two valves on each side of the heart, the interior valves separate chambers of a lower pressure gradient compared to the ventricle outlet valves. On the right side of the heart, the tricuspid valve separates the atrium and ventricle and the pulmonary valve is the left ventricle outlet. On the left side of the heart, the mitral valve separates the chambers and at the exit of the ventricle, the aortic valve keeps blood from flowing back into the heart. The valves each have three (tricuspid, pulmonary, aortic) or two

(mitral) tissue leaflets of less than 1 mm thickness. In each valve, the leaflets are shaped so that flow is allowed in one direction only. Each valve is in a different anatomical position and endures slightly different blood flow so that the structure is unique to each valve. Although failure of any heart valve is a medical concern, the failures of valves on left side of the heart are most deadly. (7)

The three leaflets of the aortic valve are attached to the wall of the aorta. (9) The leaflets are shaped to come into contact with the two other leaflets at the center of the aorta. The tissue at the connection point, called the nodulus, is slightly thickened compared to the rest of the leaflet tissue. The leaflets are constructed in layers: the fibrosa, spongiosa and ventricularis. The ventricularis layer is on the ventricle side, as its name implies, and consists mostly of elastin. (10) (11) The fibrosa, which is on the aortic side of the valve, is composed mainly of large bundles of collagen as well as some elastin. As the leaflet stretches, these collagen fibers are the main load-bearing component. The collagen structure is arranged circumferentially so the leaflet does not stretch little in the circumferential direction, but stretches significantly in the radial direction as trans-valvular pressure increases. (12)

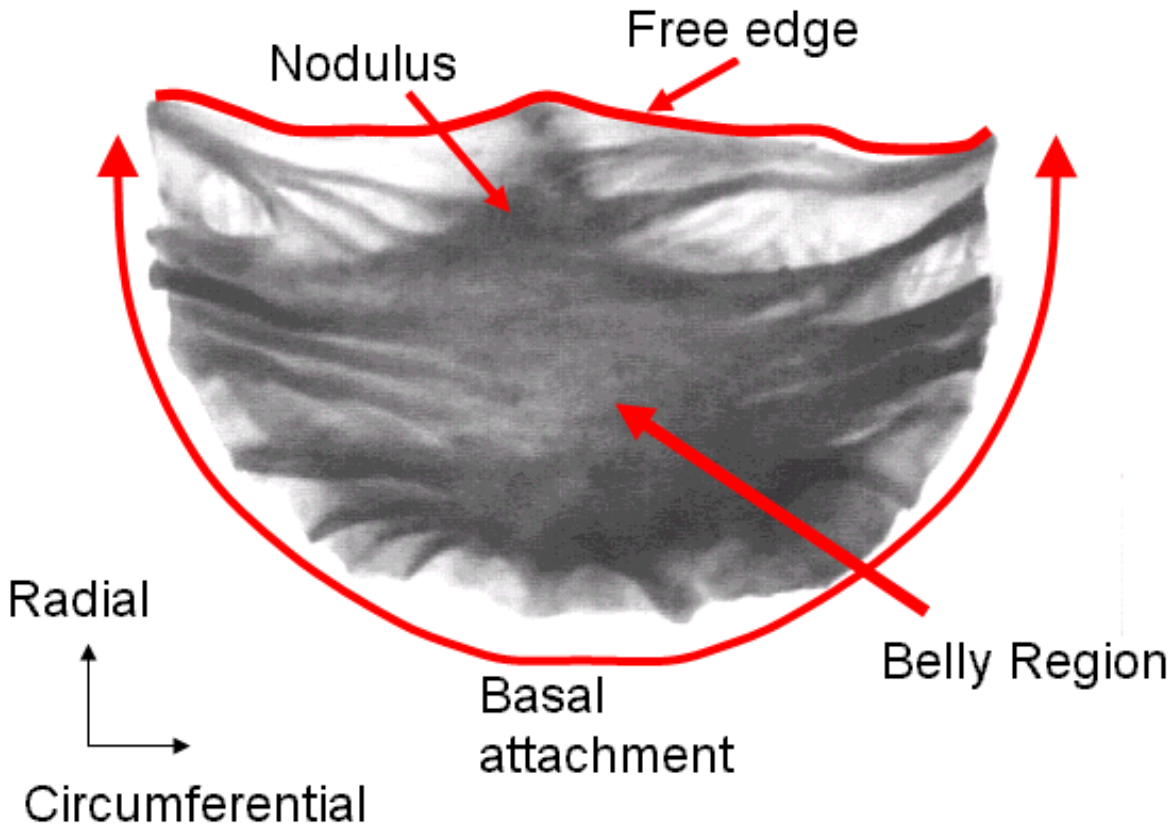

Figure 2 Image of heart valve leaflet. Leaflet is attached at the basal attachment region. The nodulus in middle of valve is a collagen fiber structure that is darken due to the thickness. The orientation axis on the left is the common terminology used for describing leaflet direction.

1.1.1 Historical Background on Aortic Heart Valve Function

The first recorded study of the heart valve dates back to the 2nd century. The renowned Greek anatomist Galen believed that the heart was a suction device rather than a pump. In the 15th century, Leonardo Da Vinci wrongly postulated that the purpose of the heart valves was to eject blood from the heart. (13) Nevertheless, his detailed drawings of the heart and valves are still considered useful in the medical field. Less than a century later, Harvey et al of England was the first one to appreciate that the

valves only allowed flow in one direction. He also dispelled the belief that the heart was a suction device rather than a pump. Much later, Bellhouse and Bellhouse investigated the influences of fluid dynamics on the heart valve and discovered that the function of a heart valve was much more complicated than originally thought. (14, 15) They postulated that the deceleration of fluid flow out of the valve is the main mechanism of valve closure. This mechanism explains why the heart valve is so effective in preventing reverse flow with minimal energy loss.

1.2 Heart Valve Disease

The category of heart disease generally includes conditions such as heart attacks (myocardial infarction) and enlarging of the heart (cardiac hypertrophy). Rarely are diseases of a heart valve included in this category. Yet valve disease is alarmingly frequent and the primary treatment is surgery. Additionally, valve disease can often cause other heart problems such as cardiac hypertrophy.

1.2.1 Types of Diseases

Malfunction of the heart valves can be the result of many conditions. The most common causes of damage to the heart valves are rheumatic fever, birth defects and aortic dilation. Additionally, a small percentage of patients with infected endocarditis, a persisting bacterial infection of heart tissue, require heart valve replacement. Treatment for endocarditis is initially through pharmaceuticals and only when this medical therapy fails is surgical treatment considered. (16)

Rheumatic fever, a childhood streptococcal infection, is a disease with a wide range of consequences (Figure 3). One outcome is scarring of the cardiac tissue, including the valves. The scarring decreases the durability of the valve tissue and leads to damage over time. Another potential result is that the valve leaflets can partially fuse together, resulting in a stricture of the valve opening, called stenosis of the valve. Rheumatic fever is the cause of 45% of stenotic valve cases. (3)

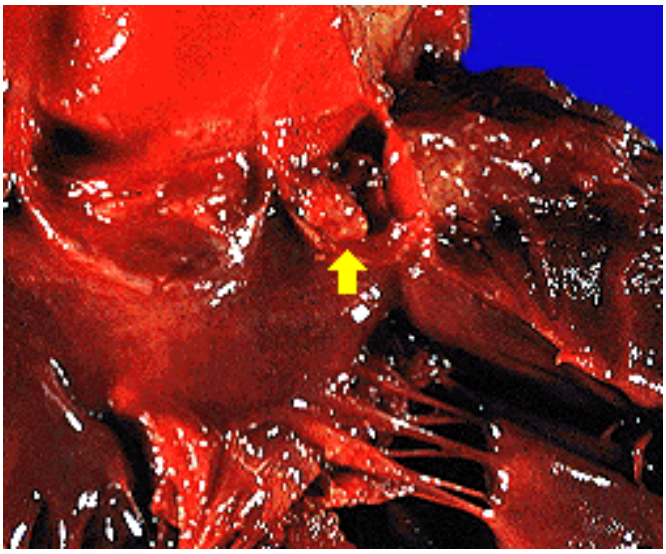

Figure 3 Arrow denotes scar tissue due to rheumatic fever. (Image courtesy of Dr. Richard B. Roberts of Cornell medical school)

Birth defects of the heart valve leaflets occur in about 2% of the population. (3) Generally, the defect is the development of a valve with an incorrect number of leaflets, including only one or two leaflets, which allow regurgitation, to four leaflets, which can cause stenosis. The most common defect is the bi-leaflet valve, where there is only a left and right leaflet. Overall, birth defects account for about 20% of heart valve disease cases (Figure 4). While some birth defects are not serious enough to require surgery, the

presence of an abnormality generally results in a reduced life expectancy. Surgery is necessary and urgent in cases of heart valves with one- or four-leaflet aortic valves (2).

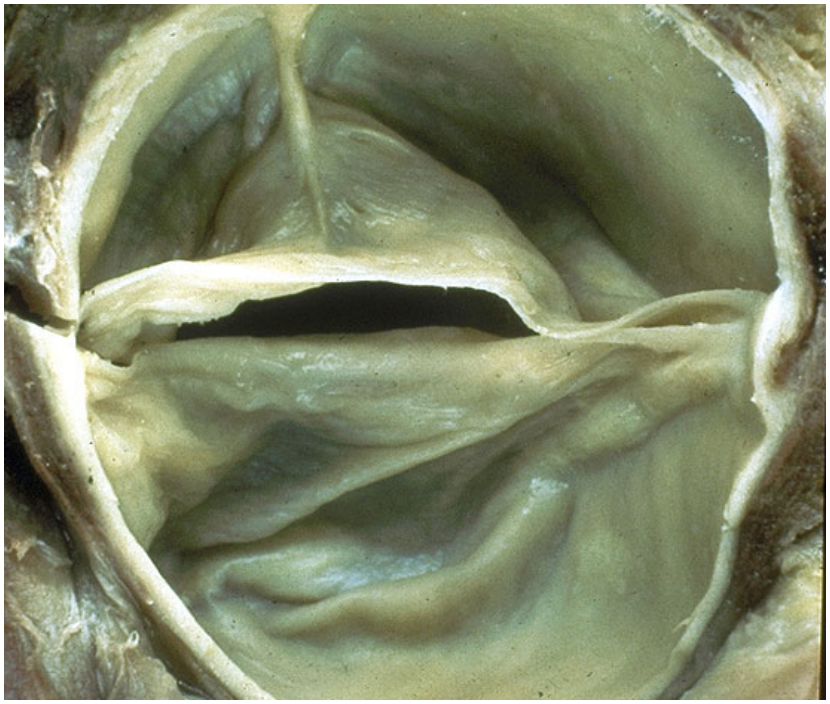

Figure 4 Congenital defect of aortic valve that has become a bicuspid valve

Aortic dilation is the enlargement of the sinuses of valsalva, where the valve leaflets are situated. (17) This dilation is secondary to other heart conditions such as arteriosclerosis and hypertension. Since the valve sinuses are often part of the prosthetic valve, depending upon the specific model, replacement of the entire valve is performed.

1.3 Therapy

Management of heart valve disease includes both pharmaceutical and surgical intervention. Pharmaceutical therapies include beta-blockers and anti-bacterial medicines. Beta-blockers are used to reduce the heart rate that can slightly improve cardiac output. Anti-bacterial medi cations are used to stop the infection of cardiac tissue. Generally, pharmaceutical treatments may be able to stop or slow down the advances of valve disease, but the only way to reverse damage caused is to surgically replace the damaged heart valve with one of four choices: an autograft, an allograft, a synthetic mechanical prosthesis, or a bioprosthetic prosthesis. (1)

The percentage of total heart valve surgeries performed where allograft and autografts are used is small. As with all donor organs, the supply of human donor cadaver heart valves is very limited. An autograft procedure is when one of the patient's valves is moved from one valve position to another. Utilization of an autograft is limited since all four valves are necessary for proper heart functioning and therefore the donor valve must be replaced. Generally, autograft are only utilized in the Ross Procedure, wherein the pulmonary valve is relocated to the aortic position and the pulmonary valve is replaced by either an allograft or a prosthesis. (18)

1.3.1 Treatment

To replace any valve, the only current surgical method is open-heart surgery. The operation takes three to five hours with the patient under general anesthesia. The access is through midline incision and the heart is stopped during the procedure. A

heart-lung bypass machine maintains the patient for the duration of the operation. In the case of an aortic valve replacement, the surgeon dissects the aorta away from the heart, dissects the valve from the heart, sews the new prosthetic valve onto the heart, and then sews the aorta onto the new valve. The heart-lung bypass machine is removed and the patient's heart is electrically shocked to return it to a regular rhythm. After surgery, the patient remains in the hospital and total recovery can take up to 6 months. Recovery is usually longer for geriatrics patients. The surgery carries an immediate mortality rate of 5%, and complications occur in 10% of the surgical cases.

1.3.2 Mechanical Prosthetic Heart Valves

Typical mechanical valves are very durable and can last up to 30 years without failure. They are usually constructed of biocompatible material and metal. Unfortunately, the durable surface tends to attract clotting factors and requires the patient to take anti-coagulants indefinitely. There are three general designs for the successful mechanical prosthetic valves used today: ball and cage, tilting disk, and bi-leaflet.

One of the first successful mechanical valve designs was the ball and cage, such as the Starr-Edwards model. (Figure 5) A small sphere of a diameter slightly less than the diameter of the aorta is encased by a ring at the ventricle outlet and by a metal cage extending into the aorta. When blood flows through the valve, the ball is pressed against the aortic side of the cage, allowing blood to flow around it, and when flow reverses, the ball is pressed against the ring near the ventricle, stopping reverse blood

flow. The ball is made out of silicon polymer and the cage of cobalt chromium alloy. Over 200,000 of these valves have been implanted worldwide.

Figure 5 Ball and cage valve (image courtesy of Edwards LifeSciences)

Tilting disk valves have a circular disk in the middle held in place by a wire frame that prevents reverse flow (Figure 6). The disk tilts when it opens, allowing blood to pass. The disks are made of graphite and pyrolytic carbon and the frame is stainless steel or titanium. The Björk-Shiley model was the first successful and most famous of this type. Around 360,000 have been implanted, however, due to a design change that resulted in many valve failures and many deaths, the use of the current Björk-Shiley model is not prevalent today.

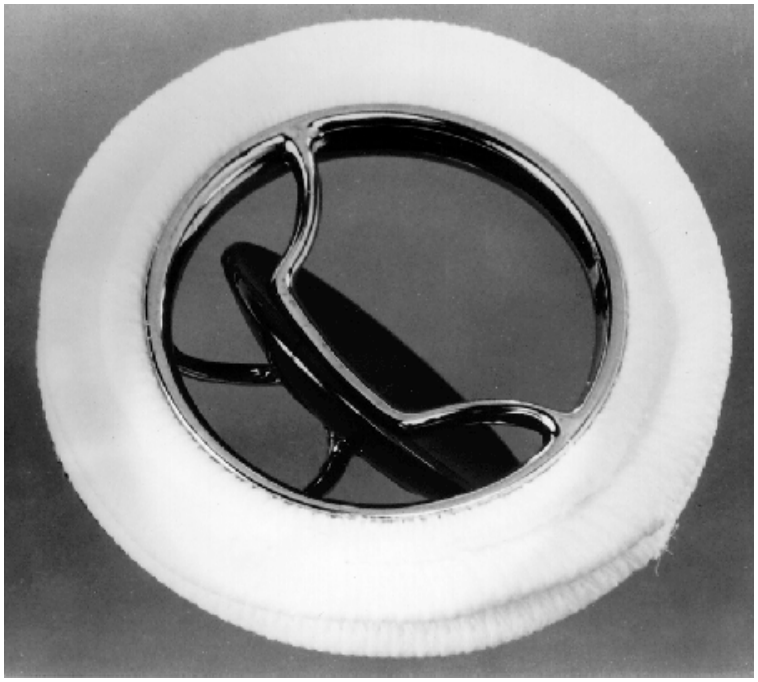

Figure 6 Tilting disk valve(image courtesy of Shiley)

The most widespread mechanical valve used today is the bi-leaflet valve design introduced by St. Jude Medical (Figure 7). Two half disks are held by a frame and the half disks swings open like a door to allow blood to flow. This valve design has the advantage of the biggest orifice area over the other models. Over 600,000 of these valves have been implanted worldwide.

Figure 7 Bi-leaflet valve (image courtesy of St. Jude Medical)

1.3.3 Bioprosthetic Heart Valves

Bioprosthetic valves can be divided into two categories, porcine aortic valves and bovine pericardial valves. Both are composed primarily of xenogenic tissue that is taken from pigs or cows, respectively. The tissue components are treated with a chemical such as glutaraldehyde to disguise the antigens on the cells so that the human system does not recognize the tissue as foreign. Additionally the chemical treatment crosslinks the leaflet's collagen fiber which stabilize and strengthens the tissue structure. Bioprosthetic valves have better hemodynamic characteristics and do not require patients to take anti-coagulants. On the other hand, the chemical crosslinking of the tissue promotes the binding of calcium and other salts to the tissue, which reduces their flexibility over

time. Unfortunately, even in the absence of calcification, tissue breakdown occurs and bioprosthetic valves usually require a replacement after 15 years. (19)

Porcine aortic valves are made from aortic valves taken from pig hearts. (Figure 8) These valves are chemically treated with 0.625% glutaraldehyde and then trimmed by technicians to fit the specific model. Depending on the model, the valve may be pressurized to different degrees during modification with chemicals such as glutaraldehyde. Additionally, the valve tissue is trimmed differently for each model, and may be sewn into either a metal or plastic frame (called a "stent"), or implanted without a frame ("stentless"). Generally a ring of Dacron or biocompatible cloth is sewn to the outside at the base of the valve to aid in surgical implantation.

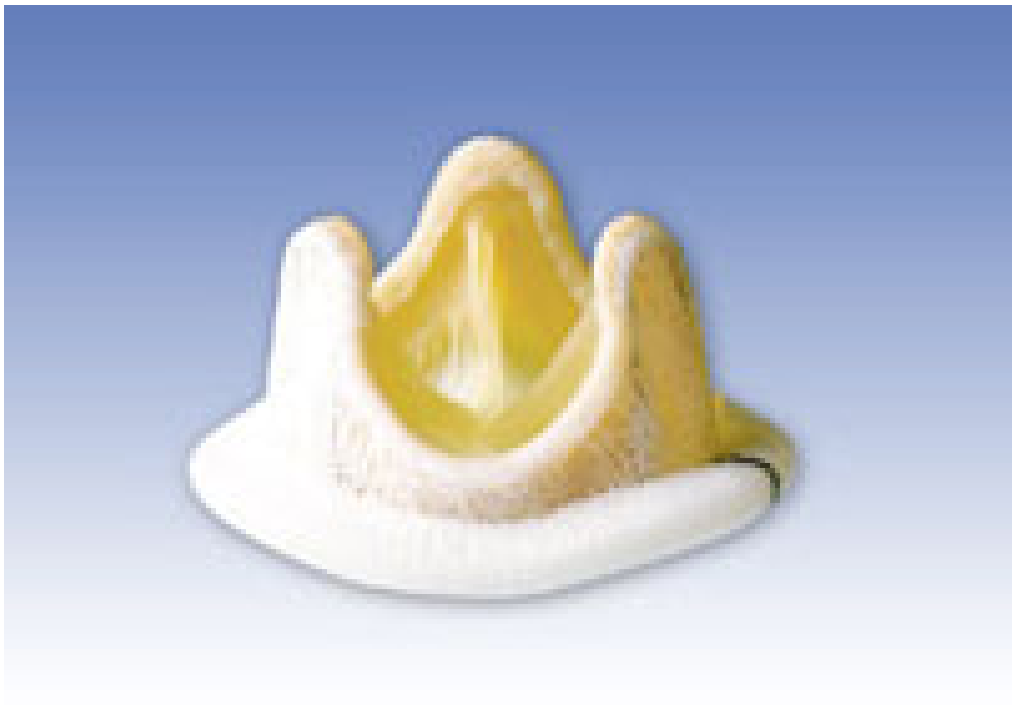

Figure 8 Bioprosthetic porcine aortic valve (image courtesy of Edwards LifeSciences)

Bovine pericardial valves are constructed from bovine pericardium, a tissue sac surrounding the heart. (Figure 9) The sac is cut out into a sheet and treated with chemicals such as glutaraldehyde. The shape of leaflets are trimmed out and sutured onto a stent with a cloth ring base for ease of implantation. Pericardial valves are thought to have better configurability as the leaflets can be cut into different shapes to form the shape of the valve.

Figure 9 Bioprosthetic bovine pericardial valve (image courtesy of Edwards LifeSciences)

1.3.4 Financial Costs

The financial expense of the treatment of heart valve disease comes from several sources related to the medical care. The cost of the surgery itself includes the use of the medical operating room, the supplies consumed and the equipment utilized during the operation, and the time of the surgical staff. The patient is generally in the hospital for several months after the surgery since open-heart surgery is very traumatic and

recovery is slow. The prosthetic valve is purchased from a medical device company and costs up to $10,000. Each year in the United States the 75,000 heart valve replacement surgeries cost an estimated 3 billion dollars. (19)

1.4 Previous Work on Heart Valve Dynamic Function

Although the basic mechanism of valve function is well understood, the specific details of dynamic function remain unknown. In order to perform these studies, imaging high speed imaging technologies are required. In the following a summary of the current state-of-the-art of heart valve imaging technologies and fluid dynamics is presented.

1.4.1 Fluoroscopic Imaging

Fluoroscopy uses radioactive dye to illuminate the inner anatomy of patients' body. It could also be used as a research tool to determine how organs function in-vitro. Thubrikar et al has done extensive studies using fluoroscopy to determine dynamic valve function. (20) (21) (22) These experiments involves submitting laboratory animals to open heart surgery, to suture lead markers onto the valve leaflets. The chest cavity is then closed and the animal was allowed wake up from anesthetics. Using fluoroscope, the images of markers and associated landmarks are recorded on film and later analyzed.

The limitation of fluoroscopic imaging lies in the need to place physical markers on a stretchable tissue. The addition of markers, some of which are made of heavy lead,

can weigh down the thin light leaflets that are 0.3 ~ 0.5 millimeters in thickness. The method to attach the marker, by use of sutures, restricts the tensile nature of the leaflet, thus miss representing the actual function of the leaflet. Fluoroscopy can only be recorded in 2D, rather than a 3D measurement. The positioning of fluoroscope detector can greatly affect the accuracy as the point of view can not be accurately verified. Thus it would be an estimation of length of which can not be verified. As the testing was done in 2D, the results do not include shape or curvature data. The lack of shape data severely hampers the understanding of valve function.

1.4.2 Ultrasound

Ultrasound study of heart function, or echocardiography, is popularly used in the clinical setting. Ultrasound can detect heart defects, abnormal rhythms, and other abnormalities. The method is also non-invasive and low cost. Many heart research studies employ the use of ultrasound to study cardiac function. Methods of 3D ultrasound are also becoming popular and are now being implemented by medical device companies.

Short comings of the ultrasound include the low temporal and spatial resolution. The ultrasound's temporal resolution is around 30 milliseconds, which is far too long to capture dynamic movements of heart valves. Spatial resolution of ultrasound is also poor because of noise and distortion that comes from use of acoustics that can bounce unpredictably. Also it can only scan in 3D by scanning several planes of view in sequence, and therefore can not capture an entire 3D field instantaneously. (23) (24)

1.4.3 Computed Tomography

The x-ray is the most commonly used tool in medical imaging. Computed Tomography, or CT, is the use of several hundred x-ray images from different view planes to form a structural analysis of the internal anatomy. Patient is placed inside the device where the mechanism would take x-ray images from all angles. The results of which is mathematically computed by a computer to develop images that can provide views that normal x-rays can not (for example, horizontal slices of human body). Many CT scanners have functions that can concentrate on a specific space to provide high quality images.

Unfortunately the method requires several hundred images to be taken to compute the final image. Thus unless the heart is in sync with the CT scanner, it would be taking images from different times of cardiac cycle. In addition, the spatial resolution of most CT scanners is around one second. Newer models (IMATRON) that can scan at 30 – 50 milliseconds are still not fast enough to capture the dynamic motion of heart valves.

1.4.4 Bi-plane X-ray Imaging

Bi-plane imaging, 3D imaging using two orthogonal point of view, using an x-ray to study heart valves was a novel idea proposed by Thornton. (5) Stereoscopic imaging is widely used in many different fields to gather data from 3D space, from mapping earth features, quality control in manufacturing, physical therapy, to video games. The short pulse of the x-ray was able to allow Thornton to capture images at short time interval. Thornton was able to achieve 1 millisecond temporal resolution

which was higher than anyone had been able to capture thus far. The study also provided a map of valve stretch as it strained during opening and closing.

Thornton's method is limited because it was unable to capture the two points of view at the same time. Once one view was captured, the x-ray apparatus was rotated to record from the other angle. Thus the two oblique images are approximately from the same time period of the cardiac cycle. They are not simultaneously captured images and thus small errors can distort the results. In addition radiographic markers had to be glued onto the surface of the leaflet. 30 ~ 40 lead markers would undoubtedly weigh down the leaflet and not represent faithful recreation of leaflet function. The glue used to attach the markers would also change the mechanical properties of the valve leaflet, preventing it to stretch normally. Markers also detached during testing due to the turbulent flow inside the sinus of valsalva and movement of leaflet (as high as 40 cm / sec). (6) (25, 26)

1.4.5 Magnetic Resonance Imaging

Magnetic Resonance Imaging takes advantage of spinning water molecules to image the body. By altering the magnetic fields to manipulate the rotational axis of water molecules, MRI can image the water content inside the body. In addition, different organs are comprised of different amount of water thus differentiating in MRI images. MRI has a high temporal accuracy and is useful in many fields of research. Also, the functional MRI which detects glucose metabolism is heavily favored in neural science research.

Unfortunately the acquisition time for MRI is extremely long. Thus MRI requires several scans to accurately interpolate the results. Thus scans of several cycles are needed in the study, which makes it difficult to synchronize the heart beat each time. Many studies of aortic valves are done in vivo under steady flow and not dynamic motion. (27) (28, 29)

1.4.6 Fluid Mechanical Studies

Fluid mechanical studies are useful to understand the flow pattern inside and around the valve. Henderson and Johnson conducted the first accurate fluid dynamical study of mechanism of the heart valve. The study was a series of experiments to show the mechanism of valve closing. (14, 15) In each of the figure below, it serves to explain the mechanism of valve closing is not due to pressure gradient, but rather by the conservation of mass due to deceleration of fluid flow (Figures 10 ~ 12).

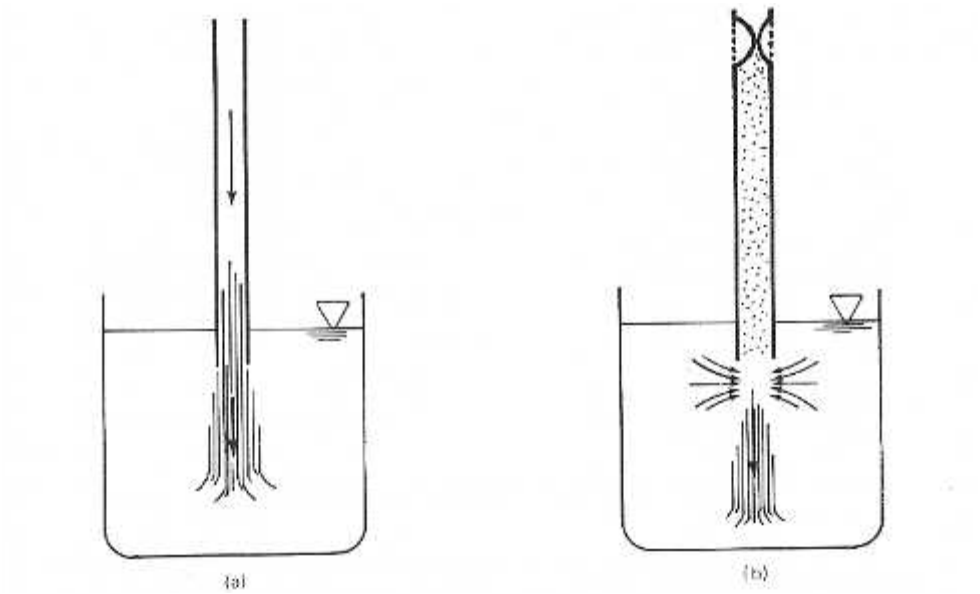

Figure 10 Henderson and Johnson's first experiment which the jet in (a) was suddenly stopped by pinching the top of the tube. What they observed was the jet has conserve it's forward motion and hence break away from the fluid in the tube and instead drawn water into the wake of the jet. (30)

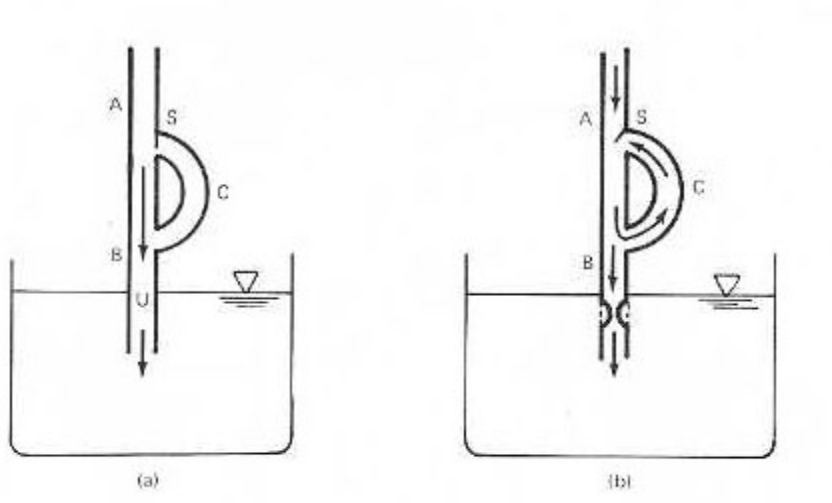

Figure 11 Henderson and Johnson's second experiment which the jet in the straight through flow in (a) was suddenly interrupted. (b) The valve in S opens indicating fluid is circulated though C. (30)

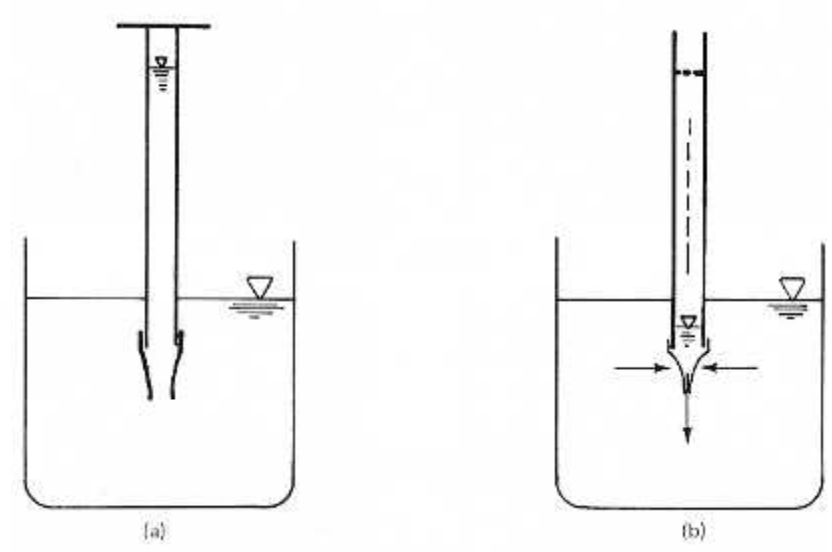

Figure 12 A tube filled with water is sealed and on the other end is a rubber sleeve. As the column of fluid is released and allow to fall, once the column falls below the water level of the tub, the fluid around the sleeve moved inward and collapse the sleeve and sealed the tube(30)

The importance of the sinuses is illustrated by an experiment conducted by Bellhouse et al (14, 15) which demonstrated that part of the flow was redirected into the sinus and behind the leaflet (Figure 13). Then it forms a vortical flow that divides into

two flows and rejoins the rest main flow. They also found the pressure at the root of the valve, p1, is lower than pressure at the tip of the valve p2. This causes more flow into the sinus cavity. This vortical motion prevents the valve cusp from rubbing against the sinus walls.

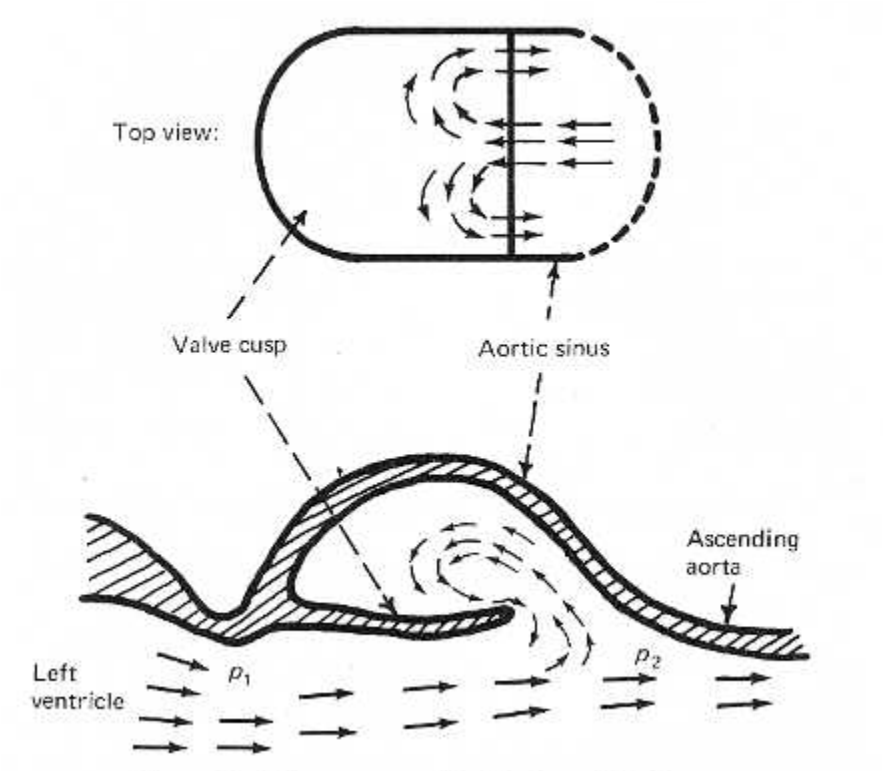

Figure 13 The flow enters the sinus in the middle of the leaflet and departs on the side. The pressure at the tip of the valve is higher than the root, which augments the flow into the sinus. (30)

1.5 Motivation

The current understandings of native heart valve mechanics are limited due to the technical difficulties resulting from the valve anatomy and the complex solid-fluid mechanical interactions. The aortic valve dynamic geometry during opening and closing is influenced by both tissue mechanical properties and local fluid dynamics.

Thus, by understanding the native valve dynamics and the effects of leaflet stiffness, we seek to improve our understanding of the valve function.

1.6 Specific Goals of this Thesis

In the present work, we present a novel optical-based valve imaging system to quantify leaflet motion and shape for the study of heart valve dynamics. The system features a structured laser-light projection technique, which eliminates the need for physical markers, to obtain images of the complete valve leaflet surface dynamically with high temporal resolution. The system employs multiple cameras along with boroscopes to obtain unobstructed views of the entire surface and has higher spatial resolution, at least three times the resolution obtained with current physical marker techniques. (5) (6) The use of boroscopes along with refractive index matching also permitted the use of realistic sinus geometry with minimal optical distortions.

The imaging system was used to quantify the dynamic geometric of the native aortic valve under simulated physiological conditions. Furthermore detailed studies of effects due to changes in the mechanical properties on aortic valve leaflet on its dynamic geometry during the cardiac cycle were performed. Native porcine aortic valves were initially imaged using our structured light imaging system (31) over the complete cardiac cycle. Next, the leaflet was stiffened by chemical treatment, and then re-imaged under identical flow conditions. The resulting changes in leaflet motion were quantified and implications to valve function discussed.

2.0 METHODS

Overall approach to examine the functioning of the heart valve, a closed physiological flow loop was designed into which the heart valve was placed for analysis. A laser imaging system was utilized to measure the motions of the heart valve during dynamic pulsatile motion. A piston controlled by a personal computer running a LabView program generated pulsatility identical to the typical pressure distribution observed at the aortic heart valve. Additionally, the LabView program acquired two-dimensional displacement data through two cameras that was then combined to produce three-dimensional displacement data throughout the simulated cardiac cycle.

The study the native heart valve functioning requires an experimental setup that reproduces a physiological-like environment. The device must be precisely controlled and the protocols repeatable so that the same experimental parameters are used for all tests. The flow loop would have to cycle the fluid through the valve without affecting the imaging system. To replicate the cardiac flow waveform, the flow loop requires many components to do so accurately.

The measurement system was composed of a system capable of estimating 3D surfaces without any contact or pre-modification (Figure 14). This was done by projecting a grid of laser dots onto the tissue surface and capturing the position of the dots on by video throughout the cycle. All these parts of the flow loop and imaging

system was controlled precisely by one computer. The software in the computer would adjust the output of the pump so for every cycle the timing would be accurate. The digital to analog devices would receive pressure and flow data which was recorded on the computer. And the computer would capture images from the Charged Couple Device (CCD) cameras, simultaneously providing pictures that are accurate in order to calculate the 3D surface.

Valves were tested using flow loop and results are captured with the laser system. Images are processed and pixel locations of the laser dot matrix recorded. The 3D location of laser dots were used to reconstructed a mesh surface. The mesh was then used to calculate curvature and geometrical properties.

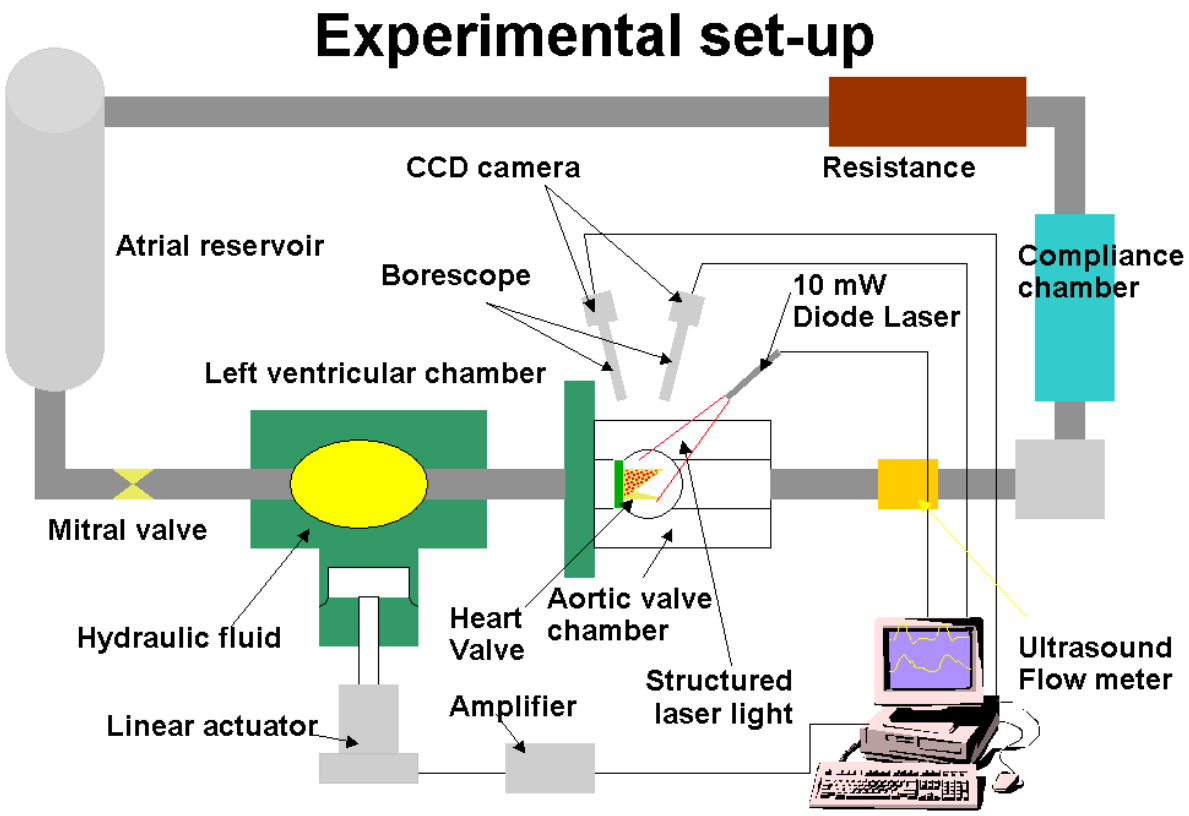

Figure 14 Overall set up of the physiological flow loop and imaging system. The linear actuator pumps the fluid in the loop. The fluid flows through the chamber that holds the valve and allows for structured light imaging. The flow is conditioned by use of compliance chamber and resistors. The water reservoir keeps the flow loop with enough liquid. The boroscopes are connected to CCD cameras which send the image to the computer. The timing of laser and camera triggering are controlled by same computer that controls the flow loop. (see text for details) published in (31)

2.1 Physiological Flow Loop

The physiological flow loop was composed of several components to produce pressure and flow conditions similar to that of the heart. Each of the parts are specially designed and connected with surgical tubing and piping connectors. The flow loop was

designed in combination with the laser imaging measurement system and instrumentation to accurately collect displacement and flow data.

The pump. As the input of the system, the pump pushed fluid medium through the loop and is therefore an essential part. There are many possible choices of pumps, however, and this decision was carefully considered.

Cylindrical pumps involve a cylinder that moves by a drive shaft. (32) As the drive shaft moves in, it decreases the volume inside the cylinder. The pump has an inlet and outlet port which has a one-way valve. The valve has a directionality that allows fluid to go only one way but not the other. Thus as cylindrical volume decreases, the inlet port closes and fluid leaves the outlet port. As volume increases again, fluid enters into the cylinder through the inlet port. The way the cylindrical pump works was ideal for this study as it mimics how a human heart works. The cylindrical pump design was an important consideration since it ensures that the output matches that of the physiological cardiac cycle. The change in volume at closure has to match the ejection output of the heart. Also the fluid has to have a symmetrical velocity profile as it is leaving the pump. These problems were solved by using a mask-valve-bag used to resuscitate respiratory arrest patients. The latex bulb was cut out and attached to circular PVC piping. The PVC piping was in line with the valve, thus maintaining a symmetrical flow velocity profile. The piping end was clamped onto the plastic acrylic wall casing. Inside the casing, it was filled with fluid to submerge the bulb. By using a fluid, the bulb can be pressurized from all sides at the same time. The fluid within the pump was viscous glycerol to minimize effects of pulsatile reflection as the pump

operates. Pulsatile reflection would cause the pump to vibrate and the viscous glycerol served to dampen the oscillation that could occur. The acrylic casing, which contained the bulb and pump fluid, is built to withstand 300 mmHg of pressure without significant deformation. The casing was the stationary container for the bulb and was bolted down to the table to stabilize it and decrease vibrations. The casing is connected to the cylindrical pump. This transferred fluid into the casing, thus increased pressure inside the casing by compressing the bulb. The cylindrical pump used could output a maximum of 125 ml of volume per stroke and was adjustable. The pump was sealed with use of a bellow. The bellow was connected to the Teflon coated piston and driven by a voice coil. A voice coil is an electrically powered device where the current through wires moves the coil. The position of the voice coil was determined by two factors, the current amperage and amount of force on the voice coil. It was powered by an amplifier (model 12A8, Advanced Motion Controls, USA) that received its signal from an NI A-D board. The amplifier had four control settings, (offset, Amp, scale, voltage limit) which allowed for fine-tuning of the signal.

Systemic vascular resistor. As blood travels through the vascular system, the blood vessels become thinner and the viscous blood generates friction against the blood vessels, this creates a natural resistivity to fluid flow. In the flow loop, the resistivity was created through the use of a device that increased the fluid-surface contact area, similar to the increased surface area of the capillaries. The small tubing resistor used in this study consisted of eighty 8 mm inner diameter of surgical stainless steel tubes packed into the flow loop's tube. These tubes increase resistance of flow by 3

mmHg/ml/sec, according to the equation below, thus approximating the resistance of human's vascular system. Resistance is given by: (R indicates resistance; r, radius; L, length of tubes; u, dynamic viscosity; X, number of tubes) (33)

$$R = \overline{P} / \overline{F} = (8 * \mu * L) / (\pi * r^4 * X) \quad \textbf{(1)}$$

Mitral valve. To prevent the pump retrograde flow out of the pump, an one-way valve is necessary. A bioprosthetic valve (Perimount, Edward's LifeSciences) was chosen because of it's negligible regurgitation flow and does not vibrate like mechanical valves. This is crucial in producing accurate pressure wave and acquiring proper pressure readings.

Compliance chamber. The healthy human aorta is naturally compliant and allows for some stretching. For this study it was necessary to include the compliance of the healthy aorta into the flow loop. However, measurement of how much the asymmetrical three-dimensional aorta stretches is difficult to quantify. For this study, the compliance measurement was estimated from a mathematical interpretation of the pressure and flow wave of the cardiac cycle.

The type of compliance used for this study was piston compliance, which involved a closed compliance system that does not have a tube. The piston was held down by a metal spring while guided by a metal bar with a through-hole. As pressure was increased, the piston moved up and was forced back by the spring while volume increased. For this flow loop, several springs were available thus providing a range of spring constants from which to choose. The compliance chamber was built with ports to

extract air bubbles trapped in the flow loop, as well as to access the fluid to measure pressure readings.

Because of viscosity, drag, and other effects, compliance can be difficult to calculate. To determine the compliance magnitude the compliance component alone was analyzed independently before testing began under hydrostatic pressure loading. The compliance device was connected with a vertical tube that was filled with water. As the height of the water increased the resultant volume change was recorded. The change in pressure and change in volume information were then used to calculate the compliance value of the component. Compliance was estimated to be 1.5 ml/mmHg, close to the value estimate using physiological data gathered by Liu et al, which was 1.47ml/mmHg. (34)

Preload. Blood enters a human left ventricle with a slightly elevated pressure due to the force of the right heart and the contraction of the left atrium. Thus, the blood can be said to be preloaded upon entry to the left heart. In a normal human, this preloaded pressure is around 15 mmHg. (35) In the study, the effect of preload pressure was added by the height of a water column raised above the system. Gravity was used to generate the water pressure within the flow loop. The usual height of water column during this study was 20 cm of water.

Fluid medium. There were many factors to consider in the choice of a fluid medium inside the flow loop. The fluid had to be optically clear and free of visible particles to allow use of the imaging measurement system. Additionally, the fluid also had to maintain the interstitial fluid balance of the heart valve and neither dehydrate

nor hypo-hydrate the leaflet tissue. Since 90% of the weight of the leaflet is water, this component had to be properly maintained within the valve tissue. Any change could potentially affect the tissue's mechanical properties or geometry by interacting with collagen and other tissue structures. The complicated conditions necessary for testing resulted in the choice of clear saline as the fluid medium. Saline, used often in re-hydrating patients in the hospital, has the correct balance of fluid particle content to maintain the fluid balance in the valve tissue. However, the viscosity of saline is only one-third that of blood, which provided a challenge during experimentation, as fluid resistance was difficult to duplicate.

Flow meter. Measurement of the flow rate was critical during the experimentation. This study incorporated the use of an ultrasonic flow meter (Transonic Inc. USA) to measure the flow rate without interfering in the flow. The unit contains both the source and the detector, angled at 45 degrees with respect to the flow direction. The ultrasound signal from the source bounces off the particles in the flow and returns to the detector, which uses the small change in sound frequency to determine the velocity of the particles. The analog output from the main unit sends information to a data collection unit, the SCXI 1120, to be recorded by LabView. The changes in flow rate were recorded at a frequency of 200 Hz.

Positioning of the flow meter was also an important factor to consider. Since flow was not constant throughout the various components of the flow loop, the flow meter was placed between the compliance chamber and the aortic valve to accurately measure flow through the valve.

Pressure transducers. The human heart works by increasing pressure in a chamber past the pressure of the subsequent chamber so that the outlet valve opens and the contents are pushed out. The muscular structure in the heart is actually composed of a series of layers of muscle wrapped around the open chamber and can thus pressurize the blood without being attached to any structure that might limit contraction. Therefore recording of pressure inside the flow loop was an important task in this study. Pressure sensors were placed before and after the valve. This was important since the differences in the pressure readings determined whether the valve opened or closed. The pressure sensors (Mer 200, Merit Medical Inc., USA) were attached to the ends of catheters that were passed through ports in the flow loop that were sealed around the catheters to prevent leakage. The sensors were then connected to National Instrument's signal conditioner SCXI 1121 to record the analog signal.

Aortic pyrex container. In the human, the aortic valve is above the left ventricle and below the ascending aortic arch. The geometry of the aorta is not a simple cylinder but a complex collection of geometric features, designed by millions of years of evolution. The features on aorta right above the valves are sinuses of valsalva , and their purpose is to facilitate leaflet closing through complicated fluid-solid interactions. In addition, the outward bulges that make up the sinuses prevent the leaflets from contacting the aortic wall, which could damage the delicate and sensitive leaflet. As has already been discussed, the magnitude of compliance available in a tube compliance vessel was not enough to approximate the compliance of the aorta. In addition, the aorta had to be optically clear to allow for measurement of the displacement of the

leaflets with in it. Therefore, the aortic arch used for these experiments was constructed from clear Pyrex, 25mm in diameter, which was then heated and expanded to create the geometry of the sinuses (University of Pittsburgh Glass shop). Each of the three bulges had a volume of 1 milliliter, a length of 10 millimeters, and each was spaced equidistant from the others, centered at 120 degree increments around the circumference of the tube. The result was optically transparent with a smooth surface and provided a perfect view into the aorta. The only remaining difficulty was the optical distortion caused by the complex geometry. The refractive index of Pyrex glass compared to air is 1.4734. (Corning, USA) It was found that this index closely matched that of glycerol (1.4740) so the aorta was placed within a chamber filled with glycerol and the tips of the borescopes used to observe the leaflet were placed within the glycerol. Calibrating the system with small objects of known dimensions within the valve space further minimized the effects of optical distortion.

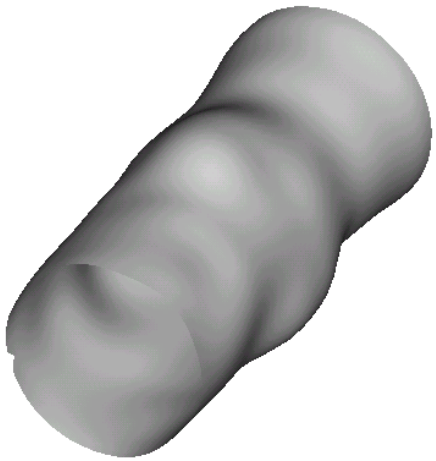

Figure 15 3D surface reconstruction of pyrex aorta used in experiments. The sinuses of valsalva is crucial in achieving accurate fluid dynamic properties.

2.2 Structured Light Imaging

To obtain a three-dimensional view of the heart valve, two CCD cameras were positioned in the same plane and distance from the heart valve but at two different angles (Figure 16, 17). Each camera recorded an image and the LabView program collected the signals. The two two-dimensional images were used to calculate three-dimensional coordinates of the leaflets. Attached to each of the two cameras, borescopes acted as lenses, the tips of which were placed within the glycerol solution near the heart valve. The borescope is a solid glass element that is very narrow at the tip yet it allows a wide field of view, and is often used in minimally invasive surgery. The combination of the borescope and the CCD camera provided the perfect instrument to capture the image of the tissue leaflet (Figure 18, 19).

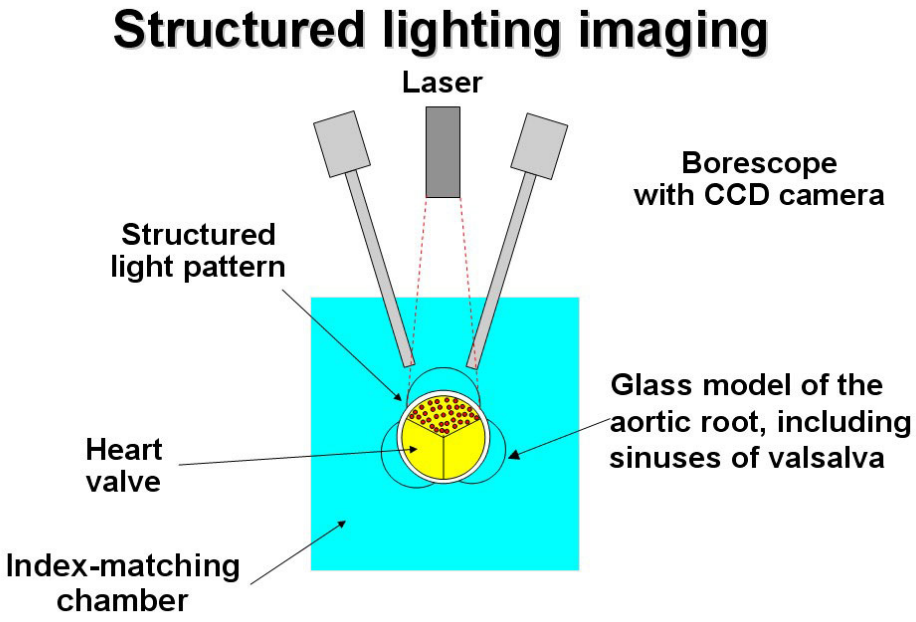

Figure 16 Arrangement of components of structured light imaging around the valve

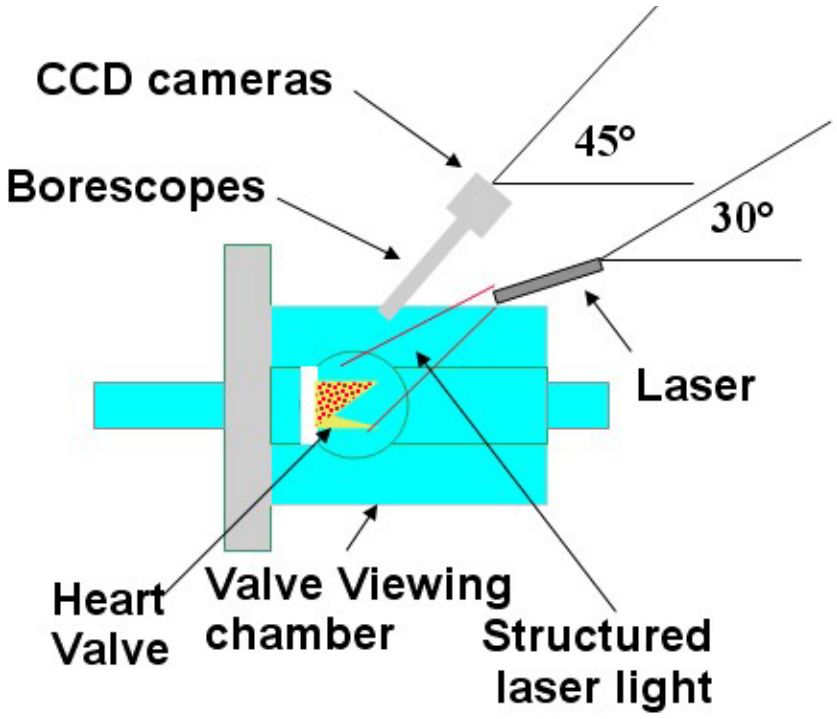

Figure 17 Angling of laser and cameras to provide optimum coverage of imaging space

CCD cameras. The two CCD cameras used were of the same brand (Watec 902C, Inc., USA) and had 380,000 pixels, or 570 TV lines. The minimum light necessary to obtain an image on this camera was 0.02 lux. This low light requirement was necessary as the laser dots to be imaged were on for less than 1 millisecond, which decreased the signal strength by 93%. Additionally, a strobe light source was used to ensure that only an instant of time was recorded at every image. The CCD cameras were arranged in the same plane and at the same distance from the camera to minimize distortion differences. The cameras were secured in their positions with a stainless steel plate of dimensions 1" x 16" x 1/8". The plate was designed to allow the camera spacing to be adjusted when necessary.

Borescopes. The borescopes were the lenses of the cameras. Like a lens, the borescopes gathered light and transferred it into the pixels of the CCD camera. (Figure 11) The tip of the borescope glass element was 4.2 millimeters in diameter and 7 inches in length. An eyepiece on the side allowed for fine focusing and adjustment. The borescope provided a wide 40 degree angle field of view. And from a position very close to the heart valve. The borescope was mounted onto the CCD camera with the use of a c-mount coupler. An outer ring adjusted the distance from the borescope glass element to the CCD of the camera to change the focal length.

Laser. The laser light was generated by a laser unit (Lasiris, Canada) that was coupled to a laser head. The laser head unit received laser from one end and diffracted the single laser beam into a 19 x 19 dot matrix in a square pattern. (Lasiris, Canada) While the observed shape of the valve was not dependent on the pattern, the density of the dots affected the resolution of the data. The angle of projection was 4 degrees and the size of the square pattern was adjustable to fit the size of the leaflet. By changing the distance between the laser and projected surface, the size of the laser dots and the square were changed. The laser could also be focused to change the shape of each dot from a circle to an oval in both axes. Additionally, the rise time, or time necessary for the laser to turn on, was a short 30 nanoseconds, thus allowing very accurate control of the time the laser was on. Thus by turning the laser on and off, a short pulse or strobe was used to illuminate the leaflet surface. The laser strobe was controlled by the LabView program through the SCXI 1121 unit via a simple BNC connector.

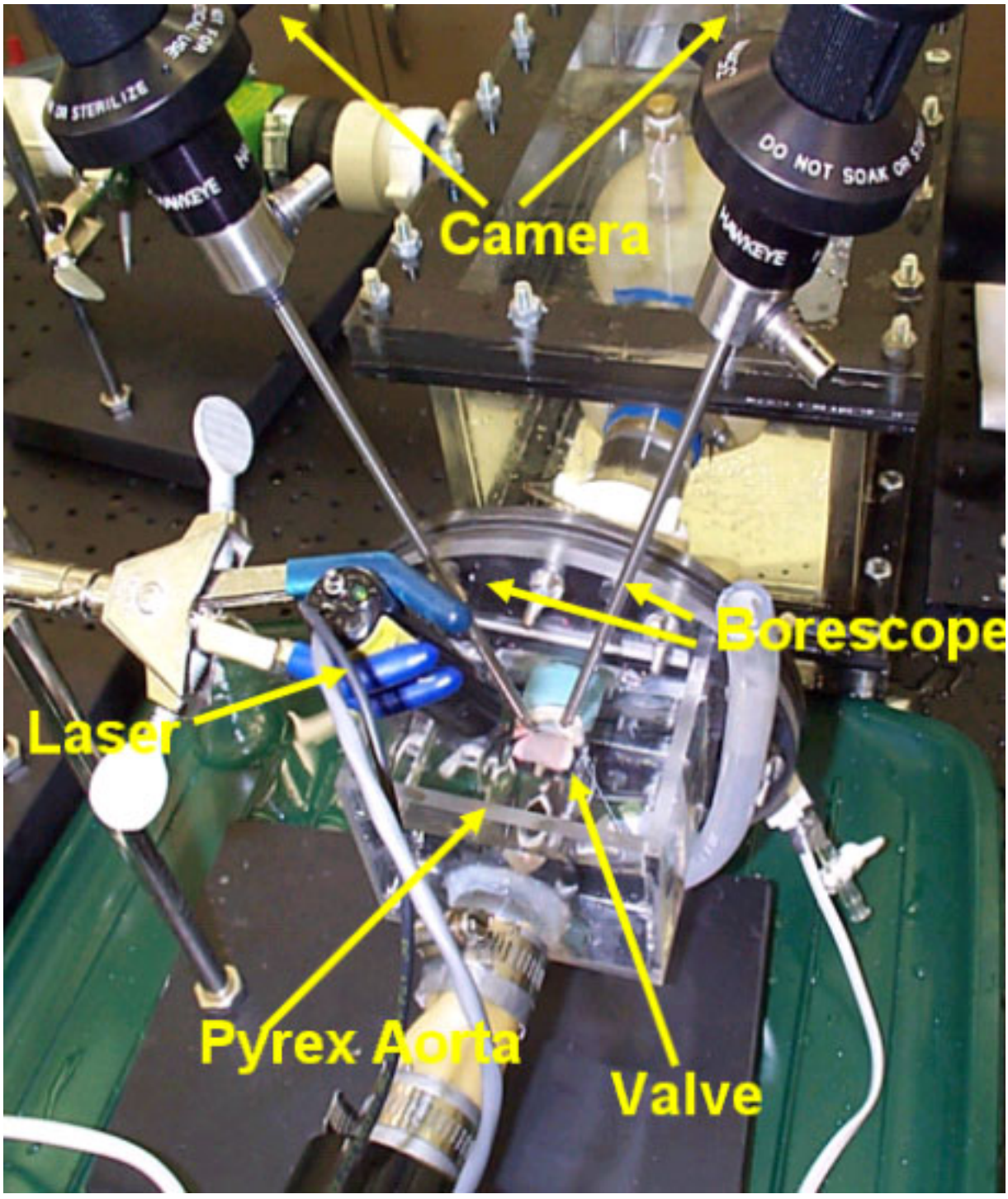

Figure 18 Close-up picture of the laser imaging setup. Both laser and borescope is focused on the same volume of space. The viewing chamber is full of glycerol that decreases distortion.

2.2.1 Frame Grabber

Due to the requirement that the two images be acquired at exactly the same point in time, the frames of each camera had to be captured simultaneously. This requirement necessitated the use of a single frame grabber capable of acquiring data from two cameras at the same time (IC-ASYNC, USA). Each channel was individually programmed yet both cameras shared a common trigger channel so that acquisition was simultaneous. In addition, this same trigger was utilized by the light strobe to coordinate the lighting and image acquisition. (Figure 19) The image acquired by the frame grabber was imported into an image capture program that displayed the views of the two cameras side by side. These screen images were saved and later analyzed using an imaging program (Microsoft PhotoEditor).

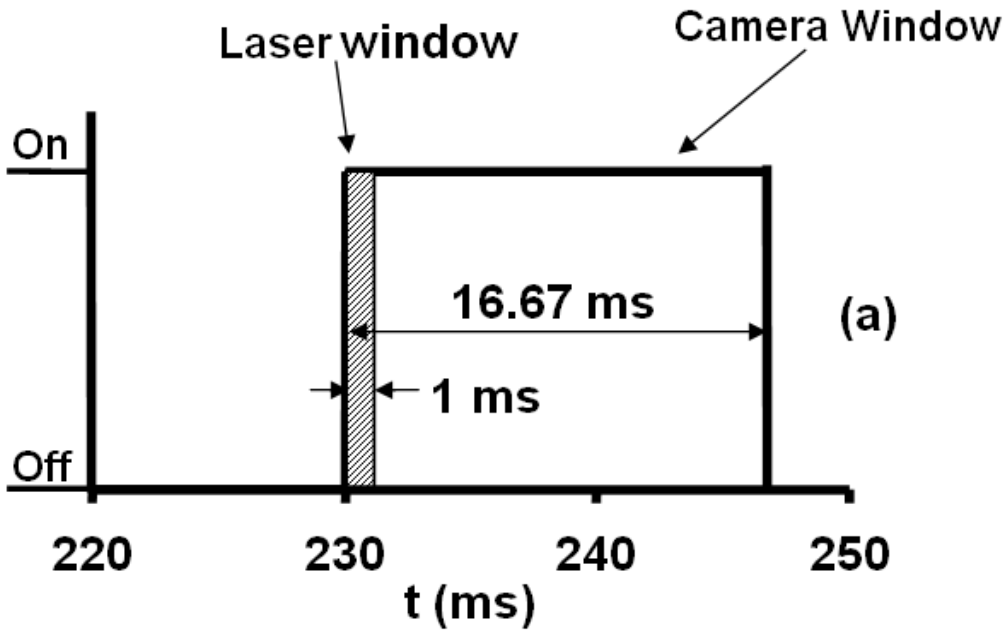

Figure 19 Triggering mechanism to shorten the image acquisition time even if the camera window time is recording at 30 frames per second, interlaced which results in image capture time of 16.67 ms.

2.3 Leaflet 3D Calculation

2.3.1 Digitization

Images captured by CCD cameras were used to calculate 3D locations of laser dots on leaflet surface. The techniques of digitations are as follows

Table 1 List of steps for laser marker digitization to acquire the horizontal and vertical pixel coordinate.

Steps	What is done	Method
1	Image enhancement	Images are contrast and brightness enhanced
2	Laser orientation	Center laser dot is located on Left and Right views
3	Boundary mapping	The boundary of the valve is mapped out
4	Leaflet segmentation	Laser markers are divided by groups using the central laser as a guide
5	Laser deletion	Laser markers not on both view of valve were deleted
6	Laser marker isolation	Lasers not on valve are excised
7	Creating columns	Laser markers are broken into groups to make digitizing more simpler
8	Recording	Each laser markers' horizontal and vertical pixel location is located
9	Verification	If errors from 3D calculation are too high, the process is repeated.

2.3.2 Direct Linear Transform

To calculate the 3D location of objects from two different views, a process termed Direct linear transformation (DLT) was used. DLT takes a calibration phantom with both the pixel coordinate from the two views and 3D coordinate of eight locations of the object (Figure 20). A mathematical formula calculates 11 parameters using the calibration phantom, parameters which describes the location of camera, the angle with respect to each other, focal distance, and etc. These parameters when placed in the original formula forms a set of 4 equations of which pixel coordinates can translate to X, Y, Z coordinates. (Equations 2 ~ 5) To solve for X, Y, Z only 3 equations are necessary

but the 4th equation can be used for error checking. (u,v denotes camera coordinates, subscript denotes camera number; ab…jk denotes camera constants; X, Y, Z denotes real world coordinates)

$$u1 = (aX + bY + cZ + d)/(iX + jY + kZ + 1) \quad \textbf{(2)}$$

$$v1 = (eX + fY + gZ + h)/(iX + jY + kZ + 1) \quad \textbf{(3)}$$

$$u2 = (aX + bY + cZ + d)/(iX + jY + kZ + 1) \quad \textbf{(4)}$$

$$v2 = (eX + fY + gZ + h)/(iX + jY + kZ + 1) \quad \textbf{(5)}$$

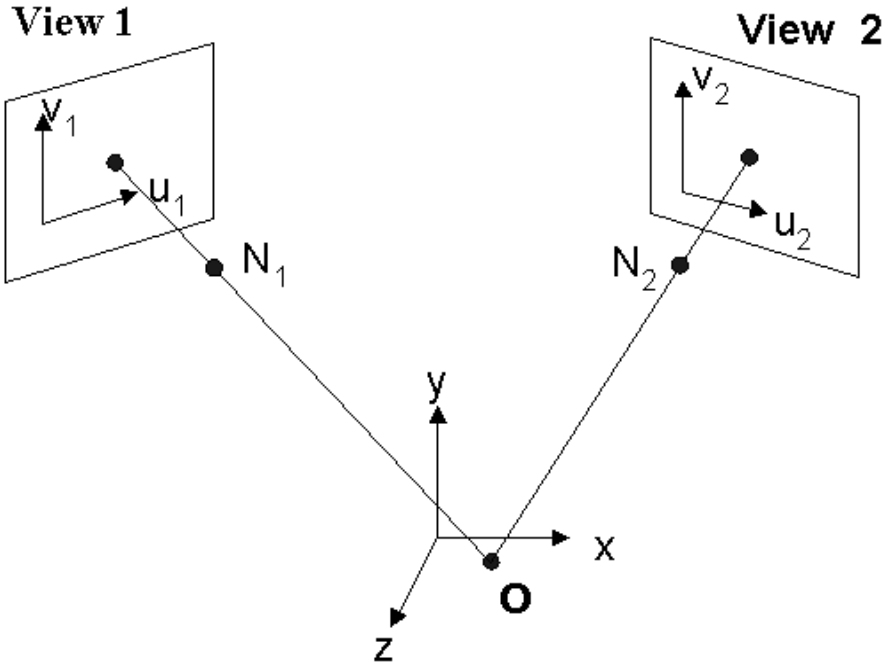

Figure 20 Schematic of how stereography works. To acquire object O's XYZ coordinates, two views, view 1 and view 2, are needed. The horizontal and vertical pixel coordinate, u,v are recorded and inserted into equations above.

Table 2 Table for steps to 3D reconstruction

Steps	What is done	Method
1	Calibration object coordinates recorder	x, y, z coordinates of 12 locations on the calibration object is entered into DLT program
2	Calibration object pixel Left Right coordinates	Pixel coordinates of the 12 calibration location on the calibration object is inserted into DLT
3	Create matrix	A matrix using calibration coordinates and pixel location is created
4	Calculate calibration parameters	LU decomposition is used to solve for parameters a ~ k from the matrix
5	Calibration parameters	Calibration coordinates are inserted into equations 2 ~ 5
6	Input of laser marker pixels	Laser markers' pixel location are inserted into equation 2 ~ 4
7	Calculate 3D coordinate of laser markers	Using three of the four pixel coordinates of laser marker, the three unknowns, XYZ are solved
8	Error detection	Using calculated XYZ coordinates, the error is detected by inserting into equation 5 to calculate deviation from fourth pixel coordinates

2.3.3 Camera Positioning

Camera positioning and angling with respect to one another was not recorded during the experiment. This step was not necessary as the calibration process negates the need to estimate 3D coordinates by calculating camera distances. The calculation of 3D coordinates of laser markers using DLT is much easier and accurate.

One of the concerns of the method was the angle between the two cameras was not at an optimal 90 degrees orthogonal to each other. The cameras line of sight was 60 degrees to each other and this positioning was the maximum allowed without losing sight of laser markers due to the complex leaflet geometries. While this was not the optimal camera angle, we have done validation testing which showed spatial accuracy

of 115 ± 35 µm and curvature accuracy of 97%. Considering the valve was 15000 µm across and number of pixel in that length was 400 meant each pixel represented 62.5 µm in length, we felt the technique was close to the technical limit at the time of the test.

2.3.4 Surface Mesh Construction

The 3D location of laser dots by themselves does not provide the necessary information about the leaflet surface. It is only the location of where the laser hits the valve leaflet. A surface mesh has to be constructed from the data using a method published by Shimada et al (36), this software forms ellipsoids through anisotropic triangulation, with the centers of ellipsoids connected using anisotropic Delaunary triangulations to construct a triangular mesh. The resulting 3D triangular mesh elements form the surface of the leaflet.

2.3.5 Curvature Calculation

The core focus of this study lies in the change of geometrical differences between native and stiffened leaflet. Or more specifically, how the surface bends or curvature changes. Curvature is the measurement of the amount of bending around a certain point. Curvature is measured linearly, as such curvature values for a surface can differ depending on the orientation and direction the quantity is measured. Thus the common convention is to divide curvature as two separate quantities; major and minor curvature.

Once the surface meshes were generated for each time point, surface curvatures were determined using local surface patch methods described in (37). The method incorporates a single bi-quadric surface that can calculate local major and minor

curvatures. For each data point, its surrounding data points were fitted with a local surface S. The surface S is a function of two vectors, u and v, with constants to describe the curvatures. Vectors u and v, is pointing in the direction of major and minor curvature and are orthogonal to each other. (Figure 21) To calculate curvature values, constants a, b, and c are fitted to local surface S using regression calculations.

$$S(u,v) = au^2 + 2buv + cv^2 \quad (6)$$

Once a, b, and c is calculated a, b, and c are inserted into equation 7 to calculate major (k_1) and minor (k_2) principle curvatures. Major and minor curvatures are the largest and smallest magnitude of curvature at the location of data point. In addition, the two curvature components are orthogonal to each other.

$$k_1 = a + c + \sqrt{(a-c)^2 + 4b^2}$$
$$k_2 = a + c - \sqrt{(a-c)^2 + 4b^2} \quad (7)$$

The number of data points contained in the local fitted surface S ranged from 10 – 40, with the average being 25 data points. It should be noted that our choice for the local coordinate system resulted in positive signed values for k_1 and k_2 when the valve was fully closed. That is, when the leaflet surface was concave with respect to the imaging system.

While major curvature is greater than minor curvature, minor curvature could bend more severely than major curvature. This is because curvature properties have directional and magnitude properties. The curvature in same direction as the normal vector is considered positive, those away from is negative. Thus the two curvature components in Figure 22 are both negative. The normal vector n is normal to fibrosa layer, thus the vector is pointing out of the aorta. Thus curvature values would tend to be positive when valve is closed, assuming the cusp is in a bowl like shape. Though $k_1 > k_2$, k_2 can be more highly curved. As k_1 is the more positive parameter, k_1 can be a positive mostly flat surface while k_2 is a negatively bent surface. Then the k_2 would be larger in terms of magnitude.

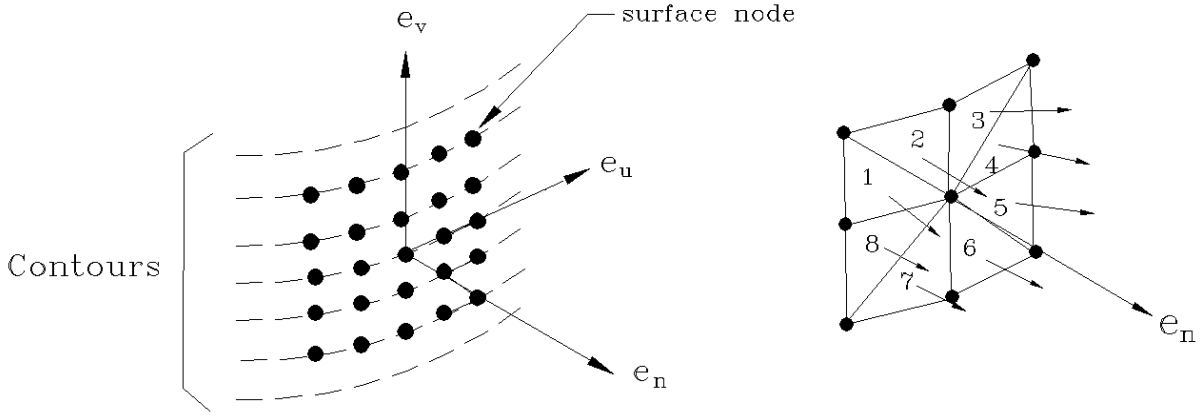

Figure 21 Nodes on leaflet is fitted to surface. Normal vector is calculated by averaging the normal vectors from each mesh triangle. Local coordinates e_u, e_v, e_n is fitted with e_n being the normal vector. e_u, e_v was fitted so that e_u is the vector for major curvature and e_v is vector for minor curvature. All three vectors are orthogonal to each other.

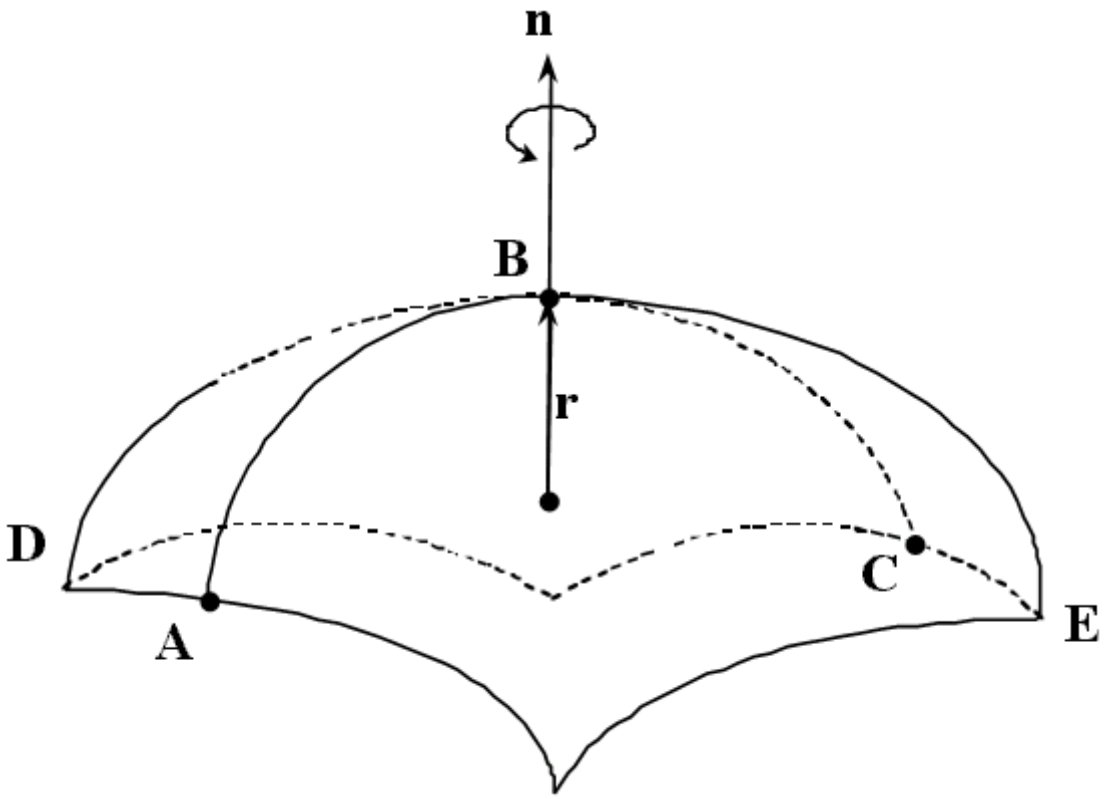

Figure 22 Figure denoting measurement of curvature of a particular surface at point B. Vector n denotes the normal vector normal to the surface. At point b, curvature is the inverse of radius r that best fits the surface. A-B-C denotes primary curvature direction for one measurement and D-B-E denotes primary curvature direction for the other measurement. The two are orthogonal in direction to one another.

2.4 Valve Preparation

Native porcine heart valves, were tested both in their natural, untreated state, and then again after chemical modification identical to that used by heart valve manufacturers.

Valve harvesting. Five pig heart valves were used for this study. After each pig was sacrificed at an abattoir, the heart was removed and refrigerated until chilled and then express-shipped to the laboratory in cold saline with ice packs carefully positioned

to avoid any tissue freezing damage. When the hearts arrived, no chemicals had yet been applied to the heart or the valves. The aortic valve was carefully dissected from the heart with portions of the aorta attached. The valve was stored in a saline solution and rapidly frozen to –30 degrees Celsius until needed. The valves were prepared by first defrosting them in cold running water and then the aorta was further trimmed to 25 millimeters. The non-coronary leaflet was identified and marked with a suture knot at the base. The base of the aorta was trimmed and flattened and extra connective tissue was excised so that the final valve was cylindrical. Many more valves were prepared than were used because only valves that were 25 millimeters in diameter were tested as this was the optimum for the device and the average size for an adult male prosthesis.

A metal stent from a medical porcine bioprosthetic heart valve was attached to the aorta with six interrupted surgical sutures. Three sutures were placed on outer surface of aorta near the three commissures where the valve leaflets come together at the aortic wall and three sutures were placed at the base and center of the leaflet. The sinuses were trimmed away leaving one millimeter of space to preserve the fiber structure that attaches the leaflet to the wall. The excision into the sinus was closely matched to the shape of the metal stent. Then the remaining portion of the sinus was sutured onto the metal stent.

Valve mounting. In order to mount the prepared valve into the piece of Pyrex glass aorta, it was first sutured onto a circular ring made from Tygon tubing (Tygon, USA). The ring was then pressure fitted into the Pyrex aorta. Friction kept the Tygon ring securely in place during high velocity flows and pressure gradient differences.

Valve installation. Once the valve was prepared and sutured in place it was inserted into the flow loop. The viewing chamber was secured onto the optical table to prevent any motion. The flow loop was primed with saline and the viewing chamber filled with glycerol. As the viscosity of glycerol tended to trap air bubbles, the glycerol was allowed to rest for at least one hour or until all air bubbles were removed.

2.5 Testing Protocol

2.5.1 Setup

Setup began by powering up the entire testing apparatus. All electronic devices were allowed the warm-up period specified by their documentation. The tips of the borescopes were immersed in glycerol and their positions were verified by viewing the image displayed on the computer monitor. Then the laser device head was positioned so that the entire leaflet was covered with laser dots. The pump was actuated manually to verify that the projected light grid stayed on the leaflet. During this procedure the pattern head was removed from the laser, focused using an adjusting knob, and reattached if needed.

A calibration object was then used to establish three-dimensional coordinates of a known geometry. This was accomplished by placing the calibration object in the volume of space to be occupied by the valve. The object, attached to a heavy-gauge stainless steel wire, was manipulated from a port attached to the compliance chamber. The wire was pushed into the flow loop, thus moving upstream towards the valve, and

positioned on top of the closed leaflet. Approximately 10 images were collected of the calibration object at various orientations and at different light settings as may be necessary during post processing.

The flow loop was always set up with normal physiological parameters, including 60 cycles per minute, 120 mmHg pressures at systole, 80 mmHg pressures at diastole, and a cardiac output of 5 liters per minute. To produce these parameters, the water level in the reservoir was adjusted to allow for the preloaded pressure and the four control knobs on the amplifier were turned to adjust the voltage output.

Additional parameters were changed as required by the specific protocol. The LabView program collected data from SCXI 1121 at 200 Hz. While the flow loop is operational, the laser and cameras strobe and trigger at precise moments during the cardiac cycle to capture the valve function at particular moments. The times examined are shown in Table 2 and Figure 23. These time periods were chosen because the majority of valve leaflet motion occurs during opening (300 – 360 milliseconds) and closing (600 – 660 milliseconds). Six to eight images were acquired for each time period.

Table 3 Frame number, Time frame, with corresponding phase of cardiac cycle

Frame	Time (ms)	Phase
1	0	Closed
2	200	Closed
3	250	Closed
4	300	Opening
5	310	Opening
6	320	Opening
7	330	Opening
8	340	Opening
9	350	Open
10	360	Open
11	400	Open
12	450	Open
13	500	Open
14	550	Open
15	600	Open
16	610	Closing
17	620	Closing
18	630	Closing
19	640	Closing
20	650	Closing
21	660	Closed
22	700	Closed
23	750	Closed
24	800	Closed

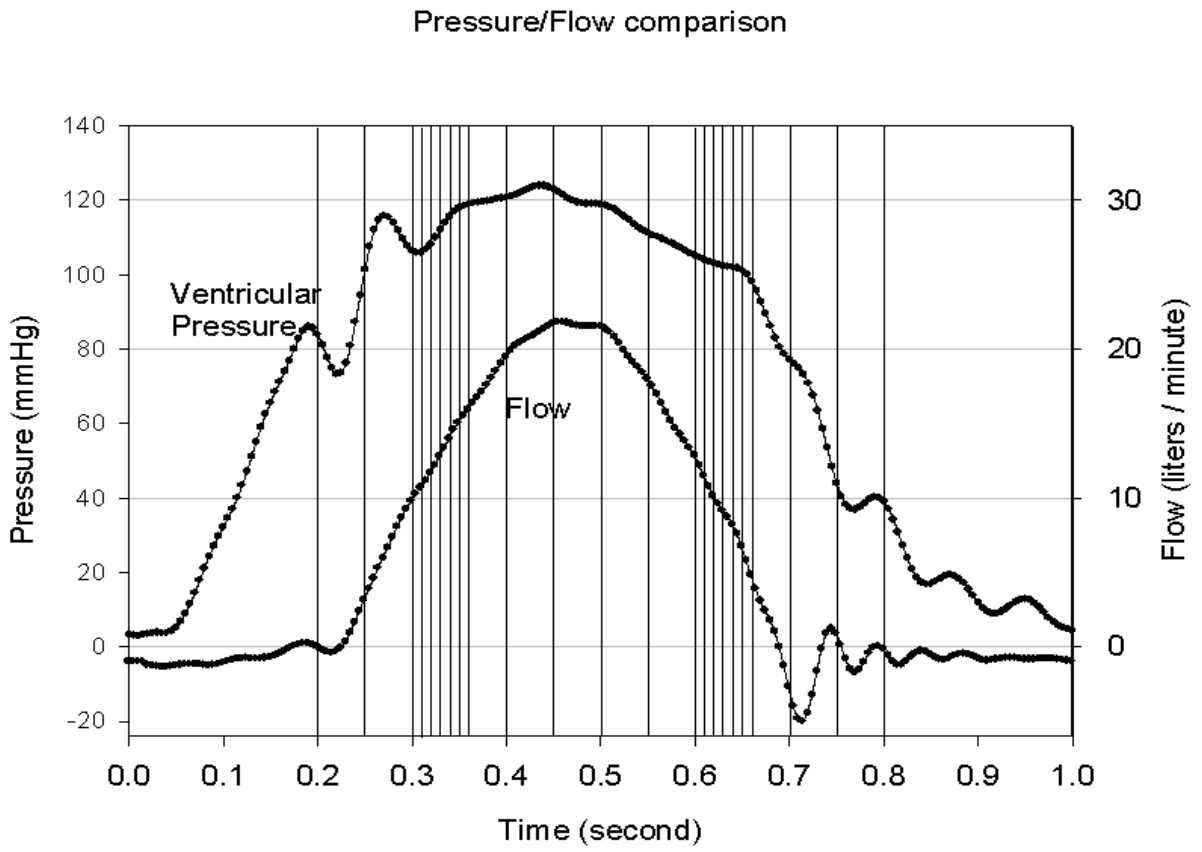

Figure 23 Plot of ventricular pressure and flow waveform recorded from the physiological flow loop. Horizontal bars indicate time points where surface was scanned.

2.5.2 Leaflet Stiffening

Once the valve was tested in its native state, it was then chemically modified. The flow loop was drained of the fluid medium, the glycerol was emptied from the viewing chamber, and the entire Pyrex tube containing the valve and the viewing chamber were placed vertically over a small tub. A glutaraldehyde solution of 0.625% concentration by volume in physiological saline was pumped onto the closed valve and drained into the tub. (38) The speed of the pump was adjusted so the rate of leakage through the valve was equal to that of the transfer into Pyrex aorta. The height of the glutaraldehyde solution column above the valve was maintained at 6 – 10 centimeters to allow for a chemical modification pressure of 4 to 6 mmHg. Chemical modification continued for 24 hours and was checked constantly to maintain the desired chemical modification pressure.

After the 24hr period, the viewing chamber was gently washed with water to remove the glutaraldehyde solution. Then the viewing chamber was then placed back into the flow loop and the flow loop and viewing chamber were filled. The settings were not changed from the native test and the experiment was repeated identically.

2.5.3 Length and Area Measurements

Dimensional measurements of leaflets indicated the physiological change that occurred during the cardiac cycle. Lengths measurements were recorded using Tecplot (Amtec Engineering, USA) which allows measurement of distance over surface from information generated from the mesh data. Thus lengths measured are true surface distance rather than inter-marker distance, unlike other studies done before.

Marker 3D location and mesh data were used to calculate area. Triangular mesh information combined with marker 3D data allowed calculation of surface area for each triangle in the mesh. Two vectors with a common end point were determined and the area between the two vectors was calculated using cross product and then divided by two. The sum of each triangle surface area was the surface area for entire surface.

2.5.4 Statistical Methods

Distances and area results were compared using one-way ANOVA. This statistical method was chosen as it took into account the error of other data sample. Thus one-way ANOVA was seen as a more comprehensive statistical method than a simple student's t-test.

3.0 RESULTS

3.1 Fluid Mechanical Performance of Flow Loop

3.1.1 Pressure/Flow Conditions

The recorded pressure and flow waveform are presented in Figure 24. The recording starts with the valve closed and covers one cycle. Details on phases of valve opening are shown in Table 3. Comparison of native and stiffened leaflets pressure and flow waveforms indicated that both were nearly identical Figure. The waveform pattern demonstrated consistent flow conditions between native and stiffened states.

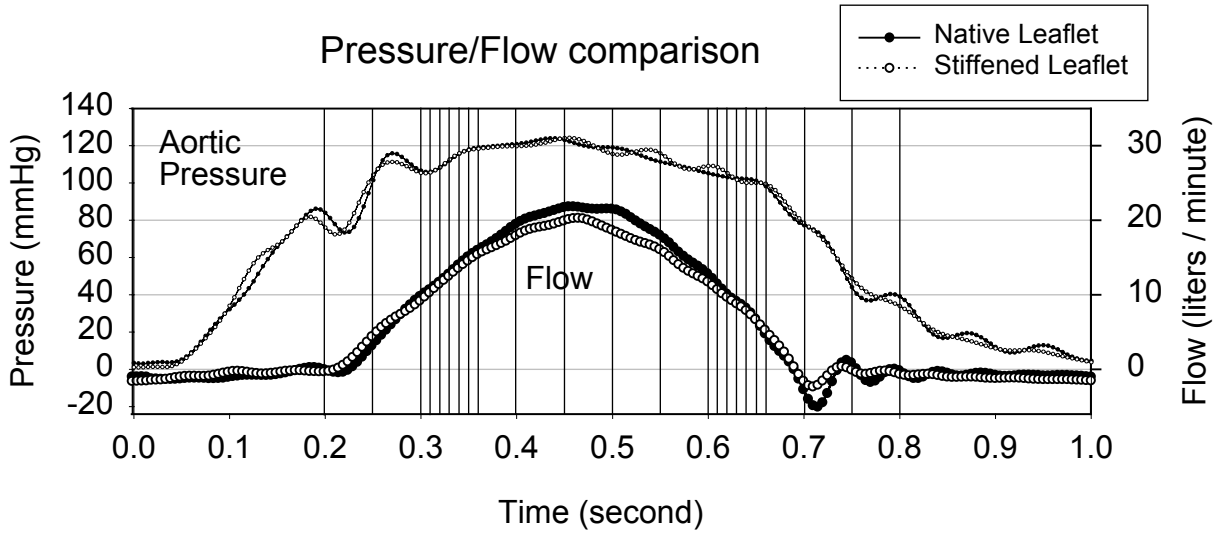

Figure 24 Generated flow pattern recorded from flow loop. Vertical lines indication time points of valve analyzed. $r^2 > 0.98$ using Pearson correlation.

3.2 Pericardial Valves

To demonstrate the feasibility and authentic reproducibility of the structured-light imaging system, we scanned a bovine pericardial valve. (Figure 25) A medical bovine pericardial valve was imaged at several time points of cardiac cycle and plotted in the same graph. To show the repeatability of the flow loop and imaging method, two images from same time point in different cycles were taken, imaged, and analyzed. (Figure 26) When the surfaces were overlaid on each other, they were nearly identical. This is only possible because of the repeatability of the flow loop and the accuracy of 3D imaging system.

We also found an interesting characteristic of pericardial valve leaflet. (Figure 27) These images were created by plotting certain segments of pericardial leaflet on the same image frame. Different color was assigned in addition to the gouraud shading to differentiate the different leaflets. The opening and closing geometrical shapes were distinctively different. When it opens, it is bended toward the center of the valve until it is fully open. When it closes, the leaflet is bent away from the valve until it finally closes. This indicated how complicated the mechanism of opening and closing of the simpler pericardial valve was, and how accurate we had to be with aortic valves.

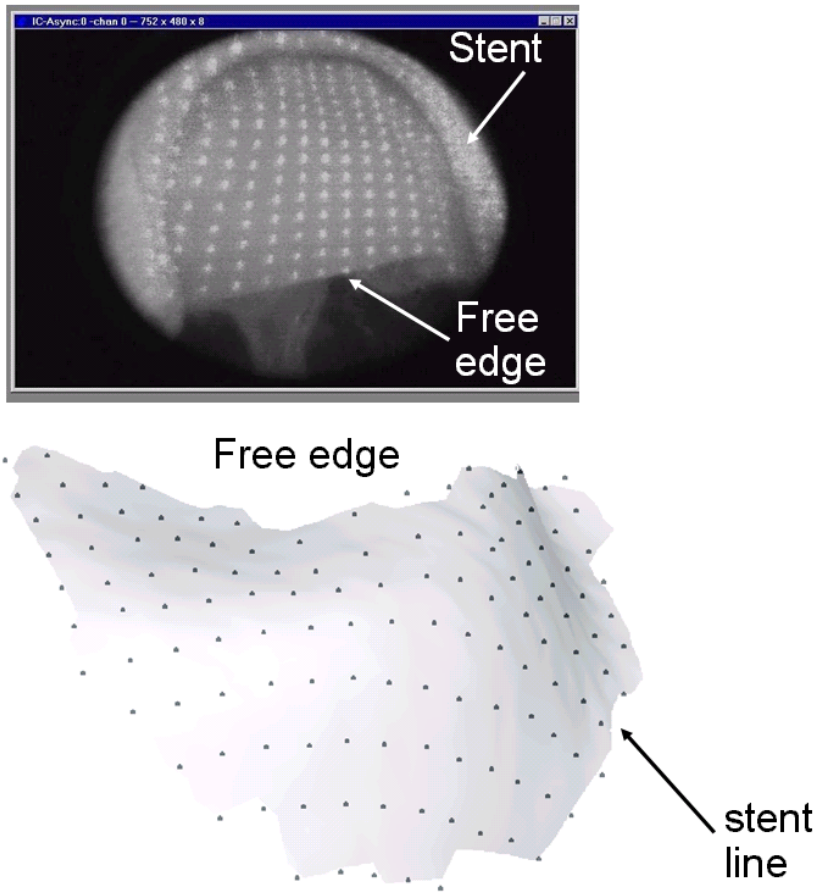

Figure 25 Picture of pericardial valve captured by left camera. Lower picture is resultant 3D valve leaflet with laser dots displayed together. Free edge and border with stent is manually defined by surface of leaflet that was digitizable.

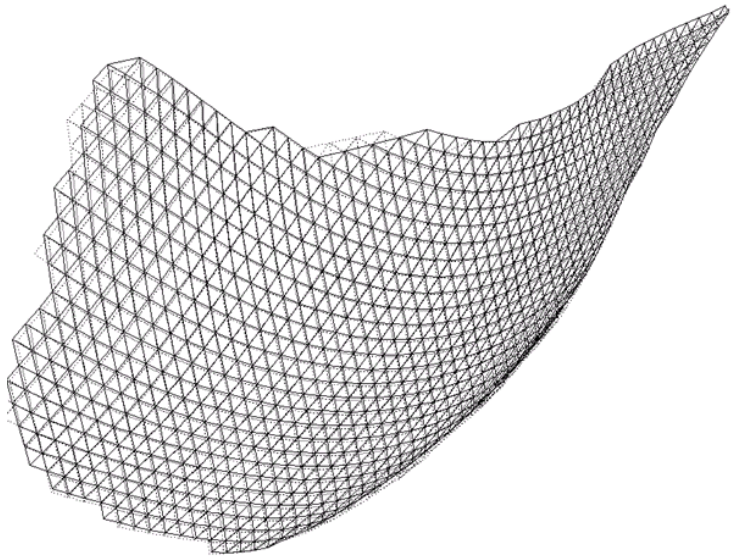

Figure 26 Two surfaces imaged by structured-light imaging overlaid on each other. The two surfaces are near identical occupying the same space. Free edge and border with stent is manually defined by surface of leaflet that was digitizable.

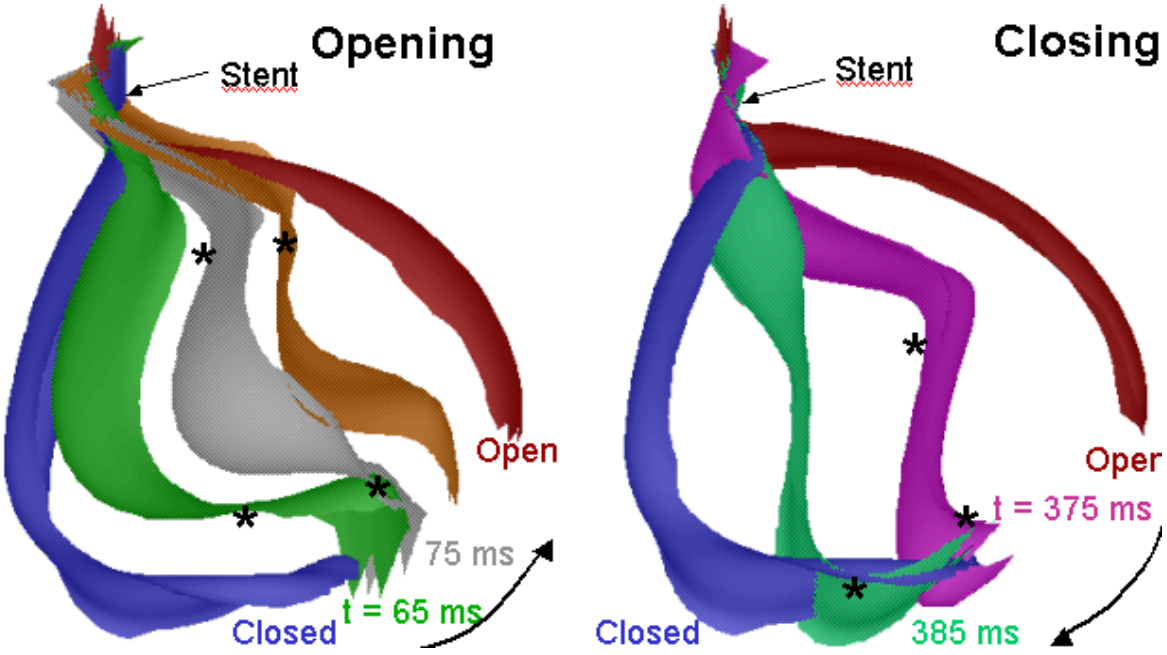

Figure 27 Sequence image of axial view of bovine pericardial valve's leaflet position and surface during valve opening and closing. Only the middle section of leaflet is shown to present multiple slices on the same frame. * denotes locations of high bending

3.3 Porcine Aortic Valve Images

Structured laser-light imaging system was able to successfully capture the leaflet surfaces at multiple time points over the cardiac cycle (Figure 28). Each frame contained an average of 140 laser dots, ranging from 90 to 190 due to the varying leaflet geometry and size. We found an exposure time in the range of 0.5 ~ 1 ms was short enough to eliminate blurring and capture valve motion. Due to the geometry of the aortic valve when it is closed, the imaging system was unable to capture a region estimated to be around 1 x 5 mm^2, which is roughly around 2% of leaflet area. This area near the basal attachment region was out of view when valve was closed and pressurized. Including closed valves' radial lengths in analysis would distort the comparison, thus radial length was compared using opening state as a base when entire leaflet is visible and no trans-valvular pressure was applied. Native valve was observed to distend significantly during fully open. Thus the borescope needs to be positioned to allow for this change.

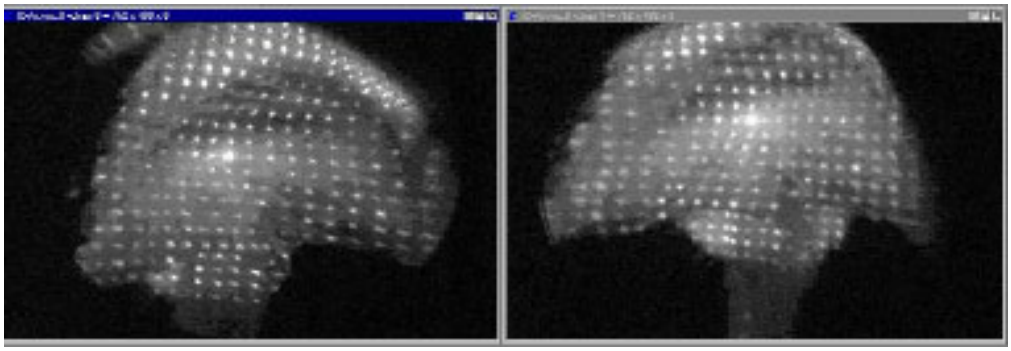

Figure 28 Image of Native Valve when closed with laser dots. Free edge is facing towards the bottom

3.4 Meshing and Curvature Calculations

Meshing and curvature calculations were accomplished by methods mentioned previously. Triangular elements to construct the mesh ranged from 150 ~ 280 elements. The curvature measurements were calculated using bi-quadric surface patch program developed by our lab that measured the fitted surfaces' major and minor curvatures.

As the valve opens, the leaflets shift from a predominately positive sign curvature to negative, so that k_2 was consistently the principal curvature component with greater magnitude. Since the major changes in surface curvature as valve opens were of major interest, we focus our graphical presentations on k_2.

3.5 Native Valve Results

3.5.1 General Leaflet Geometric Changes

Overall, we observed that the aortic leaflet underwent complex geometrical changes over the cardiac cycle (Figure 29). When the valve was closed, the shape of leaflet resembled a smooth, bowl shaped surface. As the valve opened it went thru complex geometric shape changes, often hyperbolic (i.e. saddle shaped) in the belly region. When fully opened, the shape of the leaflet continued to shift, presumably due to variations in local flow.

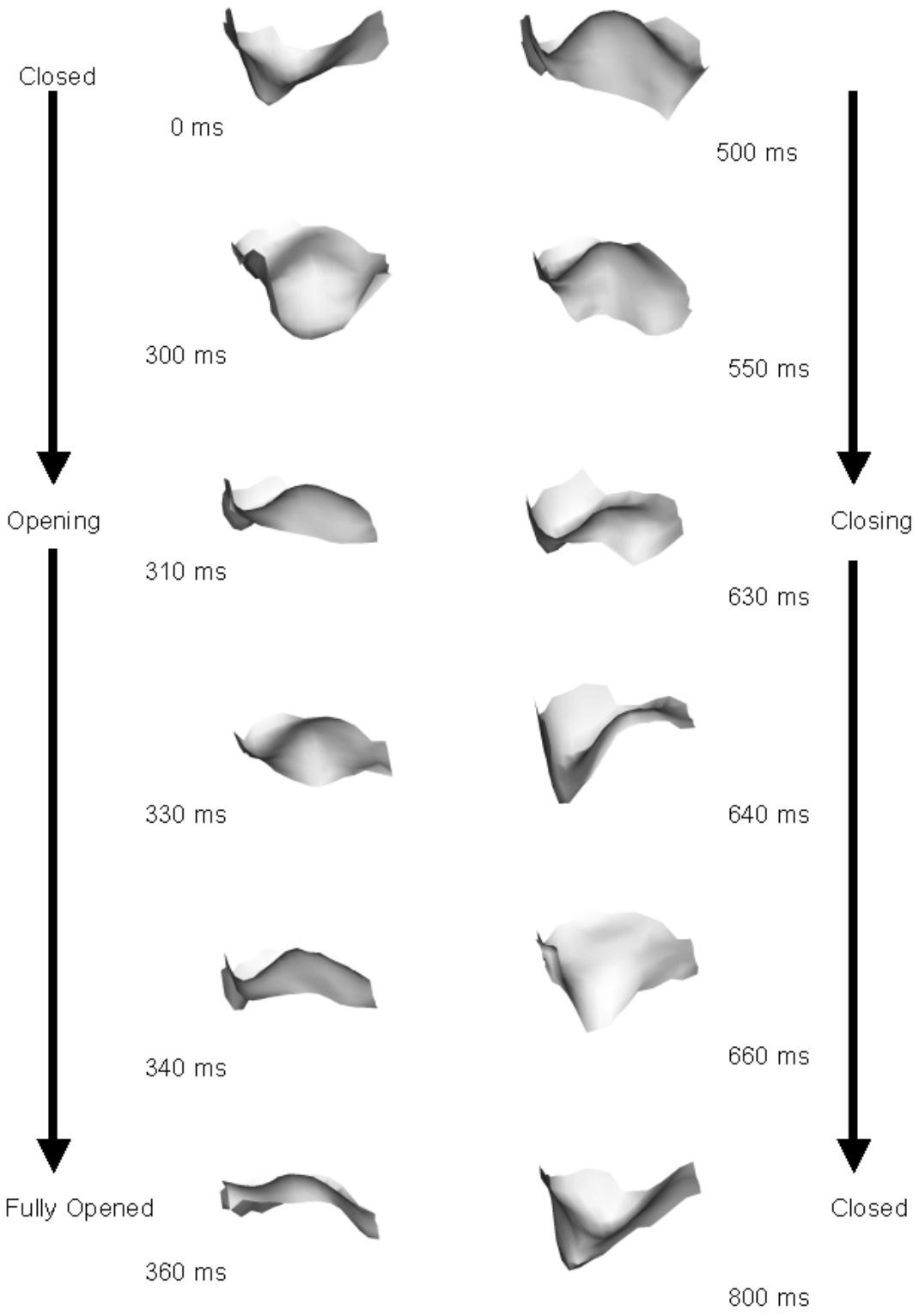

Figure 29 Sequence of shaded surface of native leaflet going through opening-open-closing cycle. View is axial view, looking into the flow. Surface is using gouraud shading with arbitrary lighting.

3.5.2 Uni-dimensional and Areal Measurements

Substantial length and areal changes were observed over the cardiac cycle (Figure 30 ~ 32). Lengths were measured using Tecplot (Amtec Engineering, USA) which allows measurement of lengths on surface generated from the mesh information. Thus lengths measured are true surface distance rather than inter-marker distance. Radial lengths increased by 30% when fully opened compared to when the valve was unloaded. Similarly, leaflet area increased by 25% when the valve is fully opened and subjected to maximum forward flow. When comparing length in radial and circumferential directions, the leaflet was less distensible in the circumferential direction, which decreased a statistically insignificant amount in length when fully open. In addition, the differences in distensibility between the free edge and circumferential lengths at maximum flow, where the free edge increases while the circumferential decreases, suggests the free edge region is more elastic than circumferential region. This result combined with radial length increase suggests the free edge of the leaflet is very distensible in the radial direction (Figure 32).

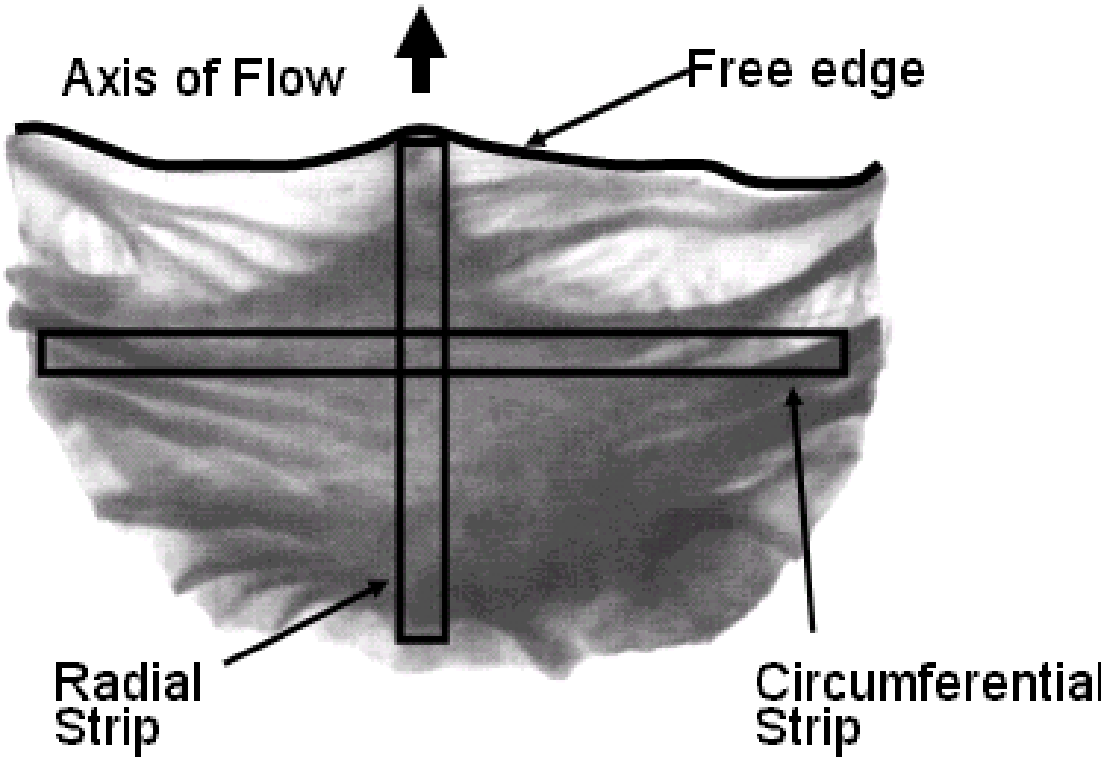

Figure 30 Locations where the length measurements were taken.

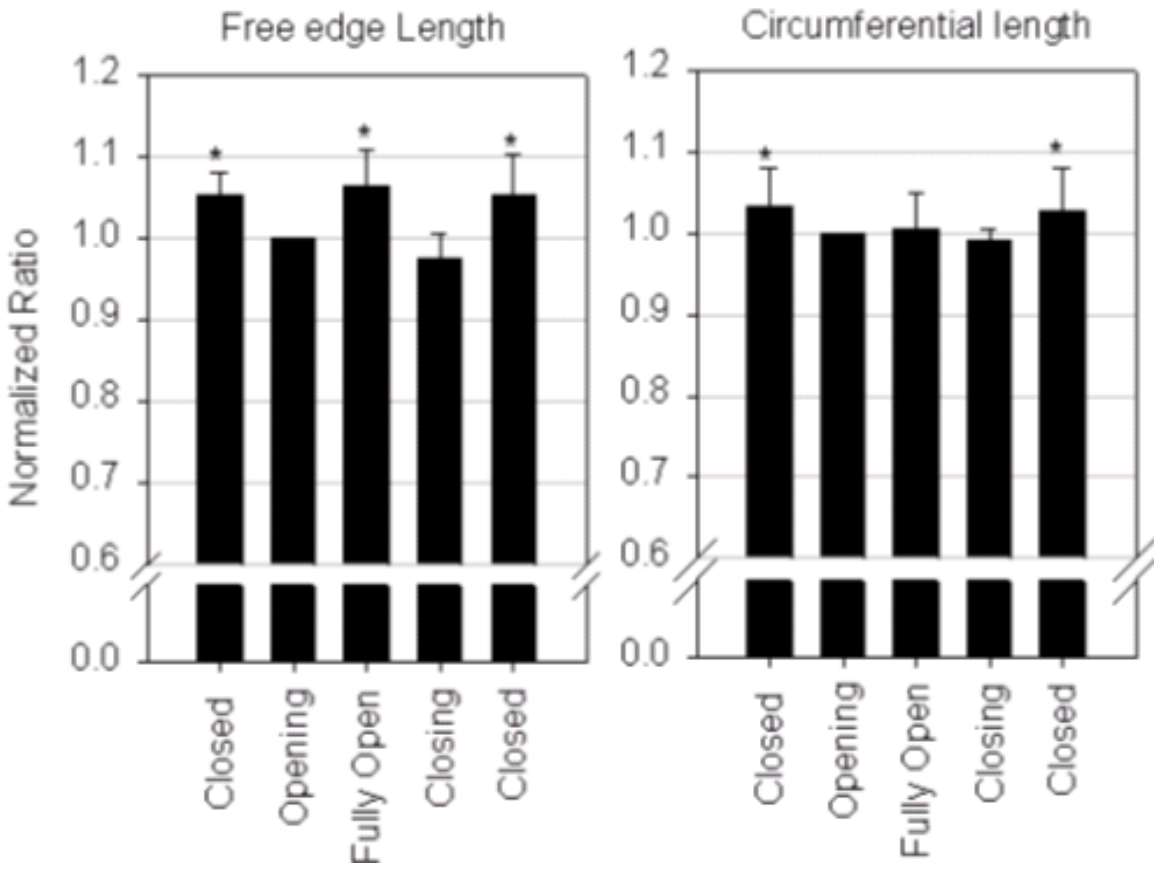

Figure 31 Graph on left is the relative length of leaflet across taken at free edge. Lengths are normalized with respect to when it is opening. The symbol indicates lengths that are statistically significant with respect to the length of leaflet when it is opening. Graph on right is the relative length of leaflet along the circumferential strip. Unlike the free edge, the length decreases slightly when it is open. * denotes statistically different compared to closed phase, $p < 0.05$ using one-way ANOVA

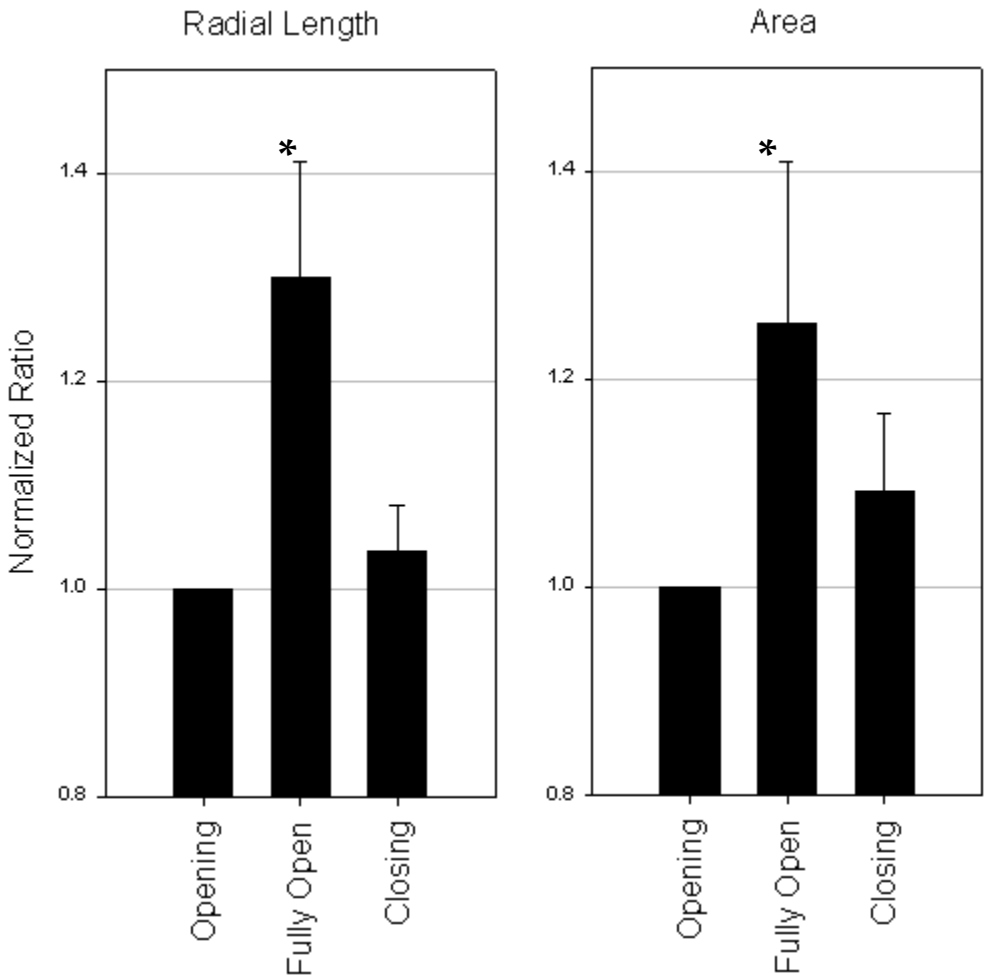

Figure 32 Graph on left is the length of leaflet in radial direction during three key phases. When flow velocity is at maximum, the valve length increases an average of 30%. Lengths during fully closed were omitted due to difficulty scanning the entire leaflet. Graph on right is the area comparison between opening, fully open, and closing. * denotes the statistically different compared to opening, $p < 0.05$ using one-way ANOVA

3.5.3 Circumferential Cross-sectional of the Native Leaflet

To more clearly present the complex changes in leaflet geometry, cross-sectional geometries were generated along the free edge and circumferential directions (Figure 33). The cross-sectional images clearly demonstrated a smooth sequential opening. It was also observed that the location of highest bending occurred to the sides of the valve rather than in the middle. In addition, the leaflet location that started to open was the circumferential region, which was one step ahead of the free edge. The behavior when closing was significantly different from opening, as both the free edge and circumferential region began closing simultaneously. Also the leaflet closing behavior was not as smooth and sequential as the opening behavior.

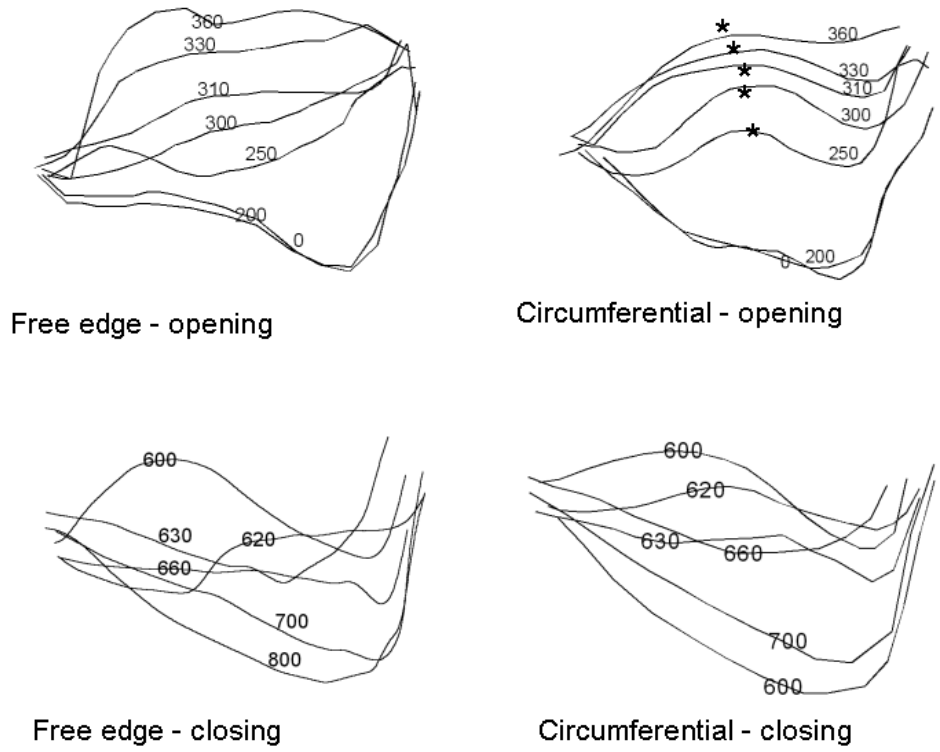

Figure 33 Cross sectional view of the native leaflet at two positions, circumferential and free edge. * denotes location of nodulus and relatively flat.. The native leaflet undergoes a smooth and sequential opening and opened from the belly region. Where as during closing the free edge and circumferential region closed together.

3.5.4 Native Leaflet Surface Curvature

As the valve opens, the leaflets shifted from predominately positive signed principal curvatures to negative, so that k_2 was consistently the principal curvature component with greater magnitude. Since the largest changes in surface curvature as the valve opens were of major interest, we focused analyses on k_2. The results for k_2 along with the corresponding isometric view for a representative valve are presented in Figure 34. Here, focal regions of high curvature were observed, but did not persist in any one location. This result further underscores the highly dynamic motion of the leaflet.

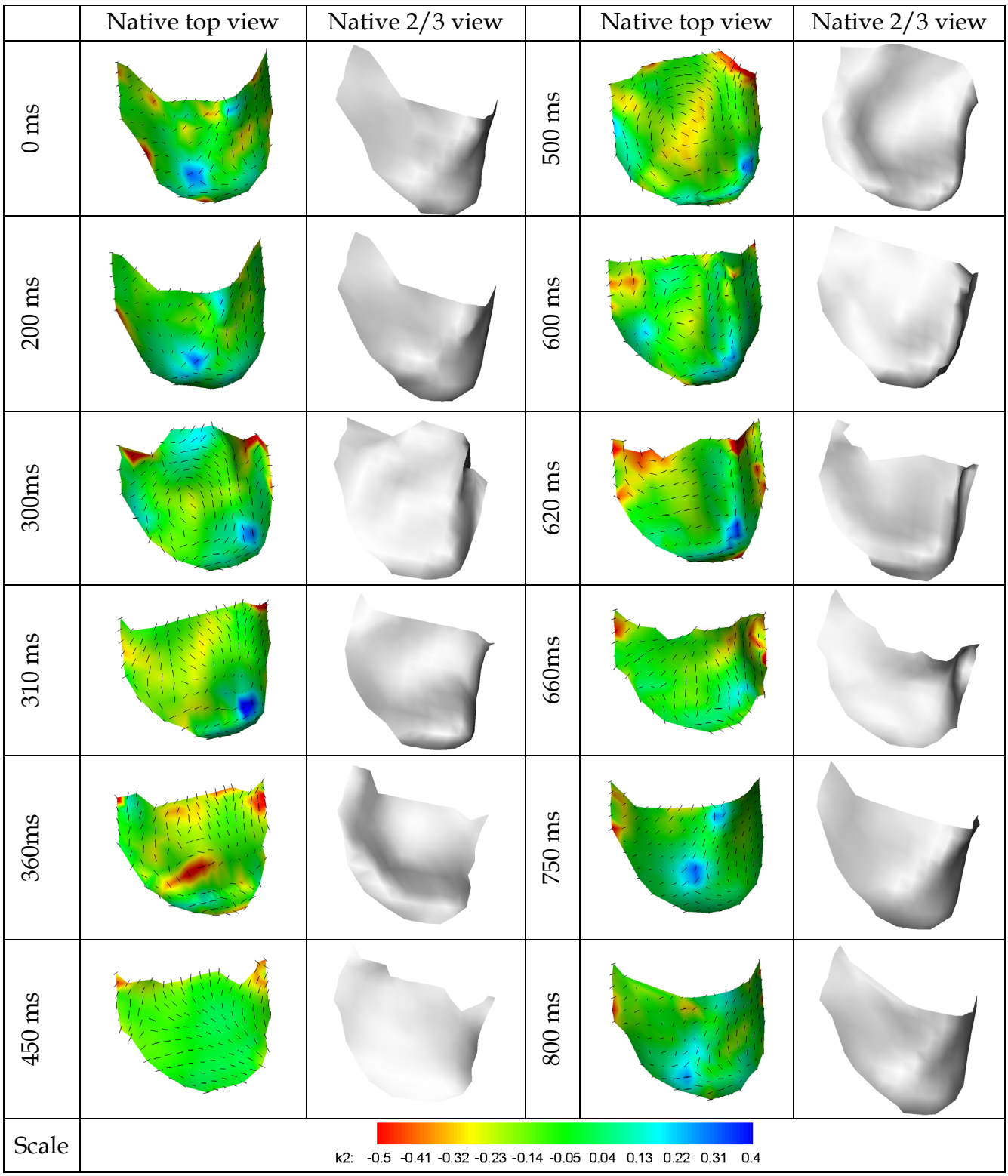

Figure 34 Figure showing minor curvature contour alongside gouraud shaded surface from an isometric view. Lines on contour indicate direction of minor curvature bending on valve surface.

3.5.5 Truncated Curvature Plot

To isolate locations of high bending, regions of the leaflet with $|k_2| \geq 0.5$ mm^{-1} were identified and plotted (Figure 35). This value was chosen as it is the upper 5% of the k_2 values observed in the present study, and thus represent regions of high bending. Small regions of the leaflet were shown to have high minor curvature and present only when the valve was open. In addition, the location of high curvature shifts in location and direction through the cardiac cycle. Some of these locations are located at the free edge and side edges of the leaflet. This indicates the native leaflet is not prevented from experiencing severe bending, but bending deformations are short in duration and constantly shift in location during the cardiac cycle.

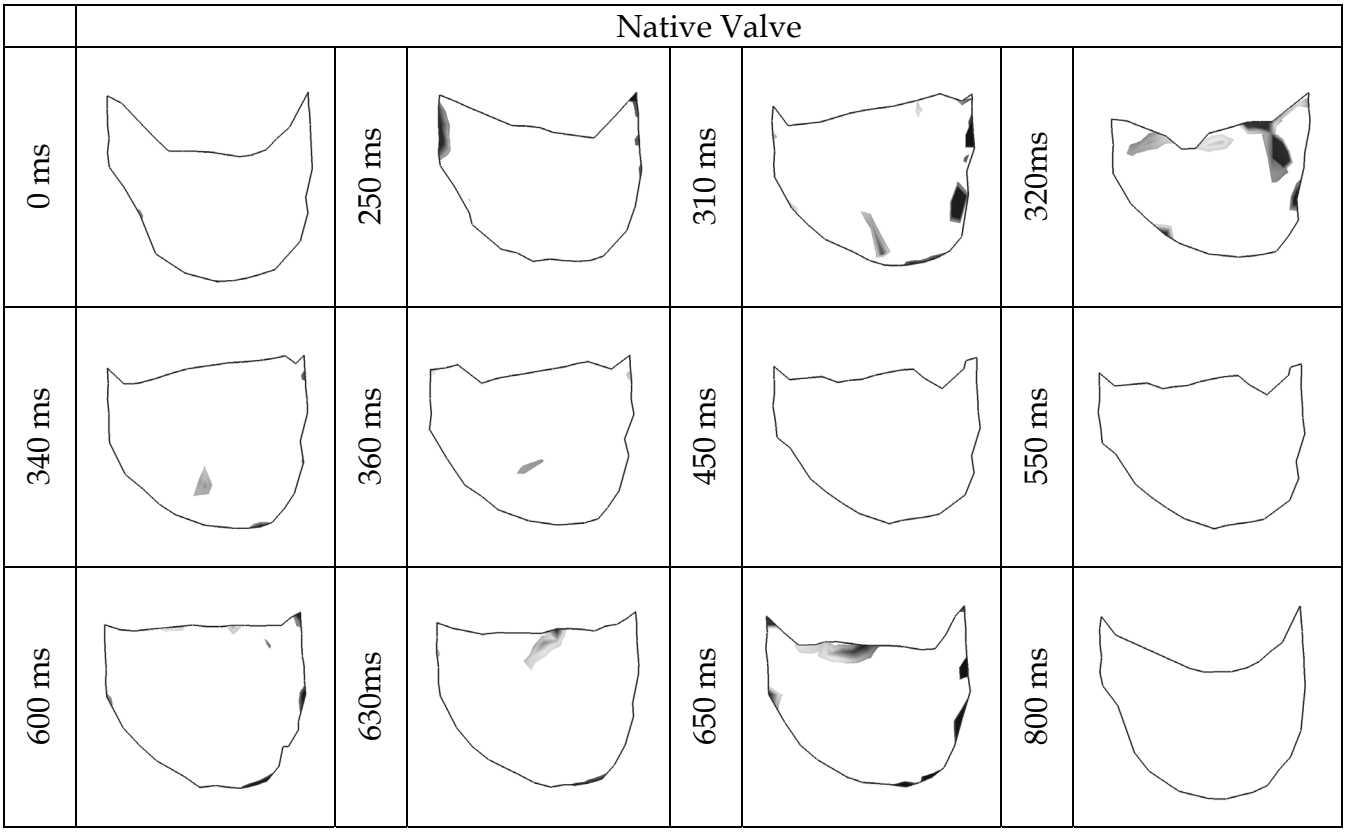

Figure 35 Minor curvature above k_2 = -0.5 mm^{-1} are removed from view. The darker the contours are, the greater the curvature. Note the location of high curvature shifts during cycle.

3.5.6 Leaflet Surface Curvature Histogram Analysis

Frequency distributions of the leaflet surface curvatures are summarized in (Figure 36, 37). In the closed position, a positive skew was observed for k_1 and negative skew for k_2., indicating that major curvatures tended to be positive, while minor curvature tends to be negative. Interestingly, as the cardiac cycle progressed k_1 tended to decrease in magnitude, while k_2 increased in magnitude. This observation indicated that the largest bending was in the k_2 direction. The highest major curvature was 0.230 mm^{-1} when the valve was closed, and highest minor curvature was -0.120 mm^{-1} when the valve was fully open (Table 4). The skew was much more highly pronounced in major curvature than minor curvature (averages of 1.01 vs -0.26). A higher skew indicates a broader range of value of curvature present, thus indicating a broader range of surface curvature or non-uniformity in bending.

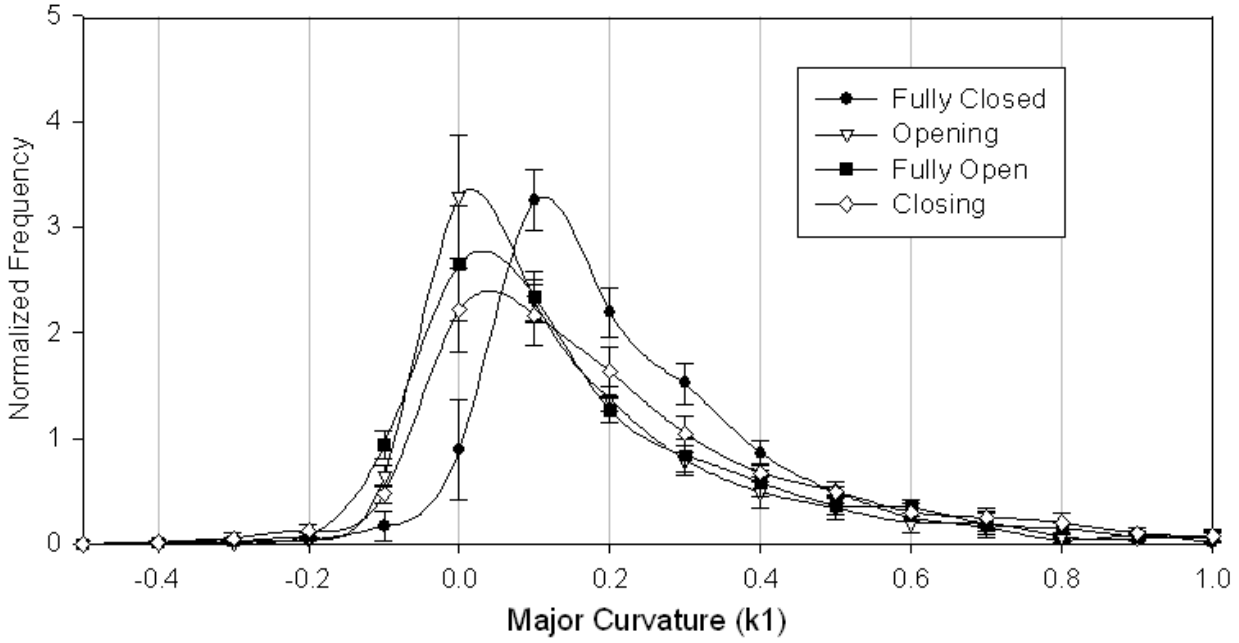

Figure 36 Major curvature histogram for all native valves averaged at important time points. (n = 5)

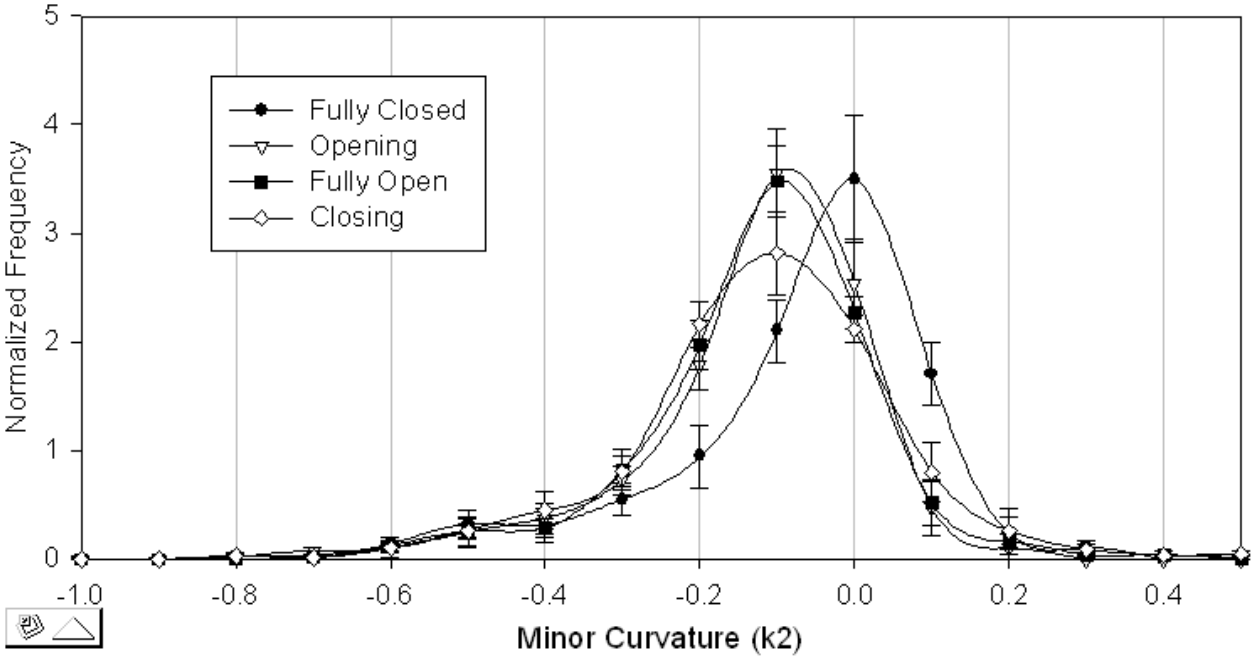

Figure 37 Minor curvature histogram for all native valves averaged at important time points. (n = 5)

3.6 Stiffened Leaflet Results and Comparison with Native Valve

3.6.1 Reproducibility of Pressure and Flow Conditions

The recorded pressure and flow waveform are presented in Figure 24. The recording starts with valve closed and covers one whole cycle. Details on phases of valve opening are shown in Table 1. Comparison of native and stiffened leaflets pressure and flow waveforms indicated that both were nearly identical with an $r^2 > 0.98$. The waveform pattern demonstrated consistent flow conditions between native and stiffened states. Other flows are presented in appendices section. (Appendix A)

3.6.2 Uni-Dimensional and Areal Changes

As previously noted, the native leaflet dimensional geometry changed greatly during opening and closing cycles (Figure 38, 39). Radial length increased by 30% ($p \leq 0.028$) and area increased by 25% ($p \leq 0.010$) when valve was fully open. The free edge length changed as well and when compared between opening and closing states it was statistically different. These findings indicate the native leaflet is compliant and stretched in radial direction during the cycle. The stiffened leaflet lengths measurement does not change statistically significant in any of the dimensional parameters.

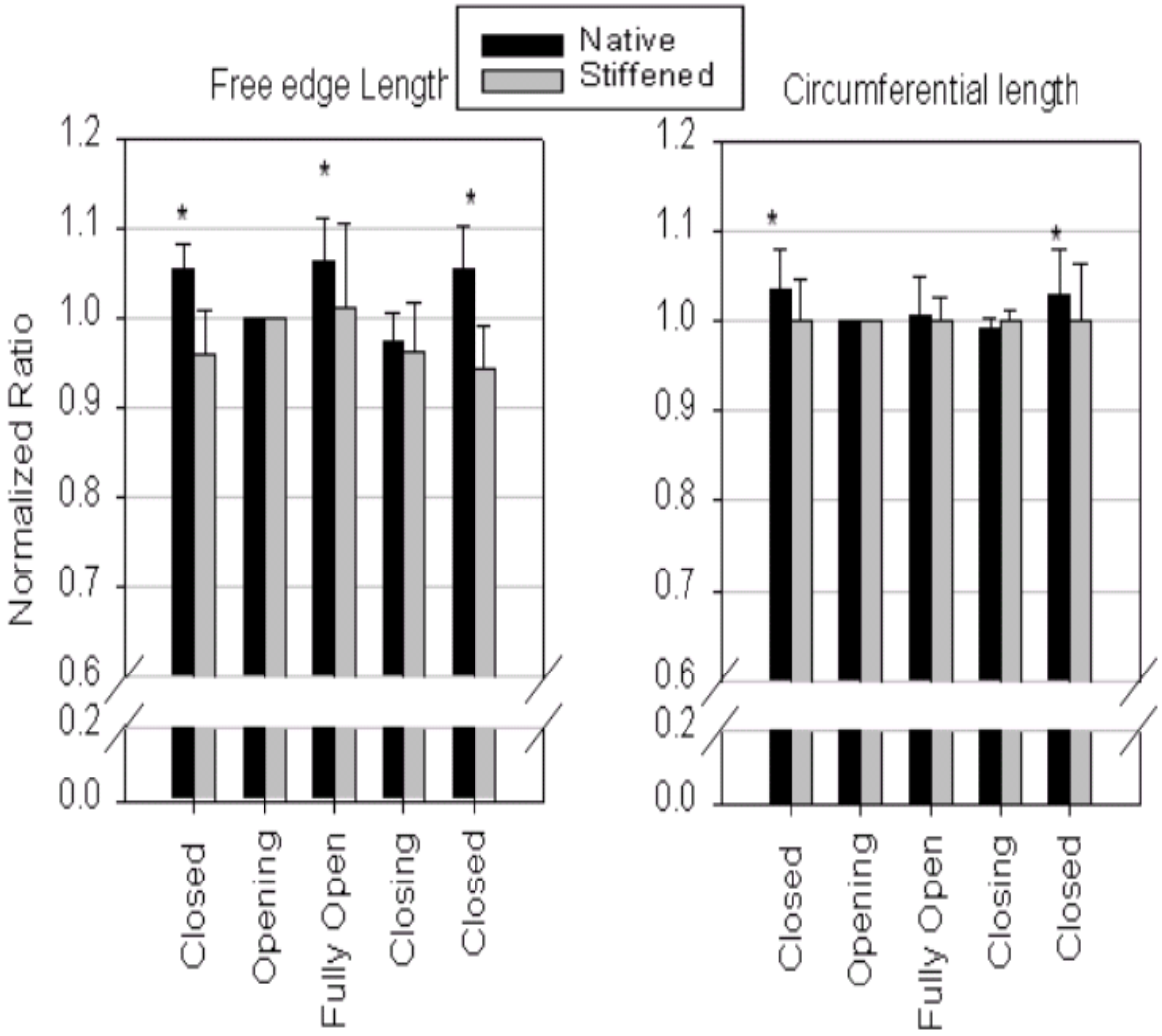

Figure 38 Lengths are normalized with respect to when it is about to open. The graph on left shows length of leaflet across free edge location. Valve radial length for stiffened valve does no increase in the same manner as native valve. On the right graph is the length of leaflet along the circumferential strip. Unlike the free edge, the length decreases slightly when it is open but statistical insignificant. * denotes length that is statistically different from closed phase, $p < 0.05$ using one-way ANOVA

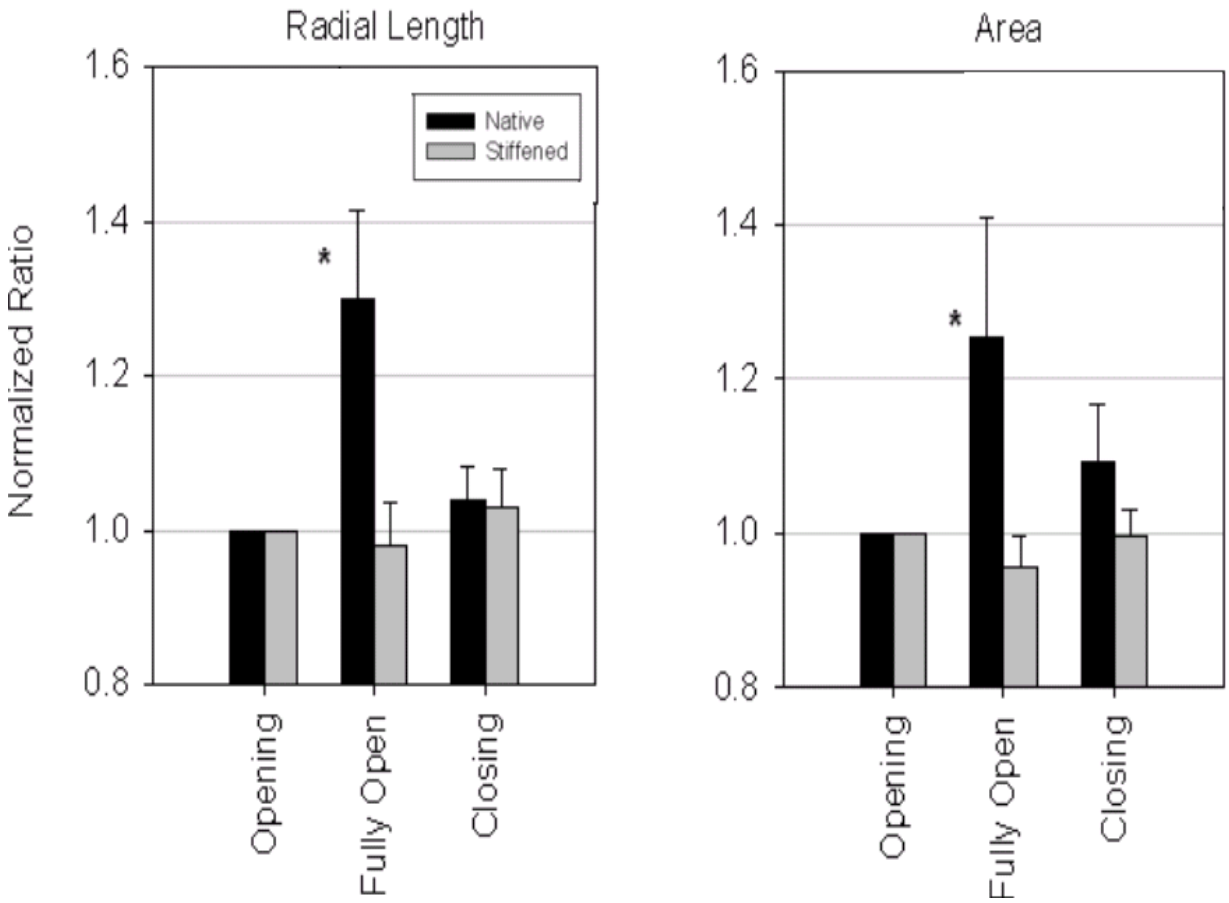

Figure 39 Radial length and area graph, all values are normalized to when it was about to open. The graph on left shows length of leaflet in radial direction during three key phases. When flow velocity is at maximum, the valve length increases an average of 30%. Length during fully closed are omitted due to difficulty scanning the entire leaflet. The graph on right shows area comparison between opening, fully open, and closing. The native leaflet is much more compliant than stiffened leaflet. * denotes statistically different from opening phase, $p < 0.05$ using one-way ANOVA

3.6.3 Overall Geometric Characteristics of Leaflets

The view of native and stiffened leaflet over the cardiac cycle is presented (Figure 40). The native valve opens early and closes later when compared to stiffened leaflet. In addition the native valve opened symmetrically, whereas as the stiffened leaflet had a "kink" on the right side. The native leaflet also continuously shifted in shape, whereas the stiffened leaflet opens and maintains the same shape until closure. Of particular note was the tendency for the stiffened leaflet to snap shut within a time period of 10 ms (Figure 40, rightmost column).

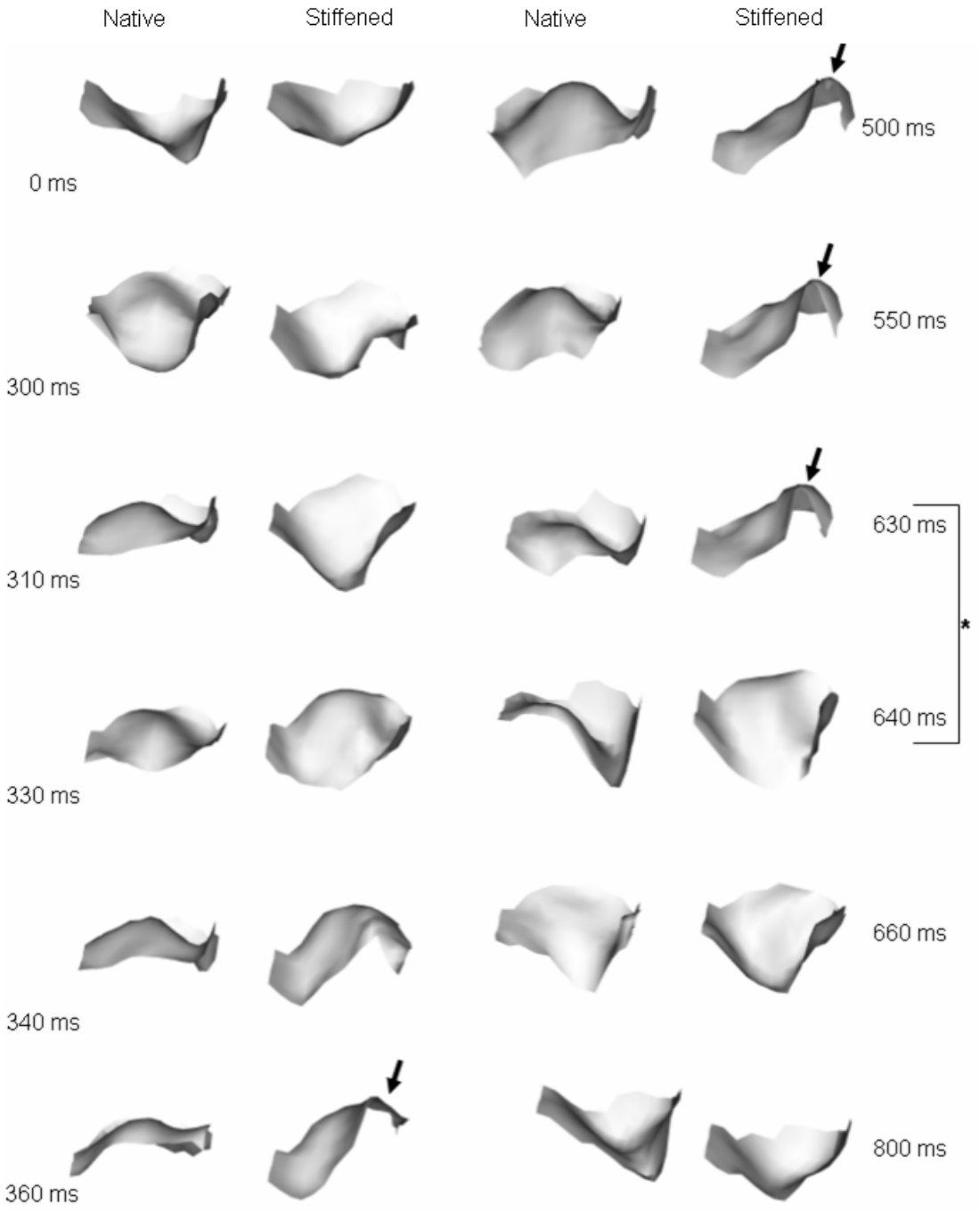

Figure 40 View showing native and stiffened leaflet opening and closing from inflow point of view. Time points are indicated to the side of the valves, opening and closing timing differ between native and stiffened leaflet. Notice it takes only 10 ms for stiffened leaflet to transition most of the closing cycle. (indicated by * symbol) Arrow points to location of high bending that does not move during the cardiac cycle or in between cycles. Surface are in gouraud shading with arbitrary light source.

3.6.4 Leaflet cross-sectional view

Circumferential cross-sections of the leaflet are presented in Figure 41 and 42. The views were taken at two locations, at the middle belly region and at the free edge. Results demonstrated that the native leaflet opens overall in a smooth, stepwise mechanism, in an orderly fashion. The closing behavior was more complex, where both free edge and circumferential region closed together and showed a continued shifting in shape. In contrast, the stiffened leaflet opened suddenly in a snap-like manner. Cross-sectional views also demonstrated the stiffened leaflet has a kink on one side, where as the native leaflet opens more symmetrically. In addition, changes in circumferential (belly region) occurs earlier than free edge, suggesting the valve opens along the direction of flow. During closing the shape suggests the entire leaflet moves towards the center of the valve, and closes from free edge to belly region.

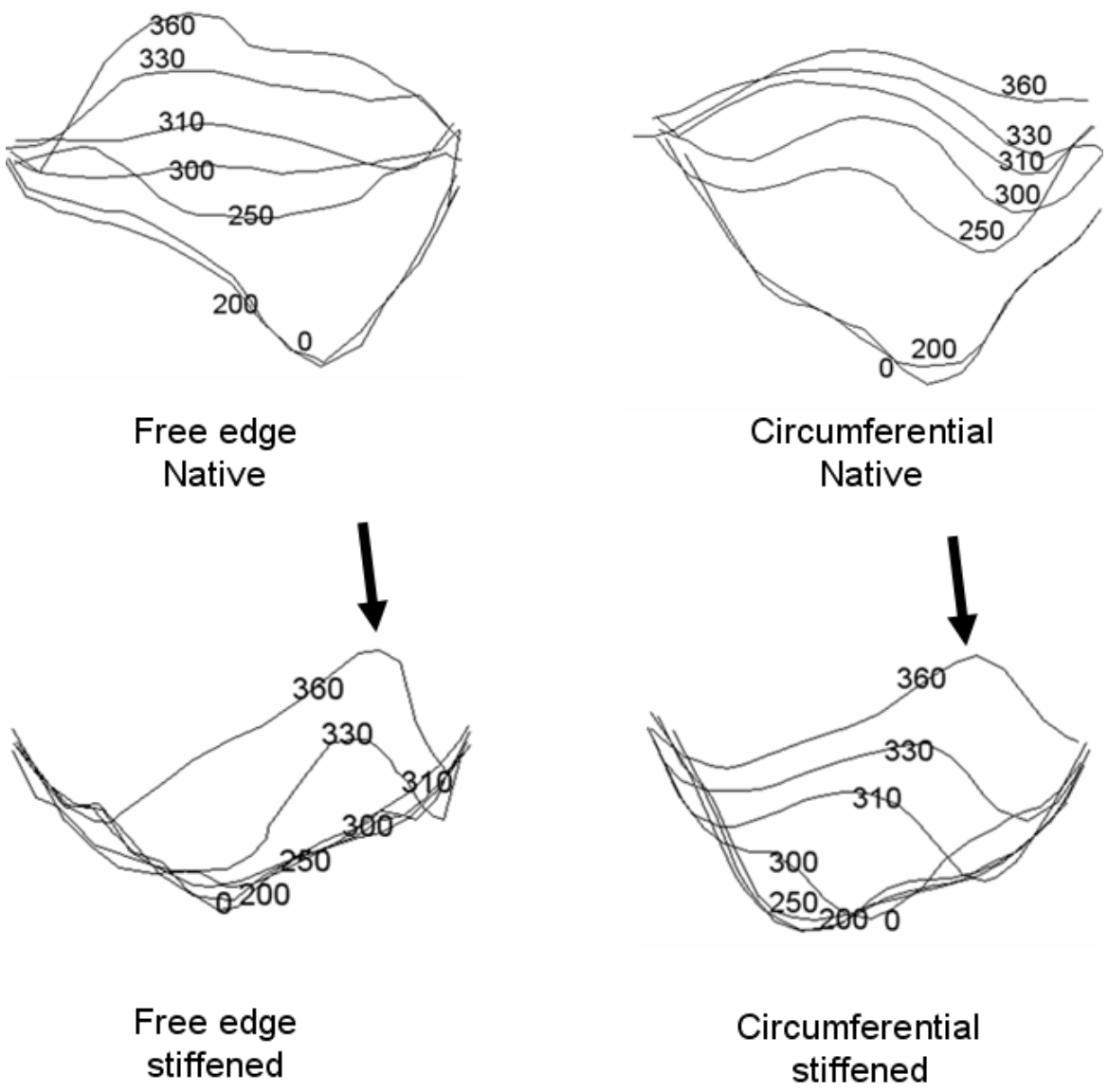

Figure 41 Cross section view of the free edge and circumferential portion of the typical valve when opening. Numbers indicate the time point when data was acquired. The native valve's free edge section shows a relatively early opening and smoothly progresses to fully open state at 360 ms. Majority of the bending occurs to the left and right, where the middle stays flat. The stiffened leaflet however stays close longer and opens faster. Arrow points to high bending that occurs only to stiffened leaflet. Circumference section shows the same smooth and gradual opening seen at free edge. Again bending occurs to the sides. Note the circumferential section opens earlier than the free edge for both conditions, indicating the valve motion opening begins from the direction the flow enters. Middle of the valve which is where nodulus is located, is flat due to the collagen bundles resistant to bending.

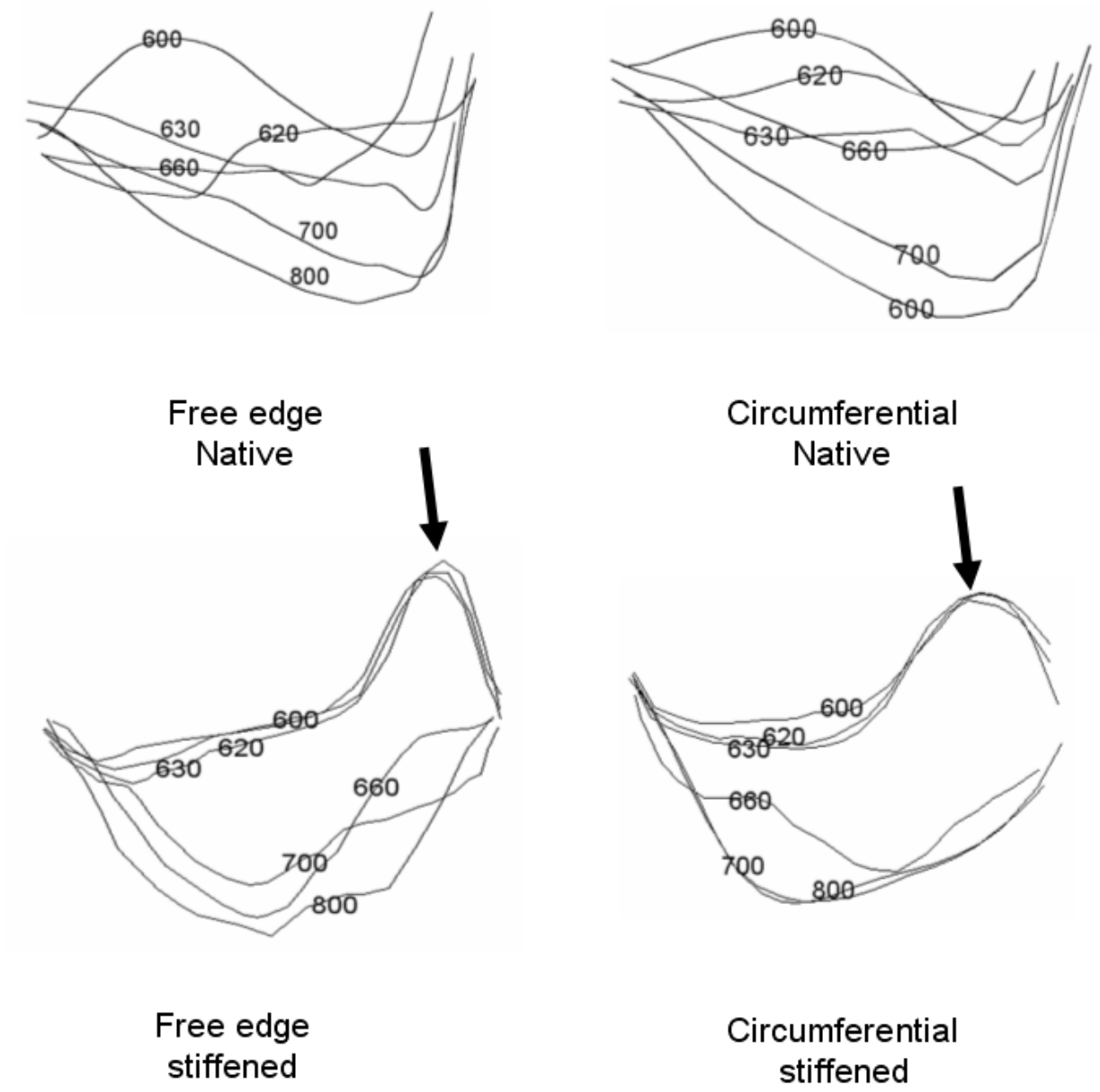

Figure 42 This is the cross section view of the free edge and circumferential portion of the typical valve when closing. Native valve closes smoothly as it settles into the close position. Unlike the native valve, stiffened leaflet closes quickly and severe bending can again be observed, highlighted with the arrow sign.

3.6.5 Surface Curvature Results of Native and Stiffened Leaflets

Minor curvature was chosen over major curvature to study because a larger curvature change occurs as the valve opens, and are shown (Figure 43 ~ 45). The leaflet experiences a reversal in minor curvature values as it opens, and is more pronounced in stiffened leaflet than native leaflet. The lines indicate the direction of bending and major portion of valve experience negative curvature, bending away from view. The portions of stiffened leaflet with severe bending consistently have bending in the circumferential direction. The native valve has uniform minor curvature and direction of bending shifts as the cycle progresses. (Minor curvature contour plots of other four valves presented in appendix B)

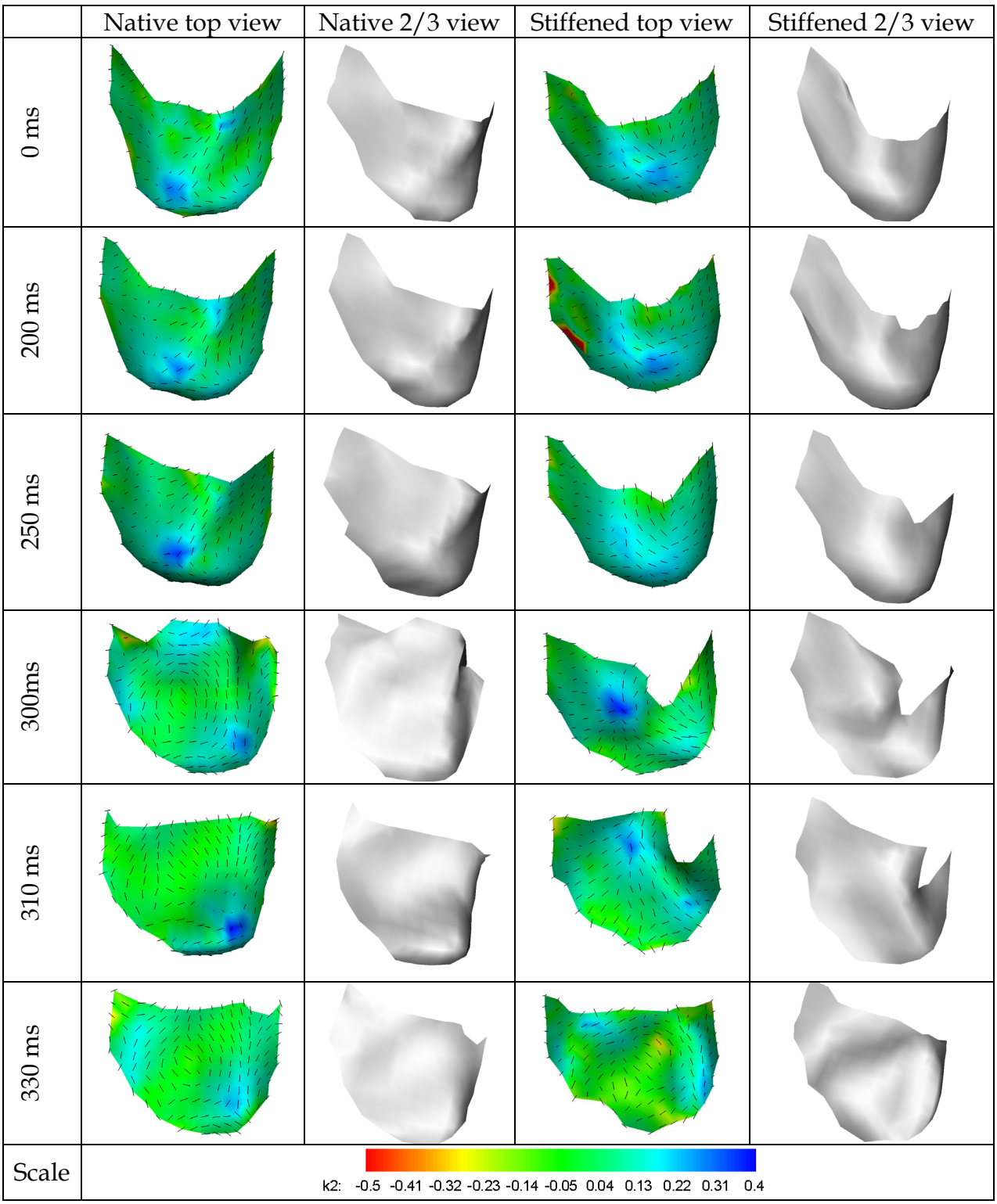

Figure 43 Contour plots and gouraud shade plot of the same valve when the valve is opening. The valve has been chemically stiffened in third and fourth column. Red arrow denotes high curvature bending. The jagged edge of stiffened valve at 310 ms is due to the point of view and positioning.

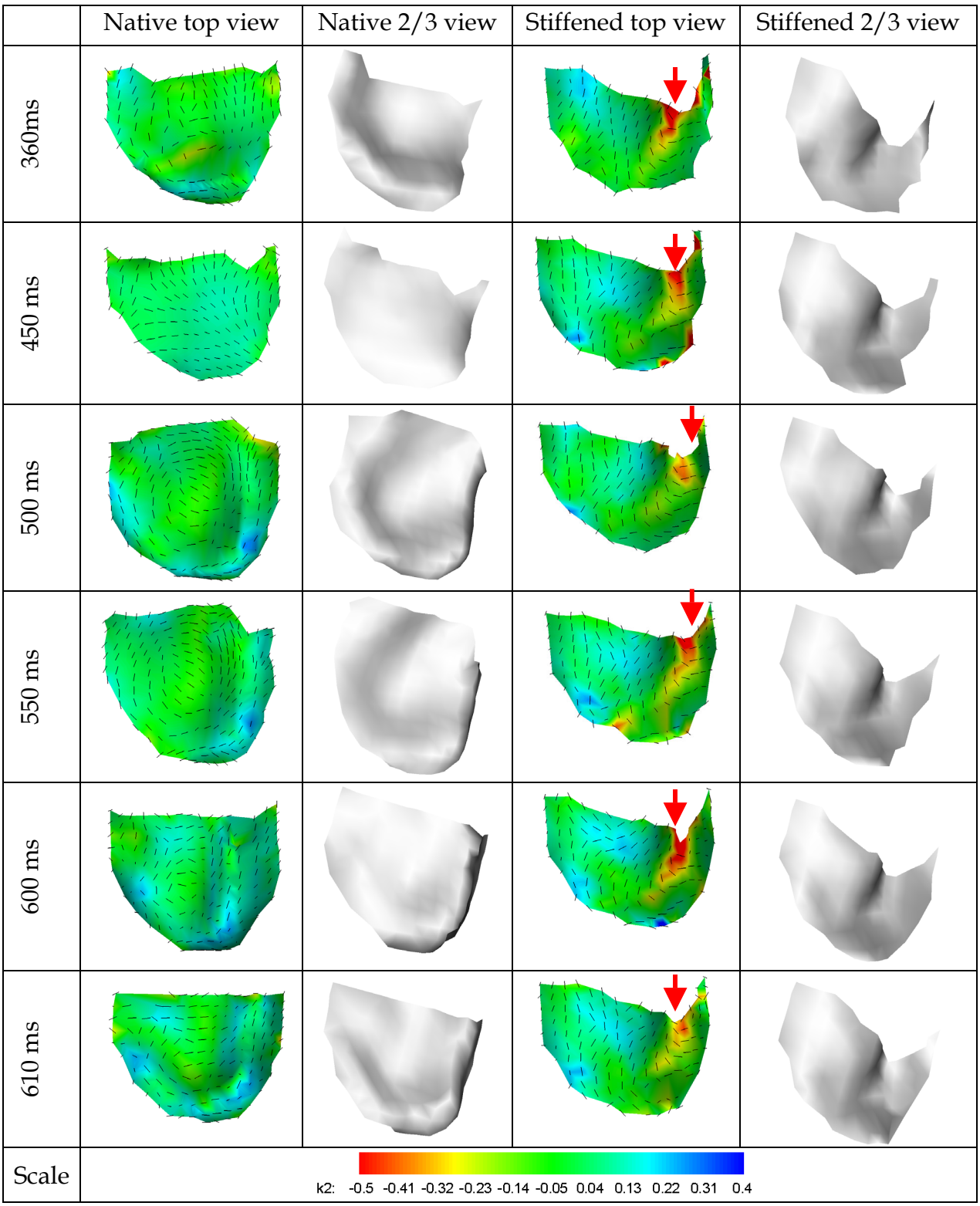

Figure 44 Contour plots and gouraud shade plot of the same valve when the valve is open. The valve has been chemically stiffened in third and fourth column. Red arrow denotes high curvature bending.

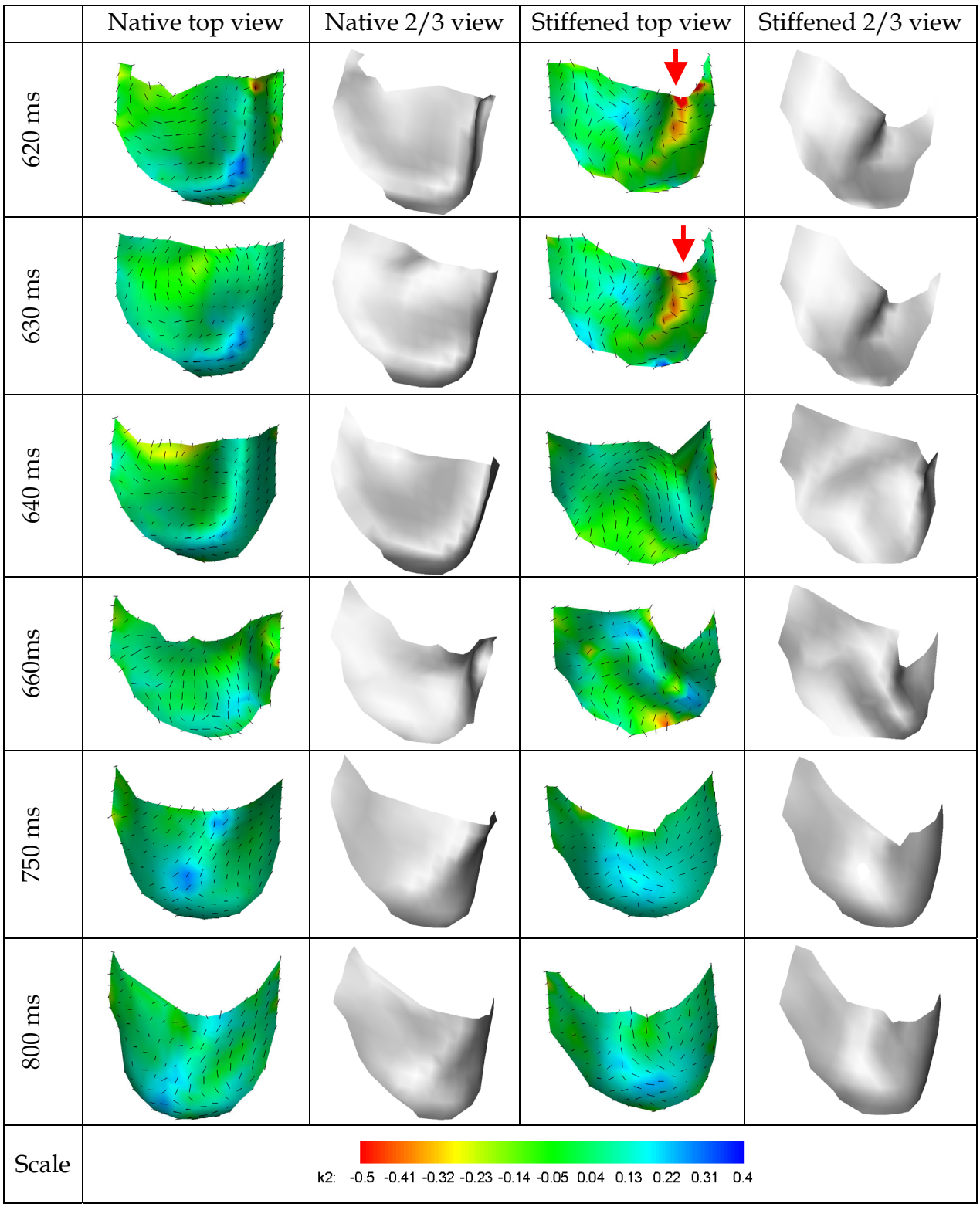

Figure 45 Contour plots and gouraud shade plot of the same valve when the valve is closing. The valve has been chemically stiffened in third and fourth column.. Red arrow denotes high curvature bending.

3.6.6 Truncated Curvature Plot

To graphically isolate locations of high bending, an additional curvature plot was generated (Figure 46). This plot only displays those regions of the leaflet with $|k_2| \geq 0.5$ mm^{-1}, regions with curvature less magnitude was excluded was the plot. This value was chosen as it is the upper 5% of the k_2 value observed in the present study, and thus represent regions of high bending. For native leaflets, small regions of the leaflet were shown to have high minor curvature and present only when valve was open. In addition the location of high curvature shifts in location and direction through the cardiac cycle. As the valve dynamically shifted geometries, the high bending area shifts around to distribute the bending stress. Some of these locations are located to the free edge and side edges of the leaflet. This indicates the native leaflet experiences severe bending, but that bending times are short and not isolated to single location during the cardiac cycle. In contrast, for the stiffened leaflet locations of high bending were consistently on one side of the valve during fully opened phase. This area of high bending is at least 10% in area and continues for around 200 ms.

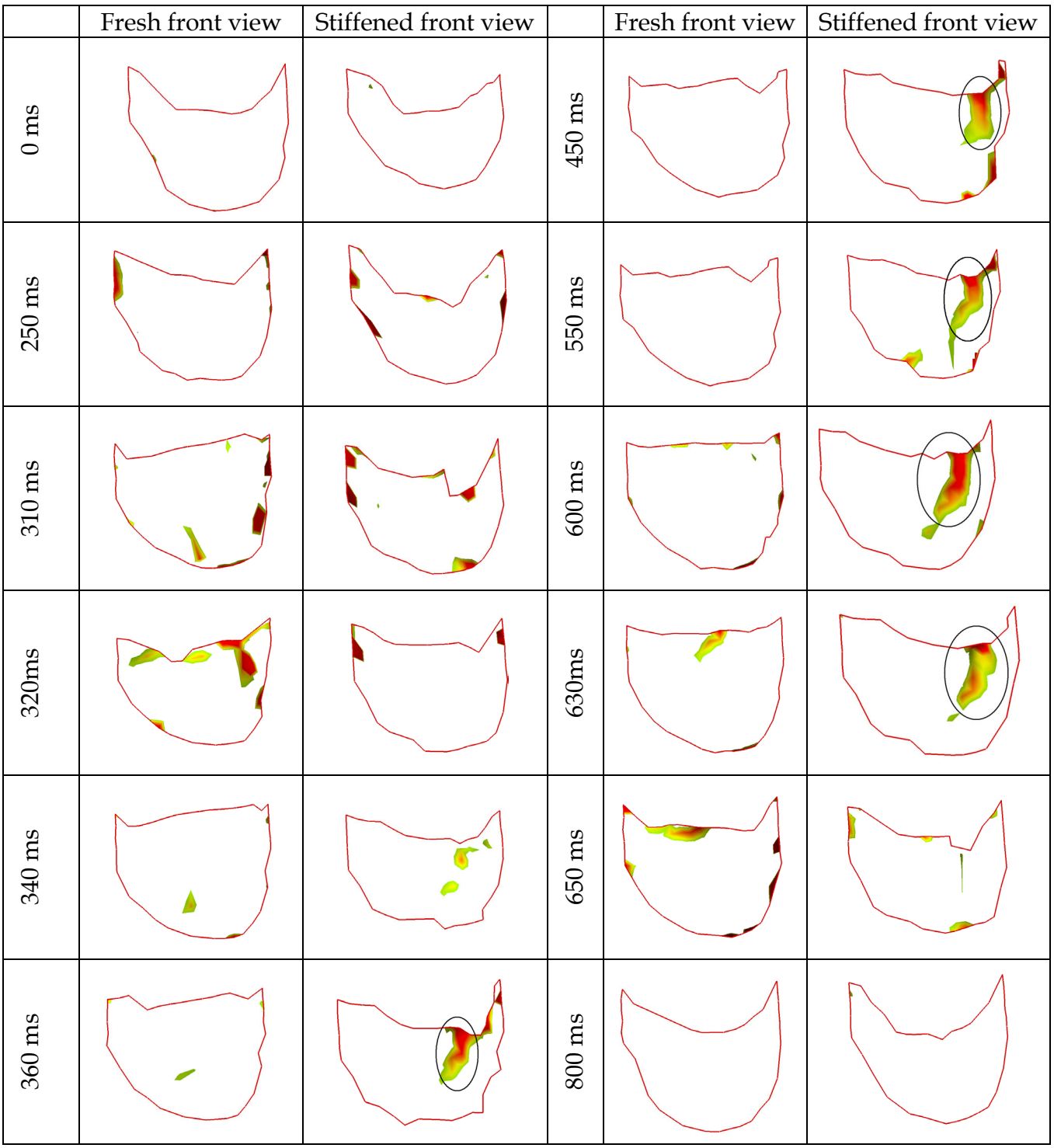

Figure 46 Plot of native and stiffened leaflet surface whose curvature value is more positive than -0.5 mm^{-1} ($k_2 > -0.5\ mm^{-1}$) were removed from view. The more red the colors are, the greater the curvature. Note for native valve, the location of high curvature shifts during cycle, where as the stiffened leaflet remains the same. Circle marks location of high bending.

3.6.7 Stiffened and Native Leaflet Surface Curvature Histogram Analysis

Quantification of complete surface curvatures demonstrated that both native and stiffened leaflet have similar trends for major and minor curvatures. For major curvature, most of the valve was positively curved, with a skew towards positive direction. (Figure 47) For minor curvature, the exact opposite was true. When native valve opens, the major curvature shifts from positive to near neutral value, indicating the valve flattens out. (Figure 48) For stiffened leaflet, the leaflet reduces the bending similar to native valve, but does not flatten out. In terms of minor curvature, native valve exhibits a more curved surface when open, and stiffened leaflet shows a complete reversal in curvature as it opens. The stiffened leaflets show twice the amount of change in peak curvature frequency. Furthermore, when the stiffened leaflet opens, the minor curvature plot flattens out, thus indicating the broad range of bending that occurs on a single leaflet.

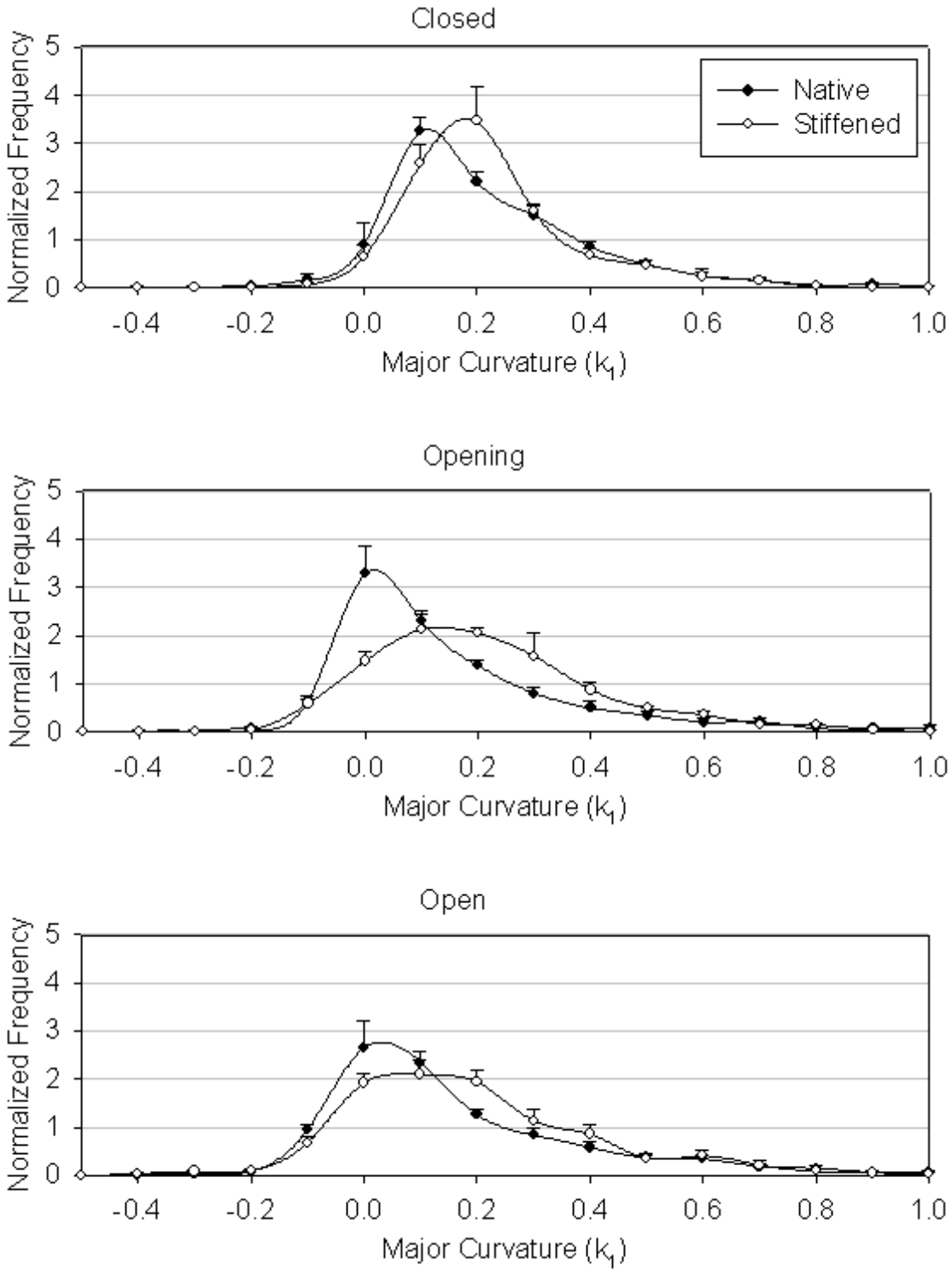

Figure 47 Major curvature histogram for all valves averaged at important time points. (n = 5)

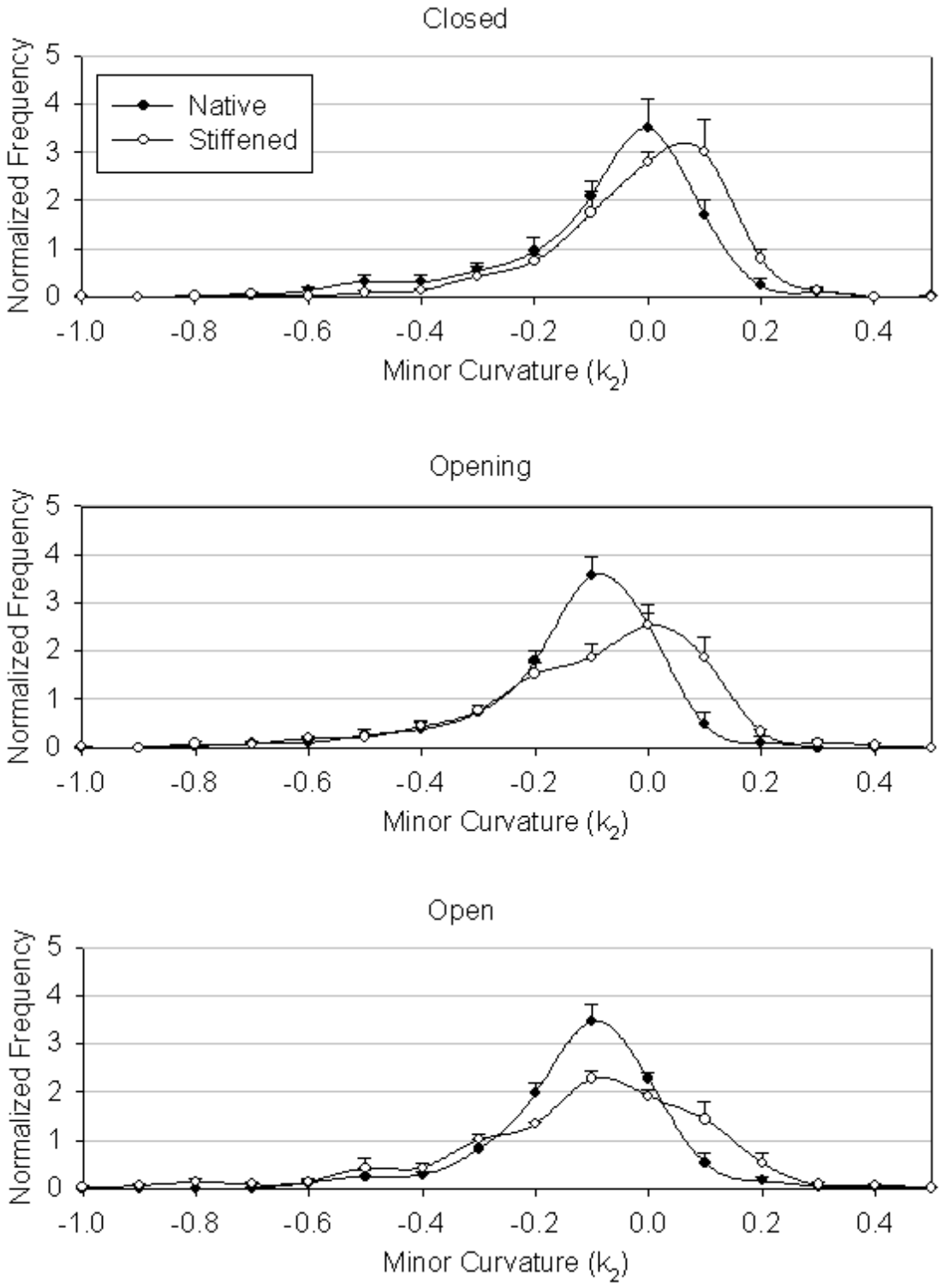

Figure 48 Minor curvature histogram for all valves averaged at important time points. (n = 5)

Table 4 Statistical table of major and minor curvature values for native and stiffened leaflets at different time points (n =5)

Valve Statistics

	Major Curvature	pre-open	opening	fully open	closing	closed
Native	**Average**	0.218	0.154	0.168	0.215	0.230
	SD	0.133	0.161	0.171	0.188	0.120
	Skew	0.887	0.956	0.985	1.144	1.079
	Mode	0.100	0.000	0.000	0.000	0.100

	Major Curvature	pre-open	opening	fully open	closing	closed
Stiffened	**Average**	0.227	0.222	0.188	0.227	0.240
	SD	0.115	0.161	0.155	0.165	0.122
	Skew	1.107	1.382	1.211	1.380	1.146
	Mode	0.100	0.000	0.000	0.000	0.100

	Minor curvature	pre-open	opening	fully open	closing	closed
Native	**Average**	-0.072	-0.125	-0.120	-0.114	-0.042
	SD	0.140	0.120	0.120	0.136	0.129
	Skew	-0.512	-0.207	-0.165	-0.105	-0.324
	Mode	0.000	-0.100	-0.100	-0.100	0.000

	Minor curvature	pre-open	opening	fully open	closing	closed
Stiffened	**Average**	-0.014	-0.089	-0.111	-0.114	-0.019
	SD	0.129	0.157	0.181	0.176	0.139
	Skew	-0.107	0.072	-0.060	-0.078	-0.134
	Mode	0.000	-0.100	-0.100	-0.100	0.000

4.0 DISCUSSION

4.1 Native Valve

4.1.1 Changes in Dynamic Leaflet Geometry

Valve leaflet motion was not always smooth, but rather underwent rapid, complex conformational changes during opening/closing. From leaflet reconstructions (Figure 29) and cross sections along the circumferential and free edge (Figure 33), it was apparent the valve opens from the belly region before free edge. During closing both the free edge and circumferential section close together, and a slight dynamic change in shape was observed. There are thus important differences between opening and closing phases, and are not simple reversals of each other.

4.1.2 Uni-dimensional and Areal Changes

The circumferential and free edge length did not change significantly during the cardiac cycle, with free edge length increase slightly and the circumferential length staying approximately the same. This stability in length is consistent with preferred circumferential alignment of the aortic valve leaflet collagen fibers (39).

The most pronounced result indicated that the valve leaflet increases in length by 30% in radial direction at maximum flow conditions. To our knowledge, previous studies have not observed such behaviors. For example, Thubrikar reported that leaflet radial length does not change significantly during maximum flow. Instead he observed

when the leaflet closes and coapt under increasing pressure, the radial length increases on during diastole (6). Thubrikar only used two markers at the basal and belly region of the leaflet, which did not cover the free edge. Further, two markers only allowed straight distance measurements, and did not follow leaflet surface. From our studies, it appears that the free edge region in the radial direction is most distensible. Yoganathan et al has reported that the shear stress at leaflet can be as much as 80 dynes/cm, whose load is estimated to be around $1.44x10^{-3}$ Newton (for a flat plate leaflet whose dimension is 15mm x 12m) (40). In a previous study by Billiar and Sacks (41) (42), high radial distensibility of the free edge region in the aortic valve has been shown in our lab using in-vitro biaxial mechanical testing. We estimate that a tension of as little as 0.25 N/m is sufficient to distend the leaflet by 40%, which translates to ~$3.75x10^{-3}$ Newton. This rough estimate suggests the loads induced by drag forces are more than sufficient to stretch the free edge of leaflet in radial direction. The physiological benefit of this increase in length cannot be answered in this study, although it likely affects the fluid dynamics inside the sinus as studies by Bellhouse and Bellhouse have suggested. (14, 15)

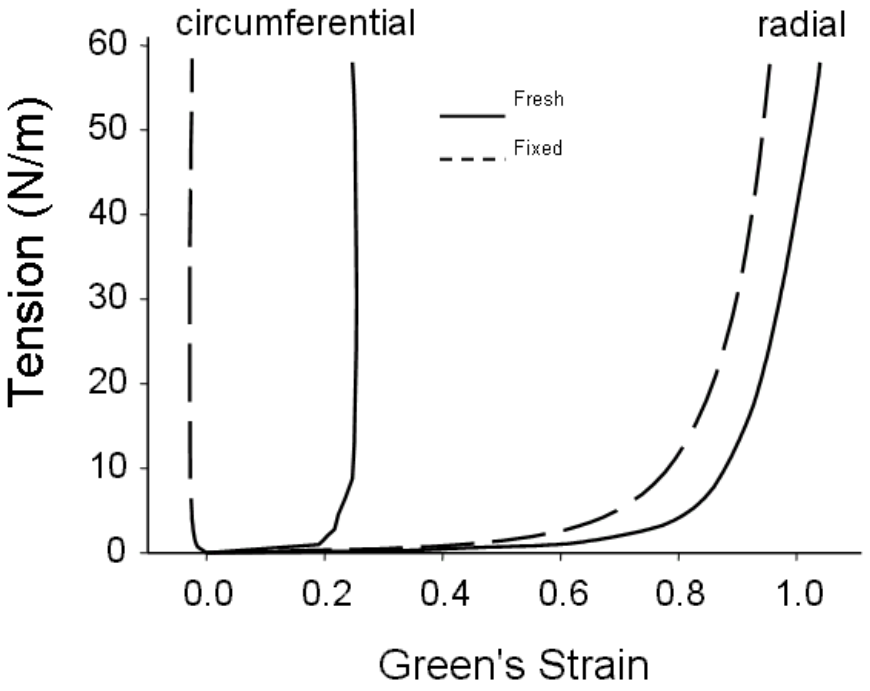

Figure 49 Stress-Strain plot of middle portion of the porcine aortic leaflet . Notice how pliable the fresh leaflet is at low stresses. (41) (42)

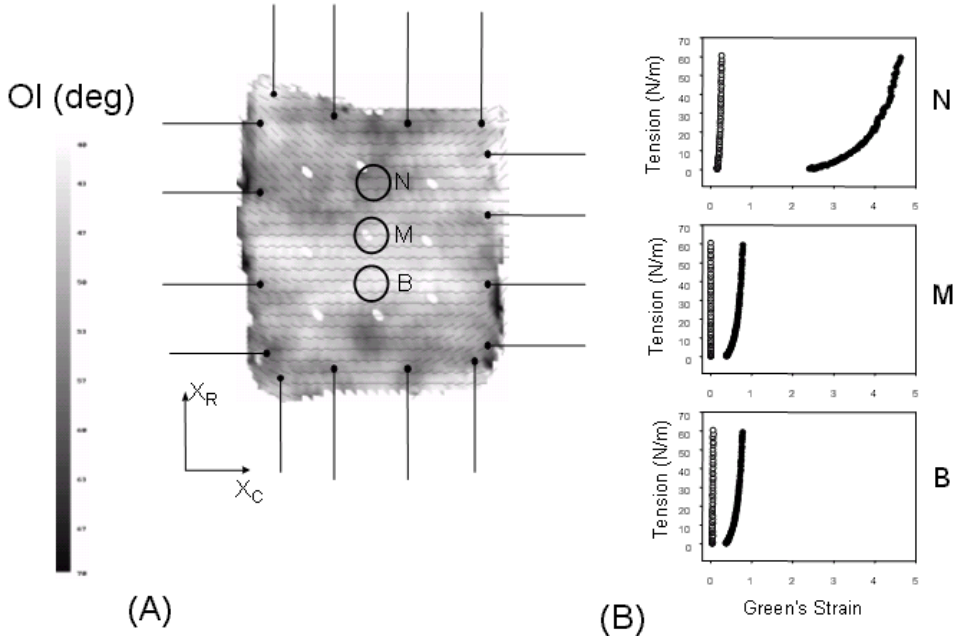

Figure 50 (A) Tissue leaflet under biaxial testing. Letters denote the location of local stress-strain curve. (B) Stress strain curve from three locations on the valve. Light circles are in circumferential direction. and dark circles are in radial direction. (41) (42)

4.1.3 Changes in Circumferential Cross-sectional Shape

Several important observations can be deduced from the circumferential and free edge surface cross-sectional results (Figure 33). Both circumferential and free edge sections showed a step-by-step progression and did not dramatically shift while opening, while when closing the sequence was less orderly. Another similarity between the two sections was the curvature of the middle of segment, near the nodulus, was relatively flat when valve is open. This is because the nodulus is a thicker segment of collagen fibers and more resistant to bending than other parts of the valve. The location with high bending and where most of bending was occurring was near the edges to the left and right of the valve.

4.1.4 Changes in Dynamic Leaflet Geometry

Major curvatures where found to shift from positive to near zero, indicating valve bends less in the major direction when opening. Throughout the cycle, the skew is towards positive indicating the severe bending in the positive direction. Leaflet also has more uniform curvatures when closed. On the other hand, the minor curvature shifts from nearly zero to negative values, indicating a reversal in direction of bending that occurs during the cycle. For minor curvature, the skew valves tend towards the negative values, indicating the severe bending in the negative direction. Therefore in terms of minor curvature, the valve is curved more and opposite is true for major curvature.

4.2 Stiffened Leaflet and Comparing with Native Valve

4.2.1 Stiffened Leaflet Kinematics

In this study, we observed several key differences in the dynamic behavior of the native and stiffened aortic valve leaflet. While the native valve would open in a complex but overall smooth manner, the stiffened leaflet tended to stay open and maintain the same overall shape until it rapidly closed. Comparison of valve geometry between native and stiffened leaflet has never been examined before, the most recent attempt by Thornton. (5) The increase is tissue rigidity also prohibited the dynamically shifted shape often observed in the native valve. In addition, a localized region of high bending was consistently observed in stiffened leaflet. The timing of valve opening and closing timing is different from native and stiffened leaflet; with the stiffened leaflet opens and closes much more rapidly. The amount of time the valve stayed open was the same but the action time to transition from open to close and vice versa was shorter. 60 ms and 40 ms were required for native valve to open and close, respectively. While for stiffened leaflet would take 40 ms and 30 ms, respectively. Both valves would open beginning from the basal region of valve leading to the free edge.

4.2.2 Uni-dimensional and Areal Measurements

The fundamental differences between the two groups studied resulted from the increased stiffness due to chemical treatment. Chemical treatment has been shown to affect the primarily the low-stress region of the stress-strain relation in bioprosthetic heart valve biomaterials (41) (43) (44) (45). In the present study, the complete lack of

change in radial length, which is perpendicular to preferred collage fiber direction (46), clearly demonstrated the effect of increased tissue stiffness on the deformation of the valve leaflet. The lack of change in total leaflet area was less dramatic than for the radial direction, as the circumferential lengths do not change as much.

Whether this change in radial direction has a significant physiological advantage cannot be directly answered in the current study. Nevertheless this geometric difference must alter the fluid mechanics of the aortic valve. Comparing the native and stiffened dimensional measurements throughout the cardiac cycle, the results indicate increased stiffness reduced changes in length in the circumferential direction, along the circumferential strip and free edge strip.

Reasons why this has not been observed others such as Thubrikar et al could be attributed to the difference in methodology in leaflet imaging. (6) The sutures used to attach the markers to the leaflet could constrict valve deformations or bending. (Figure 51) In addition Thubrikar has attached his lead marker near the center of the valve instead of at the free edge of the leaflet. In addition, his length measurement is base on two points and thus does not take into account the true length of the valve, only the distance between the two markers. Where as we have measured the entire length along the curved valve leaflet.

The biological advantage of this phenomenon can not be answered in this study. Though the increase in radial length would reduce drag at the free edge and thus decrease the local pressure. As mentioned in Bellhouse and Bellhouse this possible decrease in pressure would increase pressure gradient between the aortic root and the

leaflet free edge and thus facilitate the vortical flow inside the sinus. This vortical flow can prevent physical contact of the leaflet and aortic wall. Though it is apparent in stiffened valve that this mechanism is not crucial for valve function or durability, but could provide a slight benefit to overall valve dynamics (Figure 13).

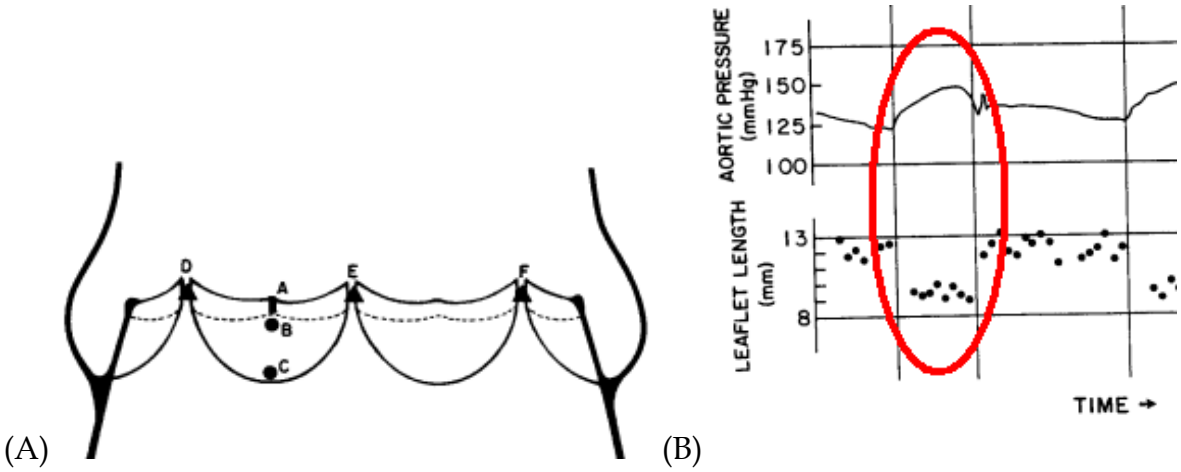

Figure 51 (A) Schematic of marker placement for Thubrikar study. He used marker BC to measure radial length. Marker A was only involved in free edge length measurement and travel. Thus the distensible free edge was not measured in radial length. (B) radial length does not increase when valve is open. He found the opposite was true as the leaflet basal region distends during pressurized but missed the radial distention occurring at the tip.

4.2.3 Differences in Leaflet Surface Shape Due to Leaflet Stiffening

The native valve showed an overall smooth opening behavior with a semi-symmetrical geometry throughout the sequence. On the other hand, stiffened leaflet showed a severe bending on one side of the leaflet while the middle and other side of the valve stayed flat. This severe bending occurred only on one side and does not switch sides during cardiac cycles. The sides the bending occurs depended on the valve, it was exclusive to one side. The native valve would experience similar severe bending, but the location would shift during cardiac cycle. Native leaflet was visually observed to quickly change leaflet surface geometries while valve was open. For both native and

stiffened leaflet, the results indicate the valve mechanistic opening starts from the basal region and leads to free edge. Where as in the closing both the circumferential and free edge close together for both native and stiffened leaflets.

In terms of overall curvature trends, there are two differences between native and stiffened leaflets. First, the major curvature values, the native leaflet has a higher peak indicating more uniform shape. The stiffened leaflet has larger portion of the histogram skewed towards positive, thus more portion of valve surface was more highly curved. First, as the valve opened, the native valve shifted its major curvature from positive to negative, thus attaining a flatter shape. On the other hand, the chemically modified valve became flatter, indicating portions of valve has higher major curvature values. Second, the minor curvature for both native and stiffened, were skewed negatively, but as valve opened, the chemically modified valve change from a positive values minor curvature to negative value.

Taken as a whole, the focal, persistent high curvatures observed in the stiffened valve are potentially relevant to the mechanism of bioprosthetic heart valve damage. In a previous study, we have observed that the leaflet bending stiffness increases significantly after glutaraldehyde treatment. (47) (48) After 200 million cycles of accelerated fatigue testing, the stiffness profoundly decreased (Figure 52). Moreover, the locations of highly pronounced curvatures we recorded in this study approximately coincide with those reported in explanted valves (Figure 53). (49-51) Taken as a whole, our results indicate that the aphysiologic shape of the stiffened aortic valve leaflets can contribute the onset and progression of tissue damage in bioprosthetic heart valves.

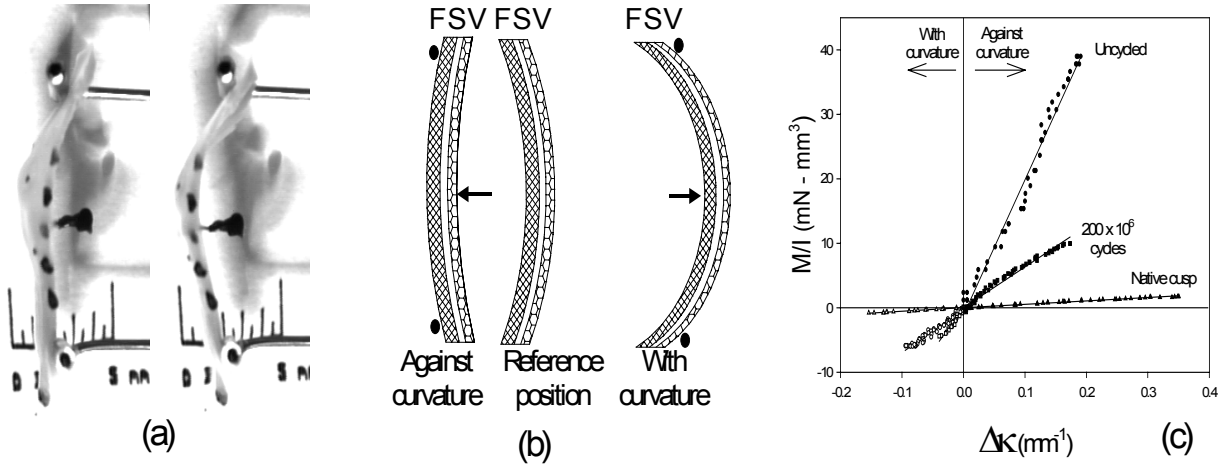

Figure 52 Results from bending test of aortic valve leaflets in the circumferential direction (a) Cuspal specimen before (left) and after (right) the application of load. (b) Schematic of the layered cuspal structure and how the layers deform with bending (fibrosa (F), spongiosa (S), and ventricularis (V)). (c) An M/I vs. Δκ curve demonstrating a linear response over the full range of flexure for the fresh aortic valve cusp. Uncycled porcine BHV demonstrated a profound, bending direction dependent increase in stiffness, while after 200x10^6 cycles the AC direction stiffness dropped substantially. (47) (48)

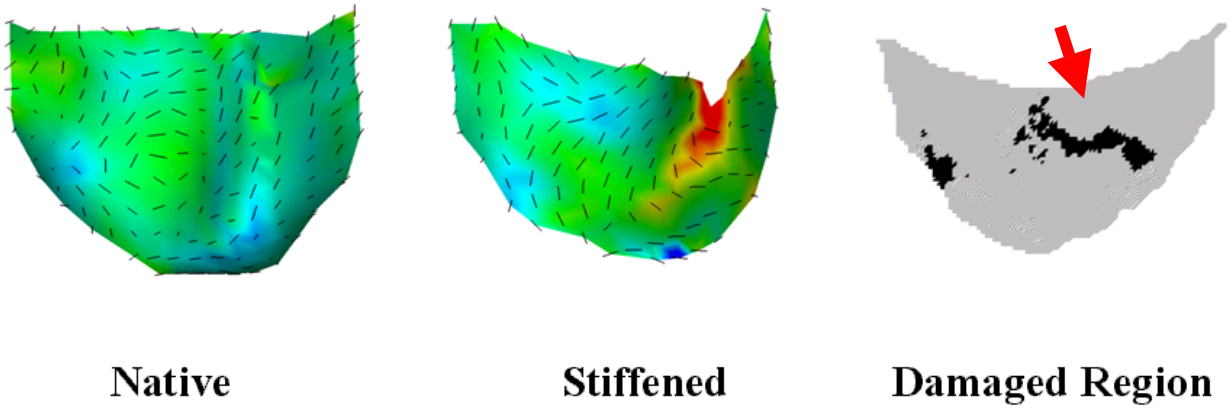

Figure 53 Minor curvature plot for the native, stiffened, and image showing regions of collagen disruption (shown in black). Damaged region image from (50, 51)

4.3 Limitations and Future Applications

The imaging technique utilized in this study was based on the use of laser on leaflet surfaces and thus points were not fixed on the valve surface. This does not allow strain analysis and the quantities measurable are limited to curvature and overall dimensional changes. Our intention was to study the opening and closing behavior of aortic valve leaflet. However, the current finding for the high radial extensibility suggests that future studies should focus on leaflet strain behavior to more precisely quantify this phenomenon.

The pressure and flow conditions of flow loop were not as precise as other flow loops used in valve studies. The design was forced to accommodate the laser imaging system which included a stiff pyrex aorta, the distance between compliance chamber and the valve, lack of time to test the native valve fresh and spend time to fine tune the waveform, and lack of a sophisticated compliance and peripheral resistance device. This shortcoming was acceptable as the focus of the study was the study of native leaflet shape rather than the study of flow condition. In addition for the comparison of native and stiffened leaflet, the testing parameters were identical and the result was compared only between each native and stiffened leaflet pairs.

Potential applications of this method include the development of heart valve bioreactors Such method of monitoring the valve while tissue culture or engineering is taking place would be valuable as it can assures the quality of the valve and doesn't contact and contaminate it. The generated data can be used to validate results from

computation fluid dynamics. The computational models are highly dependent on the parameter of the valve and any addition to the valve, such as markers or dye, can alter the experimental results and cause a disagreement between the two. An accurate model could generate results to without complex fluid experiments by running computational experiments efficiently and cheaply.

4.4 Future Applications

In the present study, the effects of leaflet stiffness on the dynamic aortic valve leaflet 3D geometry were quantified using a novel, non-contacting imaging system over the complete cardiac cycle. Area, dimensional, surface curvature, and measurements were performed. We observed that: 1) the native valve elongates in the radial direction by ~30% when fully opened, and exhibited small, high frequency shifts in shape; 2) the stiffened leaflet demonstrated a more stabile shape, as well as focal regions of prolonged, high curvature; 3) the stiffened leaflet opens and closes faster by ~10 ms compared to native leaflet; 4) for both native and stiffened states, the aortic valve opened from basal region leading to free edge 5) when closing, both the native and stiffened state valve close with both free edge and circumferential together. Clearly, valve leaflet undergo complex geometric changes during the cardiac cycle, and leaflet mechanical properties (mainly stiffness) have a profound affect on leaflet dynamic geometry.

Overall, the primary findings of this study were the extensive radial distension in the native state, and that an increase in leaflet mechanical stiffness induces high bending areas. The physiological function and advantage of the radial distension is currently unknown, but may affect the local hemodynamic patterns during valve operations, especially in the sinus regions. Our findings for the stiffened tissue have implications to valve design. For example, the high bending observed in the stiffened state correlated with known locations of tissue deterioration previously reported in our laboratory. Thus, in order to minimize leaflet tissue damage, methods of chemical modification utilized in bioprosthetic heart valves that maintain leaflet flexibility are necessary to minimize the onset and progression of tissue damage. (52)

APPENDICES

Appendix A
Valve flow/pressure waveforms

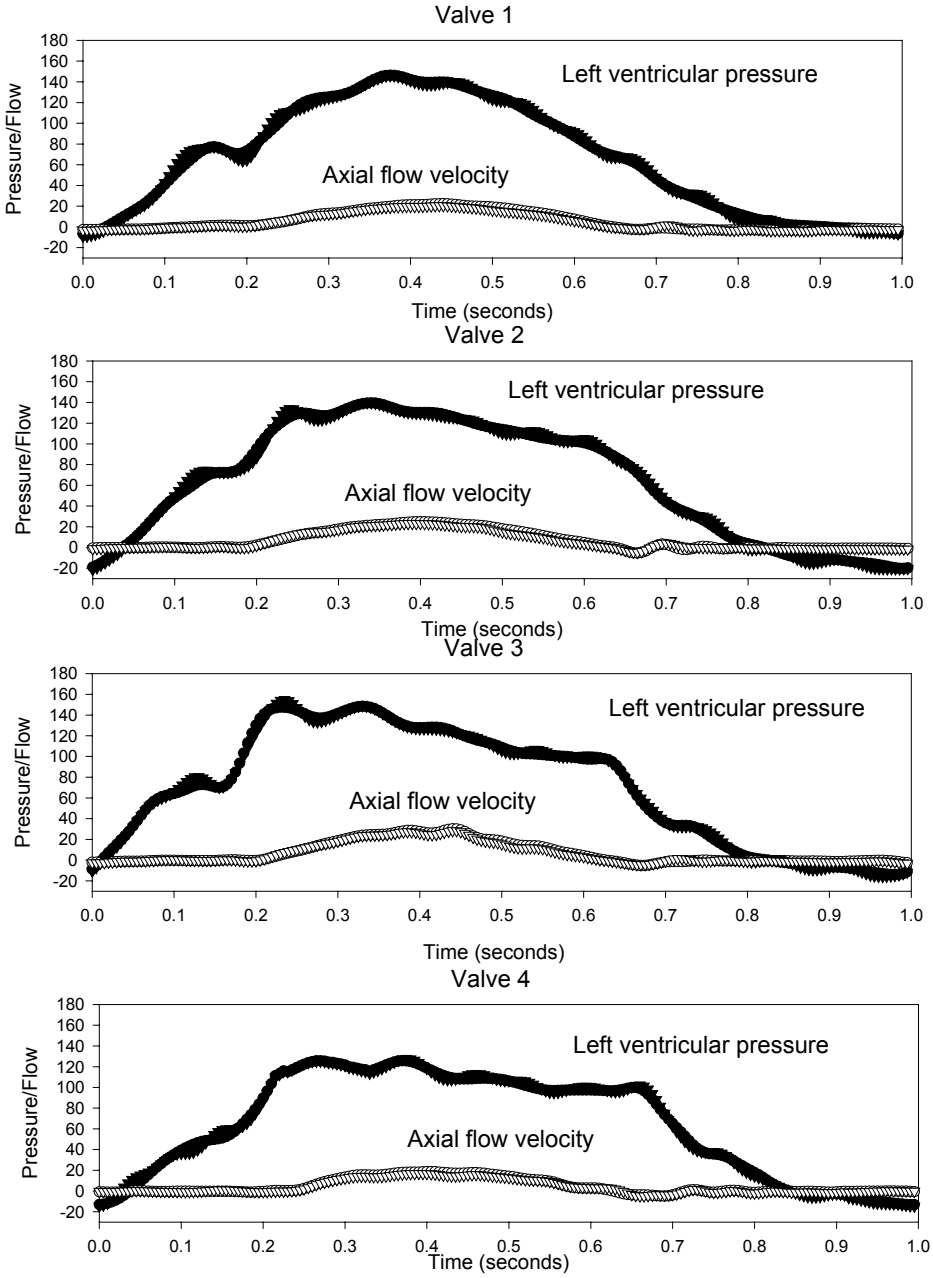

Appendix B

Minor curvature plots of other 4 valves

Valve 1

	Native valve	Stiffened valve		Native valve	Stiffened valve
0 ms	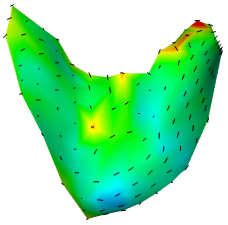	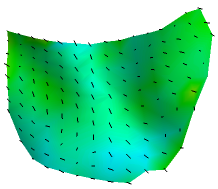	500ms	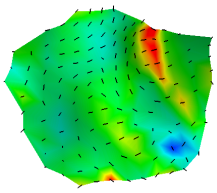	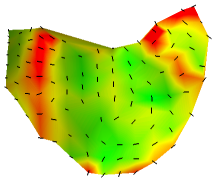
200 ms	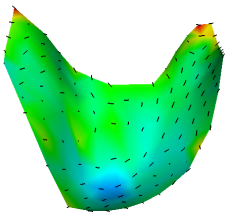	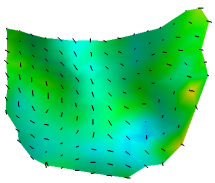	600 ms	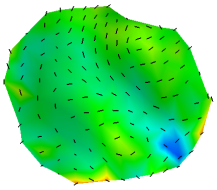	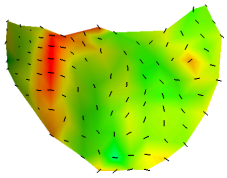
300 ms	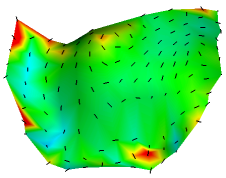	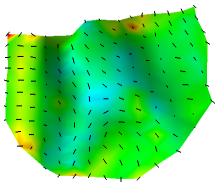	630 ms	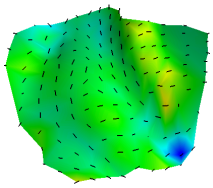	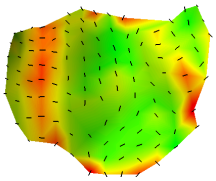
330ms	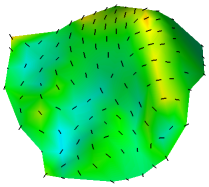	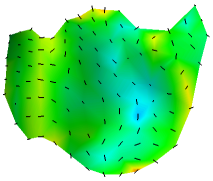	660 ms	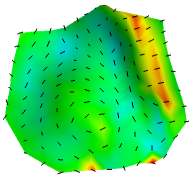	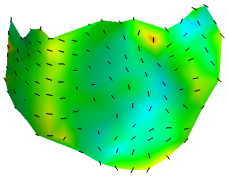
360 ms	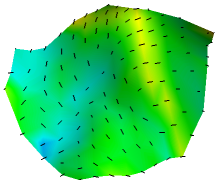	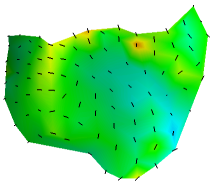	700 ms	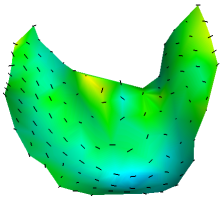	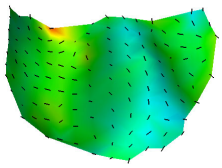
400 ms	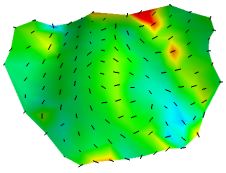	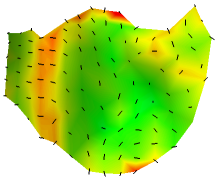	800 ms	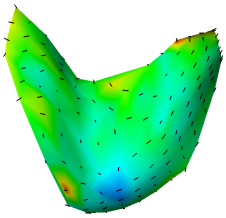	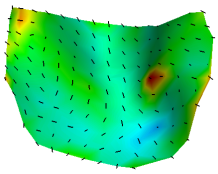

Valve 3

	Native valve	Stiffened valve		Native valve	Stiffened valve
0 ms	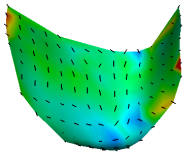	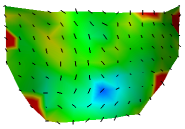	500ms	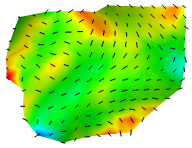	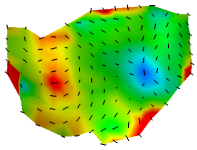
200 ms	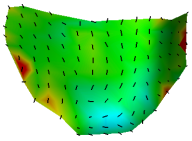	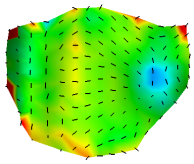	600 ms	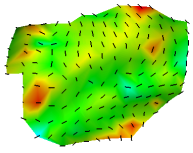	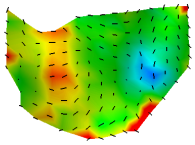
300 ms	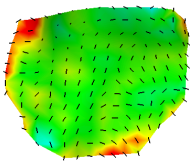	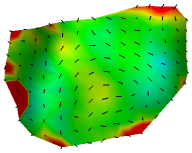	630 ms	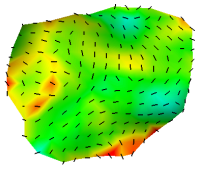	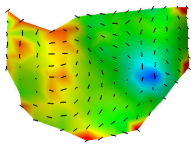
330ms	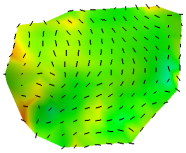	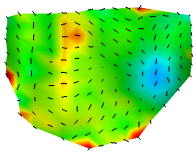	660 ms	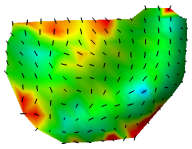	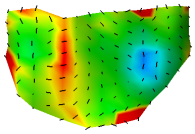
360 ms	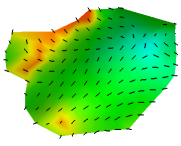	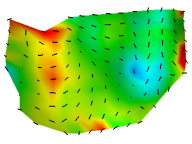	700 ms	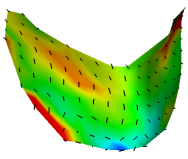	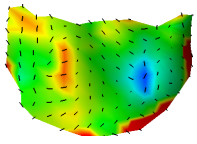
400 ms	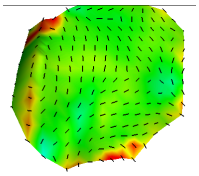	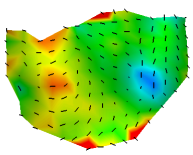	800 ms	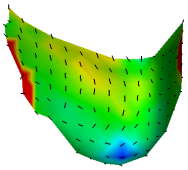	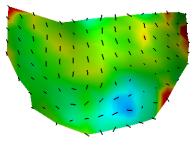

Valve 4

	Native valve	Stiffened valve		Native valve	Stiffened valve
0 ms	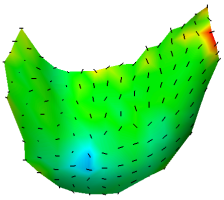	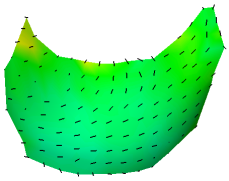	500ms	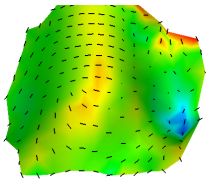	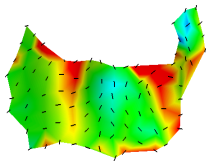
200 ms	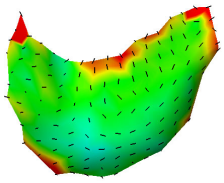	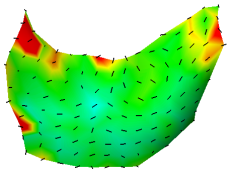	600 ms	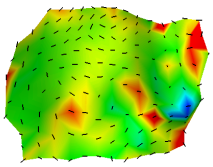	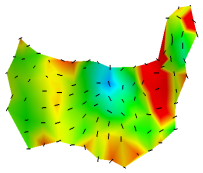
300 ms	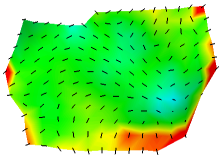	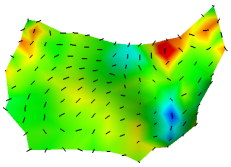	630 ms	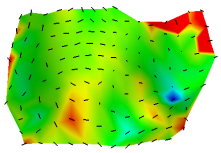	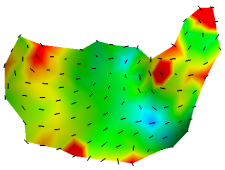
330ms	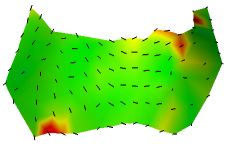	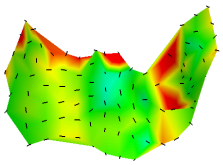	660 ms	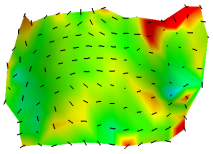	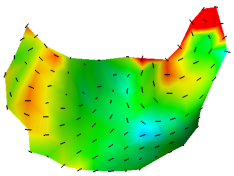
360 ms	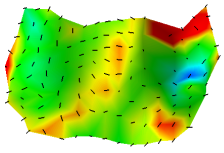	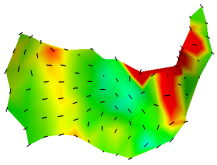	700 ms	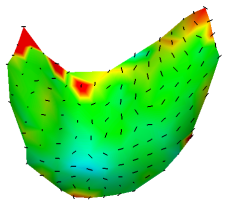	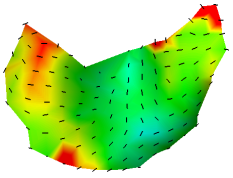
400 ms	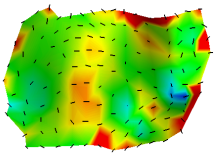	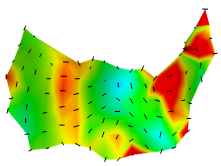	800 ms	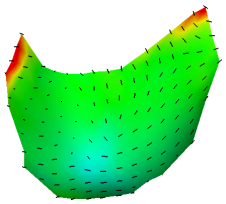	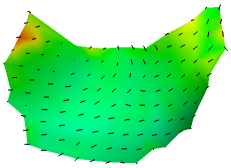

Valve 5

	Native valve	Stiffened valve		Native valve	Stiffened valve
0 ms	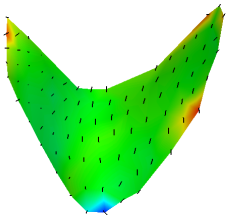	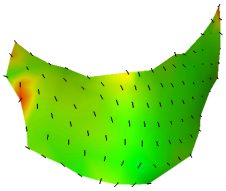	500ms	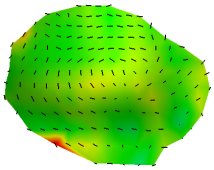	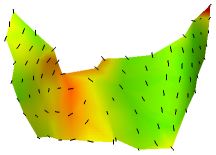
200 ms	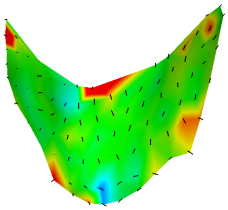	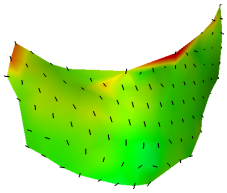	600 ms	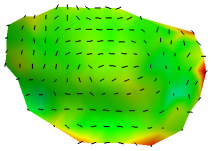	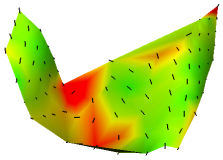
300 ms	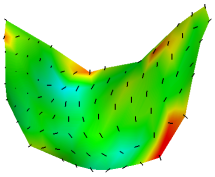	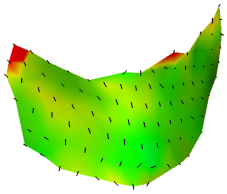	630 ms	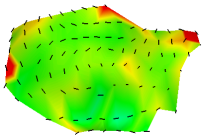	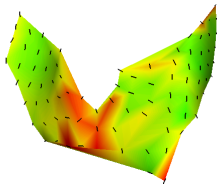
330ms	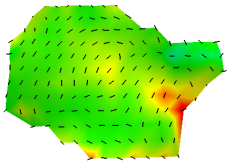	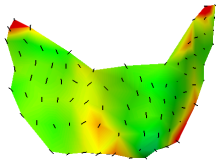	660 ms	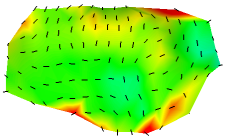	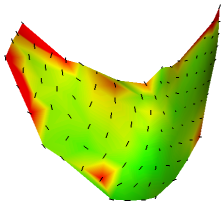
360 ms	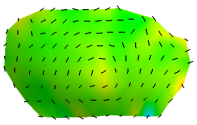	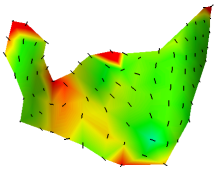	700 ms	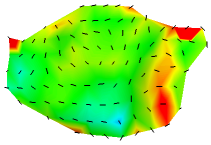	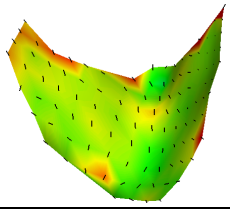
400 ms	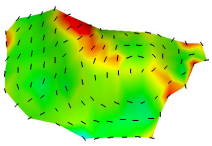	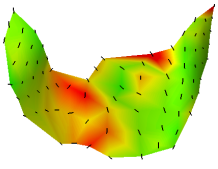	800 ms	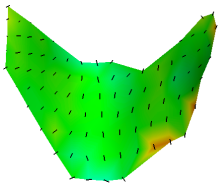	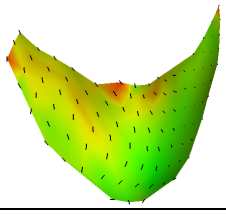

BIBLIOGRAPHY

1. Albert J, Dalen J, Rahimtoola S. Valvular heart disease. 3 ed: Lippincott Williams & Wilkins; 2000.

2. Thubrikar M. The Aortic Valve. Boca Raton: CRC; 1990.

3. Mark H. Beers RB, Mark Burs. Merck Manual Diagnosis & Therapy. 17th edition ed: Merck & Co.

4. Deiwick M, Roschner C, Rothenburger M, Schmid C, Scheld HH. Feasibility and risks of heart surgery in very elderly: analysis of 200 consecutive patients of 80 years and above. Arch Gerontol Geriatr 2001;32(3):295-304.

5. Thornton M. High Speed Dynamic, 3-D Surface Imaging [Master of Engineering Science]. London, Ontario: University of Western Ontario; 1996.

6. Thubrikar MJ, Aouad J, Nolan SP. Comparison of the in vivo and in vitro mechanical properties of aortic valve leaflets. J Thorac Cardiovasc Surg 1986;92(1):29-36.

7. Netter FH. Atlas of Human Anatomy. 2nd ed. East Hanover: Navartis; 1997.

8. Legrice IJ, Hunter PJ, Smaill BH. Laminar structure of the heart: a mathematical model. Am J Physiol 1997;272(5 Pt 2):H2466-76.

9. Wells S, Sacks M. Effects of stress-state during fixation on the fatigue properties of bioprosthetic heart valves. In: Sixth World Conference on Biomaterials; 2000; Hawaii: Society for Biomaterials; 2000.

10. Sacks MS, Smith DB, Hiester ED. The aortic valve microstructure: effects of transvalvular pressure. J Biomed Mater Res 1998;41(1):131-41.

11. Gould PL, Cataloglu A, Chattopadyhay A, Dhatt G, Clark RE. Stress analysis of the human aortic valve. Computers and Structures 1973;3:377.

12. Lee TC, Midura RJ, Hascall VC, Vesely I. The effect of elastin damage on the mechanics of the aortic valve. J Biomech 2001;34(2):203-10.

13. O'Malley CD, Saunders JB. Leonardo DaVinci on the human body. New York: Crown Publishers; 1982.

14. Bellhouse BJ, Reid KG. Fluid mechanics of the aortic valve. Br Heart J 1969;31(3):391.

15. Bellhouse B, Bellhouse F. Fluid mechanics of model normal and stenosed aortic valves. Circ Res 1969;25(6):693-704.

16. Schoen FJ. Surgical pathology of removed natural and prosthetic heart valves. Hum Pathol 1987;18(6):558-67.

17. Butterfield M, Fisher J, Lockie KJ, Davies GA, Watterson K. Frame-mounted porcine valve bioprostheses: preparation during aortic-root dilation. Biomechanics and design considerations. J Thorac Cardiovasc Surg 1993;106(6):1181-8.

18. Ross D. Aortic root replacement with a pulmonary autograft: current trends. Journal of heart valve disease 1994;3:358-360.

19. Schoen FJ. Pathology of heart valve substitution with mechanical and tissue prostheses. In: Silver MD, Gotlieb AI, Schoen FJ, editors. Cardiovascular Pathology. New York: Livingstone; 2001.

20. Thubrikar M, Skinner JR, Aouad J, Finkelmeier BA, Nolan SP. Analysis of the design and dynamics of aortic bioprostheses in vivo. J Thorac Cardiovasc Surg 1982;84(2):282-90.

21. Thubrikar MJ, Skinner JR, Eppink RT, Nolan SP. Stress analysis of porcine bioprosthetic heart valves in vivo. J Biomed Mater Res 1982;16(6):811-26.

22. Thubrikar M, Carabello BA, Aouad J, Nolan SP. Interpretation of aortic root angiography in dogs and in humans. Cardiovasc Res 1982;16(1):16-21.

23. Subramanian KR, Thubrikar MJ, Fowler B, Mostafavi MT, Funk MW. Accurate 3D reconstruction of complex blood vessel geometries from intravascular ultrasound images: in vitro study. J Med Eng Technol 2000;24(4):131-40.

24. McPherson DD. Three-dimensional Arterial Imaging. Scientific American Science and Medicine 1996;March(April):22-31.

25. Stevenson DM, Yoganathan AP. Numerical simulation of steady turbulent flow through trileaflet aortic heart valves--I. Computational scheme and methodology. J Biomech 1985;18(12):899-907.

26. Stevenson DM, Yoganathan AP, Williams FP. Numerical simulation of steady turbulent flow through trileaflet aortic heart valves--II. Results on five models. J Biomech 1985;18(12):909-26.

27. Walker PG, Pedersen EM, Oyre S, Flepp L, Ringgaard S, Heinrich RS, et al. Magnetic resonance velocity imaging: a new method for prosthetic heart valve study. J Heart Valve Dis 1995;4(3):296-307.

28. Hartiala JJ, Mostbeck GH, Foster E, Fujita N, Dulce MC, Chazouilleres AF, et al. Velocity-encoded cine MRI in the evaluation of left ventricular diastolic function: measurement of mitral valve and pulmonary vein flow velocities and flow volume across the mitral valve. Am Heart J 1993;125(4):1054-66.

29. Walker PG, Oyre S, Pedersen EM, Houlind K, Guenet FS, Yoganathan AP. A new control volume method for calculating valvular regurgitation. Circulation 1995;92(3):579-86.

30. Fung YC, Sobin SS. Mechanics of pulmonary circulation. pp. 665-730. In: Hwang NH, Normann NA, ed. Cardiovascular flow dynamics and measurements. Baltimore, Univ Park Press, 1977.

31. Iyengar AKS, Sugimoto H, Smith DB, Sacks MS. Dynamic in vitro quantification of bioprosthetic heart valve leaflet motion using structured light projection. Ann Biomed Eng 2001;29(11):963-73.

32. Abdallah SA, Su CS, Hwang NHC. Dynamic Performance of Heart Valves Prostheses and the Testing Loop Characteristics. Transactions of the American Society of Artificial Internal Organs 1983;29:296-300.

33. Geddes LA, Janas W, Badylak SF. Use of impedance ratio for the continuous measurement of stroke volume of a valveless pouch used as a cardiac-assist device. IEEE Trans Biomed Eng 1992;39(3):310-3.

34. Liu ZR, Ting CT, Zhu SX, Yin FC. Aortic compliance in human hypertension. Hypertension 1989;14(2):129-36.

35. Yamaguchi S, Tsuiki K, Miyawaki H, Tamada Y, Ohta I, Sukekawa H, et al. Effect of Left Ventricle volume on right ventricular end-systolic pressure-volume relation. Circulation Research 1989;65:623-631.

36. Shimada K, Atsushi Yamada and Takayuki Itoh. Anisotropic Triangular Meshing of Parametric Surfaces via Close Packing of Ellipsoidal Bubbles. In: 6th International Meshing Roundtable October 1997; Sandia National Laboratories. p. pp.375-390.

37. Sacks MS, Chuong CJ, Templeton GH, Peshock R. In Vivo 3-D Reconstruction and Geometric Characterization of the Right Ventricular Free Wall. Annals of Biomedical Engineering 1993;21:263-275.

38. Golomb G, Schoen FJ, Smith MS, Linden J, Dixon M, Levy RJ. The role of glutaraldehyde-induced cross-links in calcification of bovine pericardium used in cardiac valve bioprostheses. Am J Pathol 1987;127(1):122-30.

39. Sacks MS, Gloeckner DC. Quantification of the fiber architecture and biaxial mechanical behavior of porcine intestinal submucosa. Journal of Biomedical Materials Research 1999;46:1-10.

40. Weston MW, LaBorde DV, Yoganathan AP. Estimation of the shear stress on the surface of an aortic valve leaflet. Ann Biomed Eng 1999;27(4):572-9.

41. Billiar KL, Sacks MS. Biaxial mechanical properties of the natural and glutaraldehyde treated aortic valve cusp--Part I: Experimental results. J Biomech Eng 2000;122(1):23-30.

42. Billiar KL, Sacks MS. Biaxial mechanical properties of fresh and glutaraldehyde treated porcine aortic valve cusps: Part II - A structurally guided constitutive model. Journal of Biomechanical Engineering 2000;122(4):327-335.

43. Sacks MS, Chuong CJ. Orthotropic mechanical properties of chemically treated bovine pericardium. Ann Biomed Eng 1998;26(5):892-902.

44. Lee JM, Haberer SA, Boughner DR. The bovine pericardial xenograft: I. Effect of fixation in aldehydes without constraint on the tensile properties of bovine pericardium. Journal of Biomedical Materials Research 1989;23:457-475.

45. Vesely I. A mechanism for the decrease in stiffness of bioprosthetic heart valve tissues after cross-linking. ASAIO 1996;42(6):993-999.

46. Sacks MS, Smith DB, Hiester ED. The aortic valve microstructure: Effects of trans-valvular pressure. Journal of Biomedical Materials Research 1998;41:131-141.

47. Vyavahare N, Ogle M, Schoen FJ, Zand R, Gloeckner DC, Sacks M, et al. Mechanisms of bioprosthetic heart valve failure: fatigue causes collagen denaturation and glycosaminoglycan loss. J Biomed Mater Res 1999;46(1):44-50.

48. Gloeckner DC, Billiar KL, Sacks MS. Effects of mechanical fatigue on the bending properties of the porcine bioprosthetic heart valve. Asaio J 1999;45(1):59-63.

49. Sacks MS. The biomechanical effects of fatigue on the porcine bioprosthetic heart valve. Journal of long-term effects of medical implants 2001;11(3&4):231-247.

50. Sacks MS, Schoen FJ. Calcification-independent collagen damage in explanted clinical bioprosthetic heart valves. In: submitted, editor. Society for Biomaterials; 1999; Providence, Rhode Island; 1999.

51. Sacks MS, Schoen FJ. Collagen fiber disruption occurs independent of calcification in clinically explanted bioprosthetic heart valves. J Biomed Mater Res 2002;62(3):359-71.

52. Schoen F, Levy R. Tissue heart valves: Current challenges and future research perspectives. Journal of Biomedical Materials Research 1999;47:439-465.